UNIVERSITY OF CALIFORNIA,

IRVINE

Modeling Power Plant and Electric Grid Dynamics with High Renewable Use and Climate Change in California

THESIS

submitted in partial satisfaction of the requirements for the degree of

MASTER OF SCIENCE

In Mechanical and Aerospace Engineering

By

Gi Jung Lee

Thesis Committee:

Professor Jack Brouwer, Chair

Professor Scott Samuelsen

Professor Derek Dunn-Rankin

2019

DEDICATION

This work is dedicated to my parents, Heung Seob and Seon Joo, for raising and shaping me into the person I have become today. It is also dedicated to my beloved brother, KiBeom, for cheering and caring for me. All the opportunities and achievements would have been impossible without all your support. Although a few words are not enough, thank you all for everything.

TABLE OF CONTENTS

Page

LIST OF FIGURES

LIST OF TABLES

NOMENCLATURE

APEP	Advanced Power and Energy Program
CCPP	Combined-Cycle Power Plant
CFD	Computational Fluid Dynamics
DOE	U.S. Department of Energy
EIA	Energy Information Administration
GE	General Electric
GT	Gas Turbine
HHC	High-Hydrogen Content
HiGRID	Holistic Grid Resource Integration and Deployment
HP	High Pressure
HRSG	Heat Recovery Steam Generator
IP	Intermediate Pressure
ITC	Investment Tax Credit
LP	Low Pressure
NGCC	Natural Gas Combined-Cycle
PEM	Proton Exchange Membrane
PTC	Production Tax Credit
PV	Photovoltaic
RPS	Renewable Portfolio Standard
SCAQMD	South Coast Air Quality Management District
SSMT	Steam System Modeler Tool
ST	Steam Turbine
3PRH	Three-Pressure with Reheater

ACKNOWLEDGEMENTS

I would like to first thank my advisor, Professor Jack Brouwer, from whom I have so much to learn. As an advisor, he guided me through this work with his leadership and expertise; without them, I would not have been able to complete this work. As a researcher, he set the example with enthusiasm and dedication that I can always look upon. As an individual, he showed me tremendous care and support that helped me to achieve my goals.

My gratitude goes to Professor Scott Samuelsen who has been an inspiration to me ever since I got to know him. His exemplary leadership and dedication to the field of renewable energy will always have a place in my heart as the power source that keeps me going as a researcher in the field for the rest of my career.

I would like to extend my appreciation to all my colleagues and predecessors in and out of the Advanced Power and Energy Program. My special thanks go to Dr. Robert Flores and Dr. Derek McVay for productive and insightful discussions we had related to my research. Previous works by Professor T.S. Kim, Professor Dustin McLarty, Dr. Brian Tarroja and Kate Forrest were essential in setting the goal and path of my research.

ABSTRACT OF THE THESIS

Modeling Power Plant and Electric Grid Dynamics with High Renewable Use and Climate Change in the United States and Asia

By

Gi Jung Lee

Master of Science in Mechanical and Aerospace Engineering

University of California, Irvine, 2019

Professor Jack Brouwer, Chair

While advancement of power generation and grid management technologies has enabled their broader applications, recent changes in climate are projected to impose obstacles to performance and operation of the systems employing these technologies. As more renewables are prioritized over fossil fuels to alleviate changes in climate, the power systems are in need of further research to help meet public and environmental demands by complementing renewable intermittency. In this thesis, the combined-cycle plant technology was modeled in the MATLAB/SIMULINK and verified at two different scales: 1) a 19MW UC Irvine central power plant; 2) a 600MW utility-scale power plant.

Three scenarios were generated using the Holistic Grid Resources Integration and Deployment (HiGRID) tool with the renewable penetration percentages set according to the original California Renewable Portfolio Standards (RPS): 33%, 50% and 80%. Each scenario presented how various

power generating classes contribute to electricity demands for a year-long period. For the scope of this study, load-follower power plant contributions to the general load profile for a week-long period were extracted, normalized and input into the utility model for simulation.

The simulation results demonstrated possible consequences from increasing the renewable penetration to the grid. With the increasing penetration, the natural gas combined-cycle power plant needed to operate more dynamically as a load-follower to complement the renewables. The more dynamic operation of the power plant resulted in decrease of its efficiency from 63% to 44% and to 36% and its capacity factor from 75% to 59% and to 34% for the three scenarios, respectively.

1 INTRODUCTION

1.1 Consequences of Climate Change

Consequences of changes in climate have already appeared in many forms, ranging from global warming to desertification and water maldistribution. Moreover, the change in climate is posed to increase the frequency and severity of extreme weather phenomena [1]. The meteorological phenomenon in Asia, called the Yellow Dust Storm, is an epitome of such. While yellow dust storms are not totally new to the region, the occurrence of these phenomena have been severely intensified by recently accelerated desertification [1]. In the Zabol region of Iran (western Asia), the total damage costs, which includes costs for damages to the community health, due to the intensified and prolonged dust storms during 2000-2004 were approximated to be $1213.976 million USD [2]. Although restricted to specific parts of the world, the damages can potentially increase drastically if adequate steps are not taken.

According to Liu and Chen, human activities have accelerated the change in global climate and environment. Specifically, semi-arid or arid areas are more vulnerable to human intervention than areas with other climatic characteristics, thus more easily resulting in water shortage, water quality degradation, and ecosystem instability to name a few [3]. Not only to prevent further damage from human intervention, but also to support the rapid-growing population in these regions, development and adoption of new grid systems with renewable power generation is highly recommended.

1.2 Adoption of Stringent Energy and Environmental Policies

Two of the world's largest CO_2 emitters are China and the United States. Although the two countries are in different political and environmental circumstances, they have both been implementing realistic yet ambitious renewable energy strategies.

1.2.1 Renewable Policy in China

Beginning in 2005, China has demonstrated a clear vision for renewable energy promotion with a series of legal and strategic frameworks. The Renewable Energy Law of 2005 has prioritized power produced from renewable sources over power from conventional sources and penalized operators in non-compliance upon revision in 2010 [4]. Along with the Renewable Energy Law, as a part of National Five Year Plans, specific targets for cleaner future were set. The 10th Five Year Plan for Energy Conservation and Resources Comprehensive Utilization has called for development of various technologies and projects related to topics ranging from sustainable utilization and reliable substitution of fossil fuels to efficient utilization of renewable resources and effective energy-saving measures [4]. Subsequently, the 11th Five Year Plan has established realistic yet aggressive goals for emissions reduction and targets for renewable energy development. Specifically, by 2010, China aimed to increase percentages of nuclear, hydropower and other renewable energy by 0.1%, 0.8% and 0.4% respectively out of 2.446 billion tons of coal equivalent of primary energy production target. At the same time, China proposed to reduce sulfur and carbon dioxide emissions by 10% at the national level [4]. The subsequent National Plans have established even more aggressive goals in terms of energy mix and targets. For example, by 2020, China is "to increase the share of non-large hydro renewable energy to 3 % of all electricity generation," resulting in targeting capacities of 430 GW of large hydro, 200 GW of wind power, 50 GW of solar power and 30 GW of biomass power [4].

1.2.2 Renewable Policy in the United States

The United States has been one of the prominent leaders in the field of renewable energy in terms of technology. However, effective application of technological advancement requires political or bureaucratic measures to enforce advanced technologies. At the federal level, the United States has been providing tax credits and financial aid programs to encourage electricity production by renewable means. For example, Production Tax Credit (PTC) and Investment Tax Credit (ITC) respectively allow tax credit based on electricity generated by eligible energy resources and the amount invested to build the eligible infrastructure [5]. In addition, Department of Energy's Loan Program has guaranteed billions of dollars to "bridge the clean energy financing gap" for advanced fossil energy and innovative renewable technologies at their initial deployment stages [6]. At the state level, some states have been implementing more stringent goals and policies for emissions reduction and increased shares of renewables than others.

The state of California has been adopting some of the most progressive policies not only in the nation but also in the world. In 2002, California's Renewables Portfolio Standard (RPS) was established under Senate Bill 2002 and expedited under Senate Bill 107 which sets 20 percent target for electricity retail sales be served by renewable energy sources by 2010 [7]. Subsequent legislative measures such as Executive Order S-14-08, Senate Bill X1-2 and Senate Bill 350 have enhanced the previous target respectively to 25 percent by 2016, 33 percent by 2020, and 50 percent by 2030 [7]. Senate Bill 350: Clean Energy and Pollution Reduction Act (SB350) sets an ambitious target to reduce greenhouse gas emissions 40 percent below the 1990 levels by 2030 [7]. This measure is considered to be a stepping stone for California's long-term commitment to address climate change: reducing greenhouse gas emissions to 80 percent below the 1990 levels

by 2050 [7]. Even a step further from SB 350, very recently signed, is SB 100 that not only accelerates the RPS target of 50% by 2030 to 60% but, more importantly, dictates to supply the state's electricity sector with carbon-free resources by 2045 [8].

1.3 Advancement of Renewable Power Generation Technology

Although the problems have already been recognized and possible solutions are available, more extensive research is required to practically meet the energy demand dynamics and environmental constraints specific to each region with different renewable availability and climatic characteristics. For example, Southern California, well-known for its dry and sunny weather, is more appropriate to maximize solar power generation than to focus on hydropower generation. As a long term solution, the currently-used power generation technologies may be substituted with dispatchable renewable technologies that do not necessitate any trade-offs between energy and environment, such as renewable-hydrogen fueled stationary fuel cell systems. The updates on advancement of the most common renewable technologies are as follows.

1.3.1 Distributed Energy Technologies

Various renewable distributed energy conversion technologies have demonstrated potential through increased reliability and efficiency and lower cost in recent years. While fuel cells are only renewable when operating on renewable fuels, they can be dispatched to guarantee relatively high efficiency, and achieve ultra-high efficiency when combined with gas turbines [9], [10]. This fuel cell-gas turbine hybrid technology has achieved 74.4% fuel-to-electricity efficiency with molten carbonate fuel cells and >75% fuel-to-electricity efficiency with solid oxide fuel cells [9], [10].

Wind power has become more economically competitive with traditional means of power generation. Wind turbines with electrolysis and compressed hydrogen energy storage systems, consisting of salt caverns, have been proposed and proven to produce electric power and accommodate up to 14,000 fuel cell vehicles with hydrogen fuel [11]. Solar technology, along with performance advancement and cost reduction in PV panels, is predicted to supply 27% of the nation's electricity by 2050, resulting in ~10% decrease in greenhouse gas and air pollutants emissions and in 4% decrease in water withdrawals and 9% decrease in consumption [12]. When all the benefits are converted into monetary values, solar power is expected to provide benefits of approximately $250 billion in the climate sector and $167 billion in air quality and public health sector benefits [12]. As stated earlier, the research on distributed renewable energy conversion systems focuses on finding the methods to guarantee reliability and efficiency of the technologies that can potentially replace existing power infrastructures for cleaner energy.

1.3.2 Utility Grid Network Integration of Renewable Technology

Despite rapid advancement of renewable technologies, one type of the renewable technology by itself cannot substitute the entire conventional power generation system. A 100% renewable future will only be possible when various types of renewable technologies are utilized in combination to complement each other: for example, nondispatchable and intermittent renewables such as solar and wind may need energy storage and dispatchable renewable energy sources such as geothermal and hydropower for grid reliability. Gonzalez et al. have algorithmized the optimum sizing methodology for a hybrid, grid-connected photovoltaic-wind power system [13]. Valverde et al. have developed a wind-hydrogen energy system for "Hydrogen Office building" in Fife/Scotland with a wind-turbine providing the majority of power and a PEM fuel cell providing backup power,

and validated the dynamic behavior of the system with less than 2% average error [14]. Molina and Espejo have modelled a grid-connected PV energy conversion system, developed a simulation tool (PVSET 1.0) with MATLAB/Simulink and verified the simulation with a 250 watt-peak experimental PV set-up [15]. In order to fully take advantage of the renewable technologies, however, it first requires an understanding of inherent characteristics of renewable resources. Pravalie et al. have spatially analyzed global solar energy potential based on global horizontal irradiation and direct normal irradiation data [16]. Niblick et al. have assessed renewable potentials of biodiesel, solar, and wind on selected sites of the United States [17]. Feng et al. have improved forecasting of wind availability in the United States by developing a forecast model based on geospatial and instance spatial distributions of wind characteristics and forecasting error metrics [18]. Along with this knowledge of renewable resources, change in operational dynamics of the existing power systems has to be accompanied to incorporate the renewables. Huang et al. have developed an analytical ramp rate calculator to maximize flexibility and reliability of an integrated ASEAN power grid for high renewable penetration scenarios [19]. Sharma et al. have developed a model-based approach that integrates the dynamic nature of renewable resources into a conventional power demand for planning a transitioning electricity system [20].

1.3.3 Current Renewable Complementary Technology

By far, the most important and widely used power generation technology for complementing renewable power generation is load-following natural gas combined cycle (NGCC) power plant technology. In the state of California and many places around the world these NGCC plants provide the majority of the electric energy and are dynamically dispatched to enable integration of intermittent renewable power. As renewable power generation is increasingly used; however, will

the NGCC plants be able to operate even more dynamically in the utility grid network? Alobaid et al. have reinforced dynamic operation of CCPP by summarizing progress in dynamic simulation of various types of thermal power plants [21]. In a series of two papers, Liu et al. have developed a detailed off-design model for a CCPP in Aspen HYSYS and recommended a new operating strategy, EGR-IGVC that seeks to improve the part-load performance of the plant [22], [23]. Babrowski et al. have compared five different model techniques to optimize their energy system model that calculates dispatch of thermal power units, including CCPP, upon increasing need for cyclic operation [24].

2 GOAL AND OBJECTIVES

2.1 Goal

The goal of the thesis is to establish and manage the dynamic capability of conventional power generation units required to support the grid dynamics associated with a high penetration of intermittent renewable resources.

2.2 Objectives

The following objectives are established to fulfill the goal of the thesis:

1. Conduct a literature review to obtain all relevant background information.
2. Develop Dynamic Models for the UC Irvine Central Power Plant.
3. Verify the UC Irvine Central Plant Model with Operational Data.
4. Develop Dynamic Models for Utility-Scale Power Plants.
5. Verify the Utility-Scale Dynamic Model with Operational Data.
6. Apply the developed models for high renewable penetration scenarios.
7. Evaluate the system efficiency for the generated scenarios.

3 BACKGROUND

3.1 Combined-Cycle Power Plants (CCPPs)

The combined-cycle power plant is one of the most widely-used power generation technologies in the world, and is composed of three major components that are directly involved in power generation: a gas turbine (GT), a heat recovery steam generator (HRSG), and a steam turbine (ST). The basic principle of CCPP operation is a combination of a Brayton cycle with air as a working fluid and a Rankine cycle with steam/water as the working fluid. Figure 1 demonstrates a general configuration for a natural gas fueled CCPP.

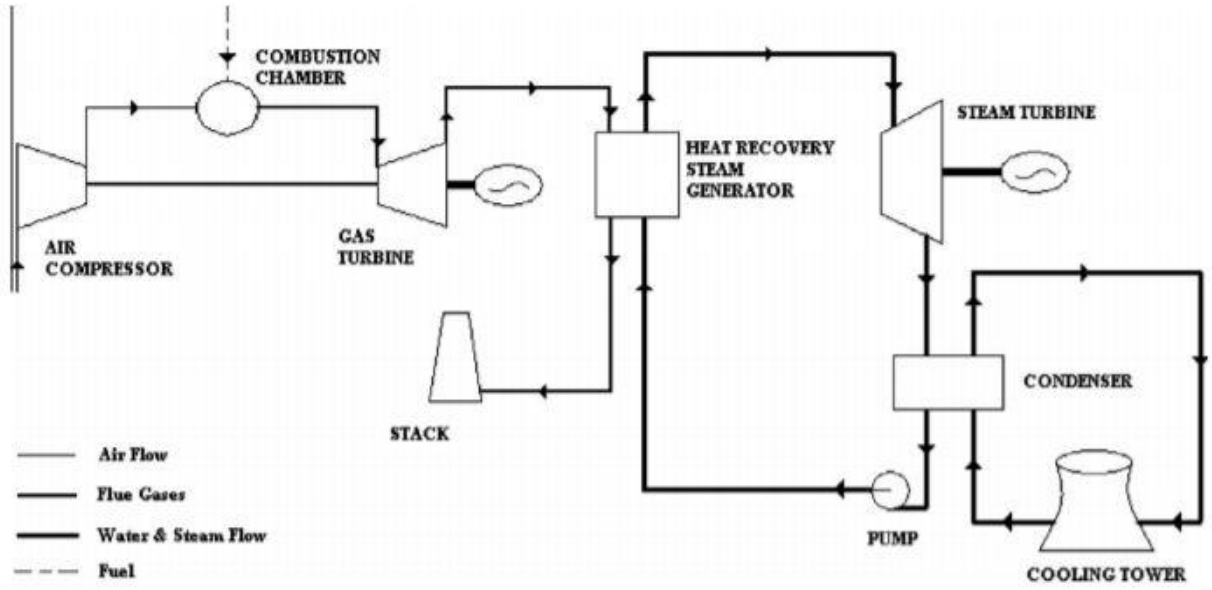

Figure 1: Schematic diagram of a natural gas combined-cycle power plant [26]

To briefly explain, atmospheric air becomes a highly-pressurized air flow through a compressor and is subsequently mixed with fuel in the combustor. The combustion of the compressed air and fuel mixture generates a high temperature flow, which high enthalpy provides energy for rotating

the GT which provides rotational power to the compressor and a coupled generator for electric power generation. The exhaust gas from the GT heats, boils and superheats water within the HRSG. The superheated steam out of HRSG is used to spin the ST and a coupled generator to generate more power as the ST exhaust is condensed using cooling towers and pumped up again to the HRSG pressure for continuous flow in the Rankine cycle.

For the last few decades, CCPPs have primarily been using fossil fuels, ranging from coal, oil to natural gas. They have been successful in supplying power with high efficiency, high flexibility and relatively low emissions. On the top of all these relative advantages, various studies have been conducted on fuel flexibility with goals of maintained reliability and, more importantly, much-reduced criteria pollutants emissions. Recently, fuel flexibility research has been focusing on using hydrogen or high-hydrogen-content (HHC) fuels for turbine-based power generation technology. Gobbato et al. have presented a CFD simulation of air-hydrogen reaction flow inside a combustor of a single shaft gas turbine [27]. Ditaranto et al. have proposed a novel concept of a gas turbine cycle with exhaust gas recirculation that utilizes hydrogen as its fuel; the proposed design minimizes compromise in efficiency while reducing formation of NOx by generating an oxygen-depleted working fluid that can limit the reactivity of hydrogen-rich fuels [28]. Cappelletti et al. have modified an existing heavy-duty gas turbine burner to investigate the optimal design for a lean premixed burner with 100% hydrogen [29].

3.1.1 Gas Turbine (GT)

The operation of the gas turbine is ideally represented as a Brayton cycle with the isobaric heat rejection step (from state 4 to state 1) substituted for by simply introducing fresh air into the

compressor at state 1. Figure 2 below demonstrates the schematic diagram of components of the gas turbine system as well as the temperature-entropy diagram of an ideal Brayton cycle.

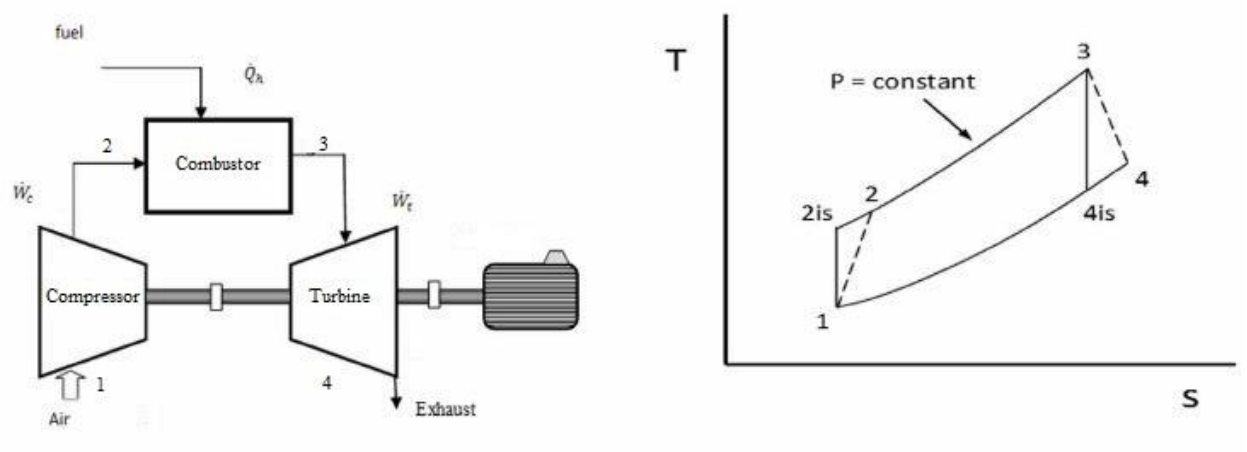

Figure 2: Simple Brayton gas cycle [30].

(Left): Cycle components. (Right): T-S diagram of Brayton cycle

The ideal Brayton cycle is a closed cycle with air as its working fluid. The steps of the ideal cycle (1-2is-3-4is-1) are as follows in order: isentropic compression (1-2is), isobaric heat addition 2is-3), isentropic expansion (3-4is), isobaric heat rejection (4is-1). On the other hand, the steps of the actual cycle (1-2-3-4-1) are as follows in order: adiabatic compression (1-2), isobaric heat addition (2-3), adiabatic expansion (3-4), isobaric heat rejection (4-1). The last step, step 4-1, is associated with cooling of the working fluid. For a typical practical gas turbine cycle, however, the working fluid in the turbine is a combusted mix of air and fuel that is not easily reused by isobaric heat rejection. Thus, fresh air is introduced to the compressor at state 1. To briefly explain the operation steps of the gas turbine system, in the step 1-2, fresh atmospheric air is pressurized through a compressor. In the step 2-3, the highly-compressed air is mixed with injected fuel and the mixture then goes through combustion to generate a high-temperature, high-pressure gas flow. In the last

step 3-4, the gas enters and expands within the turbine to produce work that spins the compressor and a coupled generator to produce electricity, followed by exhausting of the combustion mixture.

3.1.2 Heat Recovery Steam Generator (HRSG)

A Heat Recovery Steam Generator (HRSG) allows exchange of heat between the hot exhaust gas from the gas turbine and water to produce high quality steam. A general schematic of an HRSG is shown in Figure 3.

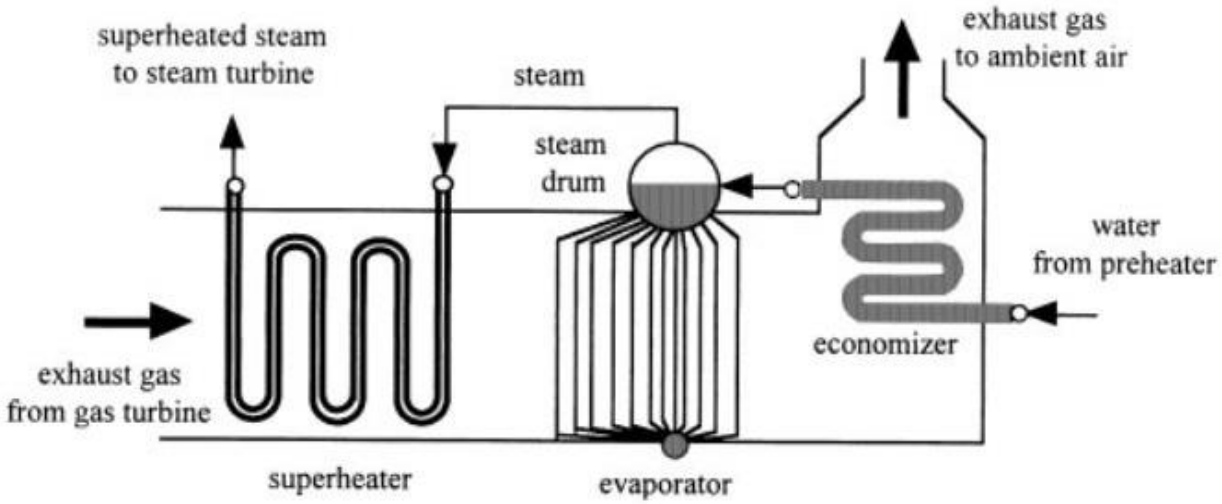

Figure 3: Schematic diagram of a heat recovery steam generator [31].

An HRSG is divided into four major parts: an economizer, evaporator, steam drum and superheater. While the heat exchange from the exhaust gas to water and consequent phase change of water can occur in any parts of the HRSG, each part has its own dominant phenomenon. In the economizer, preheated water is further heated up. In the evaporator, water is not only heated up but is also vaporized into steam. In the steam drum, steam and water mixture is separated while the separated steam is sent to a superheater, the water is sent back to the evaporator for

vaporization. In the superheater, the steam is superheated to satisfy the desired inlet conditions of a steam turbine. The significance of superheating, however, is more than to meet the desired conditions. The superheating of steam ensures high quality and dryness of the steam that is fed into a steam turbine and high quality throughout the expansion process (ideally always superheated) so that liquid water droplets that can damage turbine blades are not formed. For safe operation of the steam turbines, the quality of steam is typically to be maintained above 90% [32].

3.1.3 Steam Turbine (ST)

The operation of the steam turbine is ideally represented by one step of an ideal Rankine cycle, which corresponds to the step 3-4 in Figure 4.

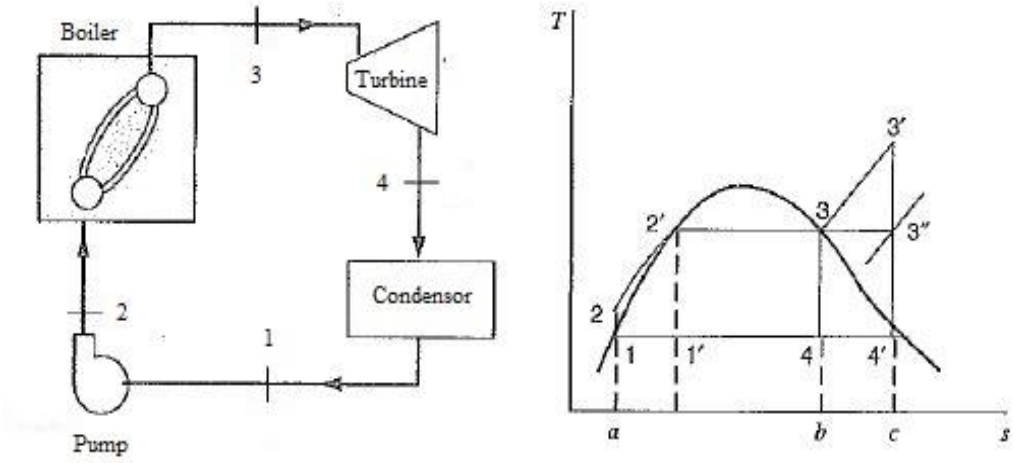

Figure 4: Simple Rankine cycle [32].

(Left) Components of the cycle. (Right) T-S diagram of Rankine cycle

Flowing out of the HRSG, the high temperature and high pressure steam is fed to the steam turbine, in which the steam expands and rotates blades within the turbine and spins a coupled generator to generate useful electrical work. Depending upon the desired power output and operating

conditions, the structural design of steam turbines varies very widely. For the scope of this study, however, two of many designs will be considered: 1) a single pressure turbine, and 2) a three pressure turbine with reheat (3PRH). Figure 5 demonstrates the schematic diagram for the combined-cycle that has a three pressure steam turbine with reheat in-between the high-pressure and intermediate-pressure turbines.

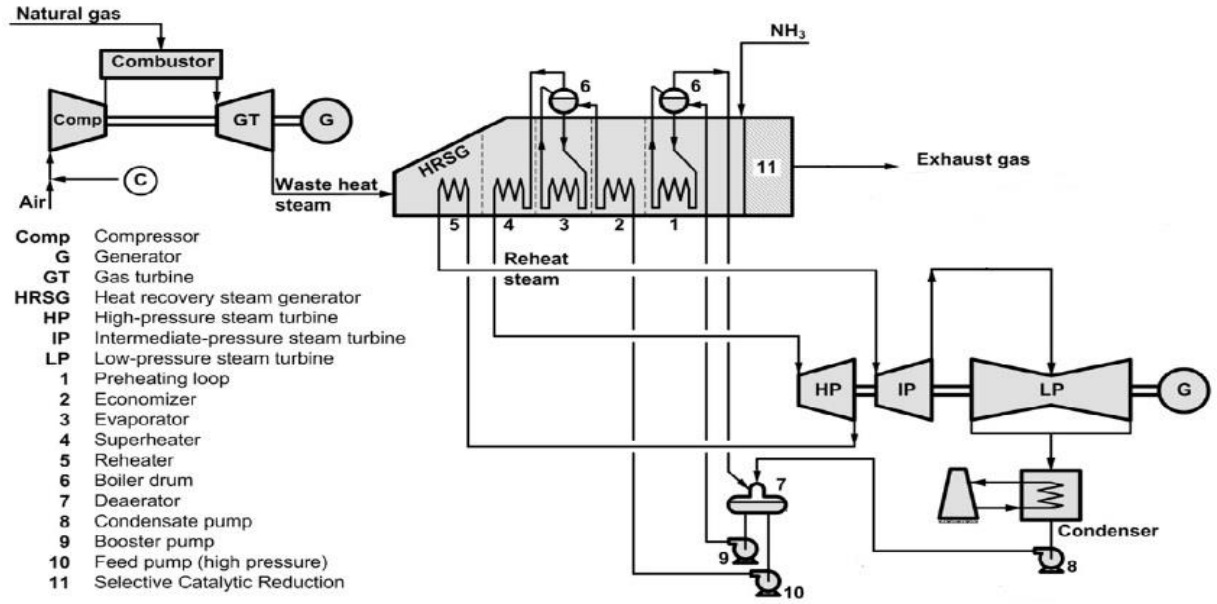

Figure 5: Schematic diagram of CCPP with three pressure ST and reheating scheme [33]

Based upon the diagram of Figure 5, a bottoming cycle with the single pressure steam turbine only includes parts 2, 3, 4, 6, and HP; that is a simple HRSG with a superheater, evaporator, economizer and steam drum as well as a single pressure steam turbine. Note that this single pressure steam turbine is characteristic of the smaller size class steam turbine, while the multi-pressure steam turbines are characteristic of large size class steam turbines. To briefly explain, a high temperature and pressure steam is produced in the HRSG as explained in Section 3.1.2 and fed into the turbine to rotate the blades of the turbine and a coupled generator for power generation. A single pressure

turbine has one steam inflow from an associated HRSG. Depending on operational modes, models and manufacturers, the number of steam outflow within a turbine may vary. On the other hand, as shown in Figure 5, a bottoming cycle with the 3PRH has a different steam flow from that of the single pressure steam turbine. Its main steam-flow is supplied from the HRSG to a turbine as in the bottoming cycle with the single pressure turbine; however, the outflow from the high pressure (HP) turbine goes through a reheater (part 5 in the diagram) and is resupplied into another turbine, intermediate pressure (IP) turbine. Because a turbine, in principle, extracts energy out of a working fluid by expanding it, an IP inlet does have a lower pressure requirement than a HP inlet has. Yet, to prevent any significant condensation of steam within the IP and low pressure (LP) turbines, the steam coming out of the HP turbine is often reheated through the reheater, located at the forefront of the GT exhaust gas flow, up to the temperature that is comparable to an HP inlet steam flow. After the IP turbine, the steam flows directly into the LP turbine. In Figure 5, the LP turbine is a dual axial flow turbine, which is often used when space is a limiting factor for turbine installation. For when space is not a limiting factor, another single axial flow turbine can be used in the place of the LP turbine just like the HP and IP turbines.

3.1.4 Utility-Scale Power Plant

For a combined-cycle, the classification of power plant technology is typically named on the basis of its gas turbine specifications. They include but are not limited to power output, firing temperature and pressure ratio. Followed by advancement in cooling technologies and materials, gas turbine technology has achieved higher outputs and efficiencies, primarily by higher firing temperature. Throughout this evolutionary history, whenever the specification gap between an existing and improved turbine technology was significant, a new turbine “class” would be defined.

So far, the most advanced commercially-available utility-scale turbine technology is entitled an H-class turbine. For example, for General Electric's H-class technology, a single 9HA.02 turbine is known to output 557 MW of power by itself and 9HA.01 in 1x1 combined-cycle configuration has achieved 605 MW with 62.22% net efficiency at full power and standard temperature and pressure conditions [34].

Figure 6: General Electric's number of operating F-class turbines around the world

Despite the ultra-high efficiency of the advanced H-class turbine technology, as shown in the Figure 6 from General Electric's statistics, F-class turbines are still the most prevalent class of turbines in the market because 1) they are proven over extended periods of operating time, 2) they do not necessitate transmission upgrades that might become necessary upon new installation, and 3) they fulfill the need for lower capacity units [35].

3.1.5 Operation Strategy

For the last few decades, a primary focus for the operation of the conventional power plants has been placed on higher output and efficiency. Ranging from as small as less than a megawatt to as big as over a gigawatt, these power plants have been supporting grids most reliably and significantly in many parts of the world. However, acceleration of climate change and aggravation of air pollutions have induced policies that prioritize power from renewable resources. In response, these conventional facilities that primarily consume fossil fuels for power generation and primarily operating continuously near full power have become subject to change and substitution. In addition, a lack of large-scale energy storage systems in market has called for increasing use of load-following operation, instead of baseload operation, by which the power facilities generate power in a constant rate [36]. The load-following operation requires very fast ramping ups-and-downs for secure power supply to grids. Although all major conventional power generation technologies including nuclear are capable of some load-following operation requirements, combined-cycle power plants are known to demonstrate an exceptional rate of load changes and thereby complement renewables very well [36]. The table below compares nuclear, coal-fired, and combined cycle power plants by the operation criteria that the load following operation mode requires.

Table 1: Comparison of operating characteristics of nuclear and fossil-fired power plants [36]

Operating requirement	Nuclear power plant	Coal-fired plant	Combined cycle plant
Average rate of load change in load-follow mode	5%/min at 50-100% load	3-6%/min at 40-100% load	4-8%/min at 40-100% load
Minimum load (% of rated power)	20-30%	35-40%*	15-25%**
Plant efficiency	36-38%	45-47%	58-59%

(100% load)			
Plant efficiency (50% load)	33-35%	42-44%	<60%
*in once-through mode, **for multiple-unit plant(2GTs+ST)			

These conventional power generating technologies have been used to provide baseload and load-following power to grids in many parts of the world. Although the table only provides an approximate range of numbers for some of the important operation criteria, the multiple-unit combined cycle power plant is better that the other technologies in the average rate of load change, minimum load, and efficiency, even at 50% part-load operation with relatively low emission levels.

3.2 Characteristics of Renewable Resources

Renewable resources such as solar and wind vary temporally and spatially by nature. To account for their variability and to be utilized at their utmost potentials, each of the resources has to be characterized in detail by region and by time. In a series of two studies, He et al. have assessed availability of wind and solar resources and characterized their spatial and temporal variation in China [37], [38]. Wang et al. have presented future projections of wind energy in California by using the state-of-the-art climate model, called Variable-Resolution Community Earth System Model (VRCES) [39]. In addition to such research on the spatially and temporally variable nature of renewable resources, Bukhary et al. have highlighted and analyzed additional requirements such as land and water resources for further deployment of solar energy systems in the Southwestern United States [40]. These natural and systematic complications further require that the existing power infrastructures and associated grids be operated in different ways from now as more of these renewable resources account for a larger proportion. In response, Mikkola and Lund have

developed a model for an economically optimal and flexible operation of existing power plants in a grid perspective to prepare for higher renewable penetration [41]. Moreover, because each power grid needs rather a unique operational strategy specific to each grid, most of the studies are conducted on regional basis. In subtropical Australia, for example, Shafiullah has developed a hybrid renewable energy integration system to be installed into the existing grid in Queensland [42]. In arid Algeria, Koussa et al. have considered a grid-connected renewable energy system (GCRES) and evaluated the integrated system from economic and environmental perspectives [43].

3.3 Electric Grids

The term, electric grid, refers to an interconnected network delivering electricity from producers to consumers and includes, but is not limited to, power generating stations, transmission lines, sub-stations, and distribution lines [44].

3.3.1 University of California, Irvine Campus Electric Grid – Micro-Grid

Serving over 30,000 students and staff, the UCI campus electric grid serves a 24MW peak electric load to various types of buildings and end-uses such as classrooms, offices, laboratories, and housing. Figure 7 demonstrates UC Irvine campus grid composition.

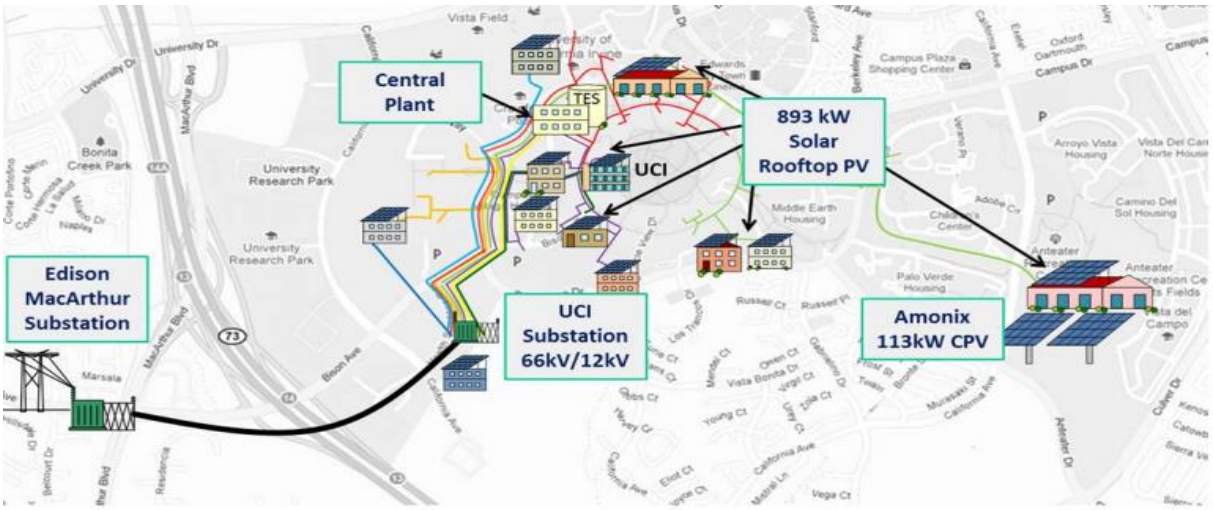

Figure 7: UC Irvine campus grid composition [44]

The campus typically experiences diurnal variations in power demand that vary between approximately 16 MW maximum and 9MW minimum electric load [44]. The grid is powered by two main power generation facilities: 1) a 19 MW-scale on-campus combined cycle power plant, and 2) several PV systems with total peak capacity of about 4 MW. The on-campus central plant consists of a 13.5 MW gas turbine generator and a 5.6 MW steam power plant with 8 electric vapor compression chillers, and cold water thermal energy storage; the roof-mounted solar panels total almost 1 MW of peak PV power, while three systems structurally supported above parking structures can produce about 3 MW of peak PV power [44]. Battery systems, including a 2.0 MW, 500 kWh battery energy storage system, and 100 kW, 100 kWh battery energy storage system, and smart electric vehicle charging are all included in the UCI Micro-Grid [44].

3.3.2 UC Irvine Grid Dynamics

Figure 8 and Figure 9 demonstrate power generated by a GT and ST at UC Irvine central plant during a week of summer 2014 and of winter 2014.

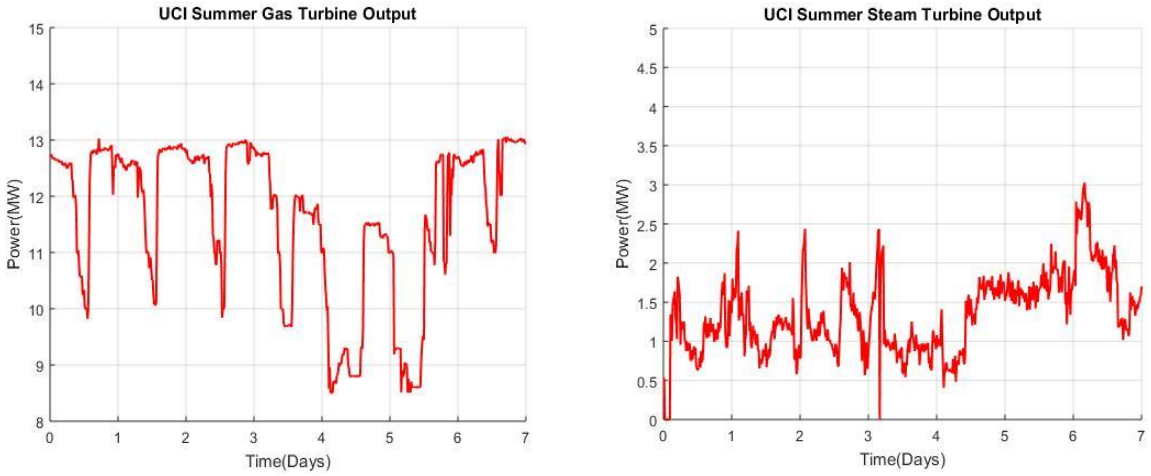

Figure 8: Power generated by UC Irvine central plant in summer.

(Left): Gas turbine. (Right): Steam turbine.

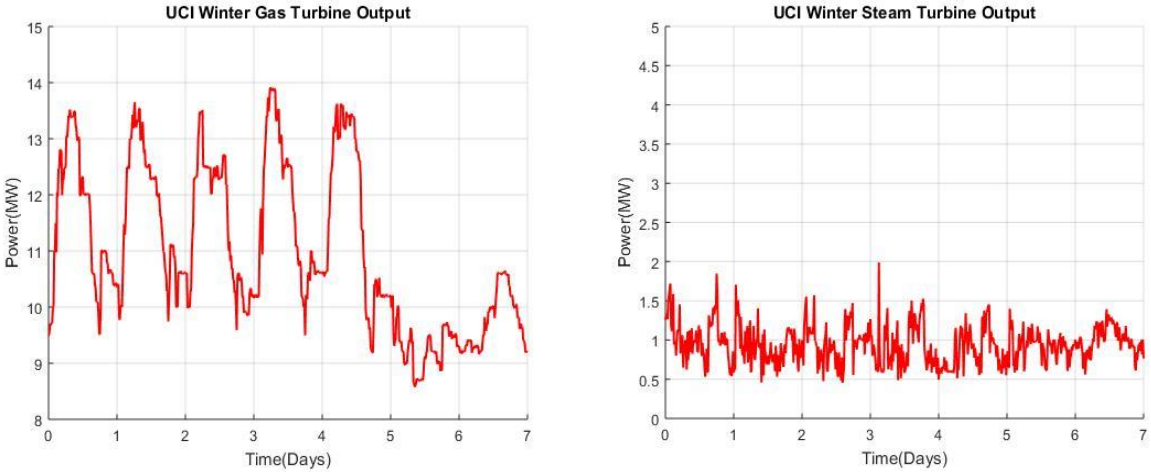

Figure 9: Power generated by UC Irvine central plant in winter.

(Left): Gas turbine. (Right): Steam turbine.

UC Irvine campus grid experiences seasonal and diurnal variations in its load and heat demands. Upon these variations, the central power plant has operated differently. In terms of the demand loads, diurnal variation is more notable. Throughout a day, just like any other grids, the grid experiences a higher demand load in the evening and a lower demand load in the morning. On the

other hand, for the heat demands, seasonal variation is more notable. The demands for heat affect the operation of the bottoming cycle of the central power plant. During winter when the demand for heat is high, steam produced by its HRSG is used to meet the campus heating demands (by making hot water that circulates around campus via heat exchange with HRSG generated steam). During summer when the demand for hot water and heat is low, steam produced by its HRSG is used to run a steam turbine to generate more electricity to meet power demands of the campus.

3.3.3 Future Grid Projections

The increased renewable use (market penetration) in existing utility grid networks has changed grid management and operation strategies. As renewables take up a larger proportion in power composition in the future, further changes in these strategies are inevitable for efficient grid operation. For example, with its state government's aggressive energy policy, California has been setting ambitious goals for the state's power composition that its grid is expected to require various changes in operation of the state's power sources. Figure 10, an excerpt plot out of Eichman et al. [45], presents a week-long snapshot for projection of 33 percent renewable penetration into California grid. As shown, the 33 percent renewable penetration, a goal to be achieved by 2020, demonstrates significant changes in grid characteristics.

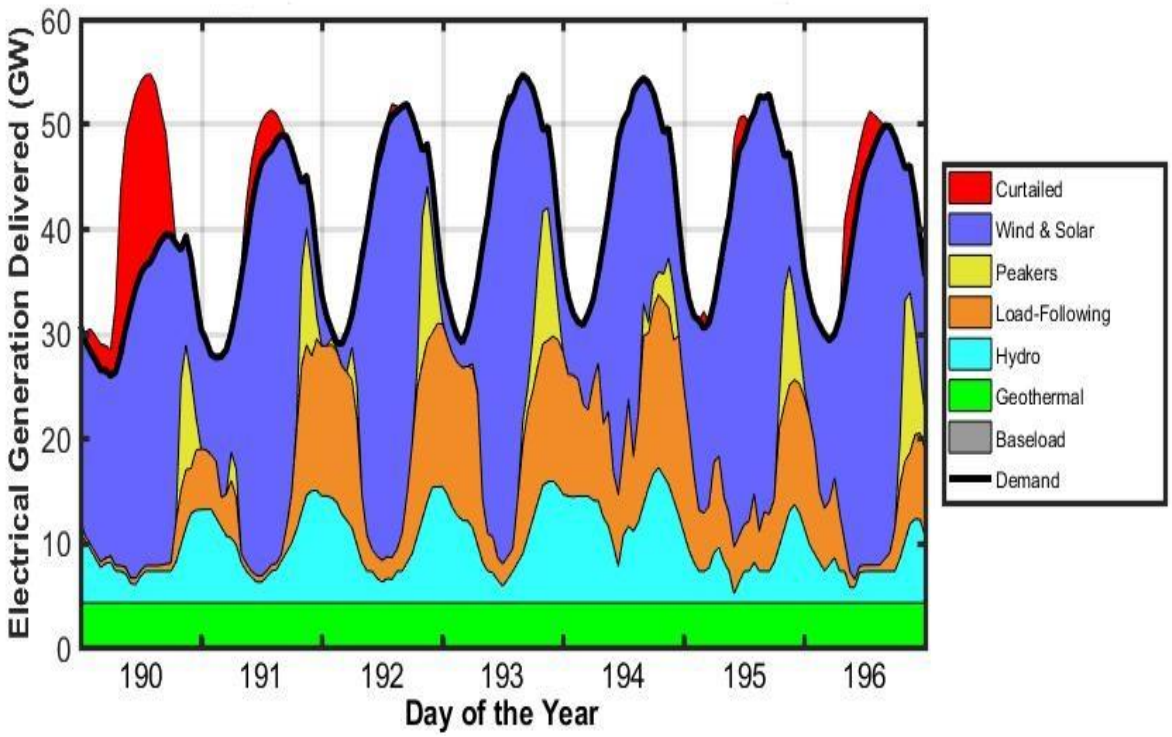

Figure 10: An example of HiGRID projection for future California grid [45]

Specifically, the grid operation will vary significantly from day to day depending on the availability of renewables. For days with high solar and wind energy, a significant portion of generated power will be curtailed to meet a demand load. For days with low solar and wind source, an additional operation of peaker plants will become necessary. On the other aspect, with more renewables penetrating into the grid, less power will be generated by fossil fuel-based baseload and load-following plants. The baseload plants will experience shut-downs or reduction in generation depending on many factors such as life-cycle, efficiency, and emissions [36]. At the same time, although the load-following plants will also experience reduction in generation, they will remain active and operated in a more dynamic manner with more generator starts and stops and faster ramping ups and downs [36]. The abovementioned characteristics that appear in the

projection are not limited to the California grid but they may appear in any other grids as well, as more renewables become available and prioritized.

3.4 Summary

Although many studies have dealt dynamic operability of a combined-cycle power plant and its parts, a study analyzing the dynamic operation of the CCPP in a grid perspective has not been found in the literature at this time. In order to better understand the role of these power plants in future grid, this work is justified. The current work aims to characterize the maximum variable range of operation that a single fleet of natural gas combined-cycle power plant can undergo in future California grid with high renewable penetration and to determine the possibility and consequences of such power plant operations.

4 APPROACH

The current section describes the technical approach developed for meeting each of the objectives, with a Task established for each of the objectives of the thesis.

4.1 Task 1: Literature Review

The scope of this research extends from meteorology, renewable energy, control to engineering design. In order to propose a potential solution for such an interdisciplinary problem, it is essential to begin with a detailed understanding of the status quo, especially of current meteorological circumstances and how these circumstances impose problems on the existing power generation systems. To do so, this thesis includes a review of literature that has examined and predicted the climate change of the regions of interest as well as the literature that has asserted the limits of conventional power plants and grids under these climate change circumstances.

More importantly, because the core of this research is to demonstrate how to integrate renewable power generating components into electric grids under specific circumstances, a review of literature that deals with various types of renewable energy sources and operation of the grids must be conducted extensively. Since the field of renewable energy is a fast-growing branch of science, the literature review has to be focused on up-to-date technological capacities of various renewable sources for practical application. Yet, for a complete design of the grid, several subsystems should be integrated into one larger system; the integration might result in fluctuations in efficiency and/or performance of each individual component. Therefore, a review of literature must encompass the possibilities and consequences following the integration along with specific methodologies to connect each component to the overall system.

4.2 Task 2: Development of a Dynamic Model for the UC Irvine Central Power Plant

Task 2 is to develop a dynamic combined-cycle power plant model. After carefully scrutinizing APEP database for any previously-built models, a gas turbine model built by a former APEP student, Dustin McLarty, is chosen as a starting point. The gas turbine model is modeled after Titan 130 by Solar Turbine. Any alteration of the model is to be made upon necessity. In accordance with the past model, the rest of model building process will continue within the MATLAB/Simulink environment. In addition, just as UC Irvine Central Plant is structured, a HRSG is modeled after Deltak Model Split Cross-Flow DINO and a steam turbine after 3T-5729 by Murray Turbine. The model development of these components is based on knowledge of thermodynamics, heat transfers, differential equations, mechanical design and control. Initial parameters are to be determined through product specifications provided by manufacturers while initial conditions are to be determined through trial-and-error.

4.3 Task 3: Verification of the UC Irvine Dynamic Model with Operational Data

Upon completion, the developed models are to be verified with available operational data. The model verification will be done simply by inputting data for generated power by the central plant's gas and steam turbines. One representative week will be selected: a week from January will be used to represent the winter-month operation, and a week from August, to represent the summer-month operation. The variation in validation data not only verifies the models' dynamic capacity but, more importantly, contributes to visualization and understanding of operational strategies of the central plant and of the UC Irvine grid that varies dramatically by season.

4.4 Task 4: Development of a Dynamic Models for a Utility-Scale Power Plant

In Task 4, a utility-scale combined-cycle power plant is to be modeled. The research on commercially available combined-cycle power plant products is to be preceded, and the range of the research includes but is not limited to power output, configuration and working fluid properties at inlet and outlet. The model development of industry-scale GT, HRSG and ST models will be based on the small-scale (19MW) UC Irvine models. Building a utility model is to be as simple as scaling-up from the UC Irvine model but as complex as building a whole new model. Due to a confidentiality issue, extensive research on any available product specifications is to be accompanied to gather as much information as possible.

4.5 Task 5: Verification of the Utility-Scale Dynamic Model with Operational Data

Just as the campus models are in Task 3, the developed utility-scale models are to be verified by comparison to operational data. It is difficult to obtain operational data of a large-scale power plant; if the data to validate the utility models are not obtained by the time of verification, then simulation results from other parties presented in the literature or a set of created demand loads associated with a series of ramping ups and downs can be used for verification of the model and its dynamic capability.

4.6 Task 6: Application of the Designed Models under High Renewable Scenarios

The combined-cycle power plant model, built in Task 4 and validated in Task 5, is to play a major role in simulating a grid with various scenarios of high renewable penetration. The different

scenarios are to be specified using the HiGRID tool, developed by Dr. Eichman [46]. The percentages of renewable penetration are to be determined according to California's previous Renewable Portfolio Standard targets. For each scenario, the designed models are to be used in dynamically simulating whether or not the predicted load for conventional power generation is feasible.

4.7 Task 7: Evaluation of System Efficiency and Grid Dynamics

Each of the proposed scenarios set in Task 6 will be evaluated and compared in terms of two main categories: system efficiency and grid dynamics. The system efficiency is to be evaluated mainly in the context of fuel-to-power efficiency and capacity factor. The grid dynamics is to be evaluated based on whether or not the ramping capability of the CCPP model is sufficient to match the dynamics of the renewables and if so, how well each of the model simulation results matches the demand load profile in respective scenario.

5 MODEL DEVELOPMENT

5.1 UC Irvine Models

All of the models have been built in the MATLAB/SIMULINK® environment. The schematic representations of the models as developed in this environment are presented in **Appendix B: Utility S**.

5.1.1 Gas Turbine (GT) Model

The gas turbine model used in this study has been adapted from a gas turbine model developed by a former NFCRC student, Dustin McLarty. The model is intended to simulate Solar Turbine's Titan 130, a 14250 kW single-shaft axial flow turbine. The details about development and utilization of this model are shared in Chapter 5 of Dr. McLarty's thesis and in a series of his publications about a fuel cell-gas turbine hybrid system [47], [9], [10]. This turbine system model incorporates thermodynamic design analysis of the turbine system and dynamics of its turbomachinery parts by using performance maps and interpolation strategy.

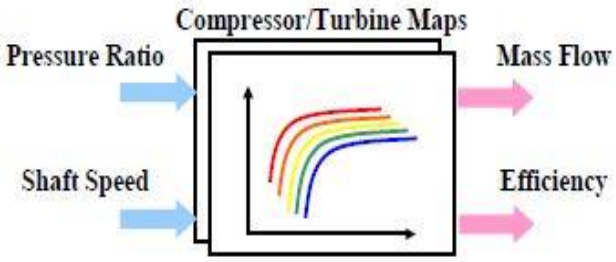

Figure 11: Turbomachinery interpolation strategy [47]

The interpolation strategy requires normalized inputs of pressure ratio and shaft speed to look for corresponding operational mass flow rate and isentropic efficiency on compressor and turbine maps. The strategy then uses the obtained flow rate and efficiency along with temperature and species concentration inputs for thermodynamic analysis. In order to apply the interpolation strategy with given conditions such as inlet temperature, species concentration, and flow rate, a back calculation of turbine inlet and compressor outlet pressure from ambient air pressure as is preceded within in the model. Also preceded within the model is an iterative approach to find the matching mass flow rate from the performance maps that keeps pressure ratio constant [47].

5.1.2 Heat Recovery Steam Generator (HRSG) Model

The central plant of UC Irvine currently employs a Split Cross-Flow model of HRSG from Deltak. The HRSG produces steam at a nominal mass flow rate of 10.34kg/s, temperature of 260 ℃, and pressure of 12 bar. Figure 12 demonstrates the schematic flow diagram showing more details about the UC Irvine HRSG system.

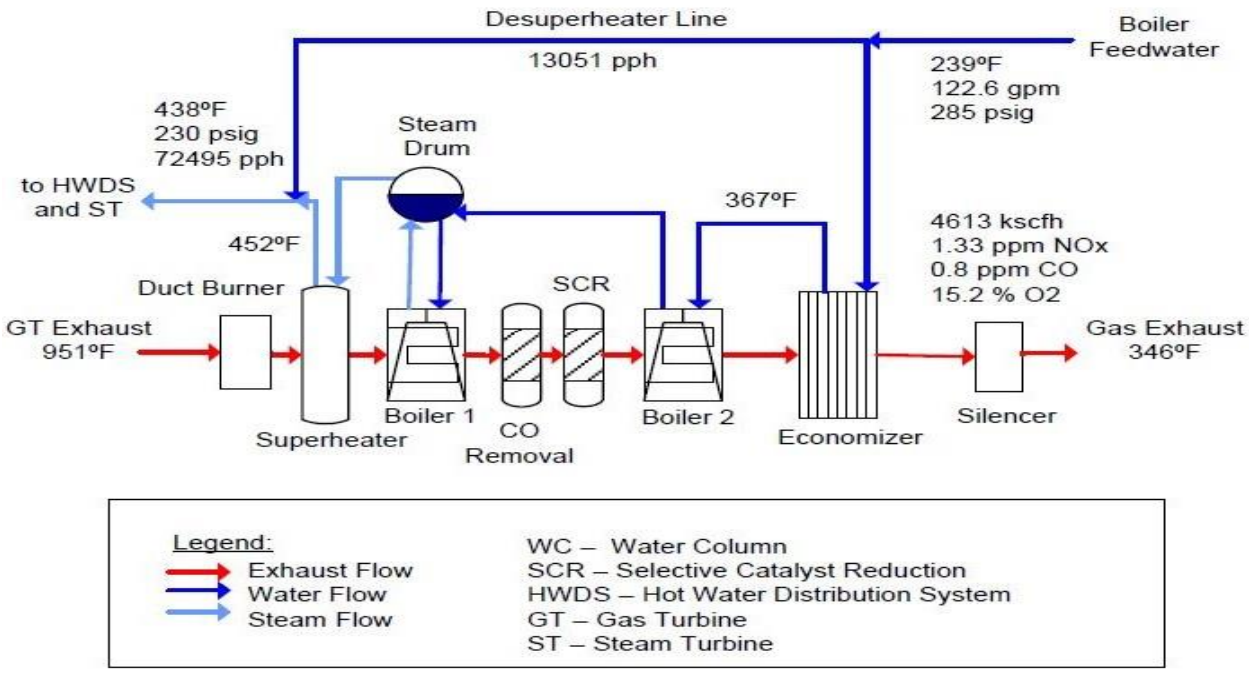

Figure 12: Schematic flow diagram of UC Irvine central plant [48].

In terms of modeling, a lack of boundaries between an economizer and an evaporator or an evaporator and a superheater turns a seemingly simple heat exchange problem into a series of moving boundary problems that cannot be easily solved mathematically. For scope of this study, the problem is simplified into a series of simple boundary value problems by making the following assumptions [31]:

1) Water at the economizer outlet is at its saturated liquid state.
2) Phase change from liquid to gas (boiling) only takes place within the evaporator.

The two assumptions set boundary conditions in-between the three sections of HRSG: the first assumption in-between the economizer and evaporator, and the second assumption in-between the evaporator and superheater. These two assumptions simplify the moving boundary problem not

only by setting the boundary conditions but also by restricting the variable parameters into only temperature that can otherwise vary in temperature, pressure and quality.

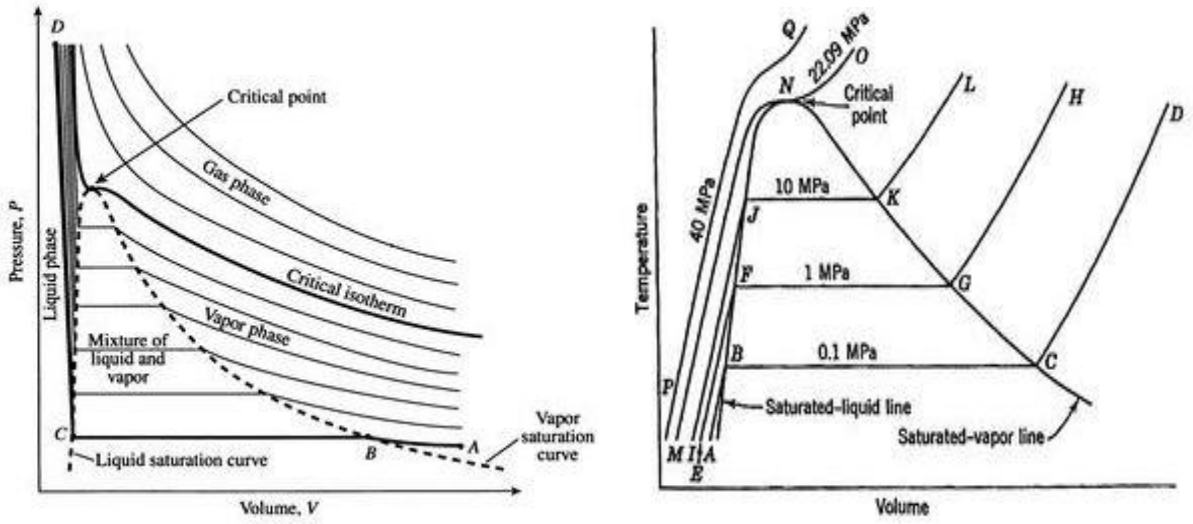

Figure 13:Two-phase diagram of water [49], [32].

(Left): Pressure vs. Volume. (Right): Temperature vs. Volume.

With these two assumptions, heat exchange within HRSG pipes is simply modeled with the energy conservation principle inside control volume along length of the pipe.

$$\dot{E}_g - \dot{E}_w - \dot{E}_{pipe} = \dot{E}_{st} \tag{5.1}$$

For the given control volume, there are a few more assumptions to note in order to complete the energy conservation equation [31]:

3) Because of relatively slow thermal response of pipe metals compared to exhaust gas flow speed, inertia of the gas is neglected.
4) Convection is the only mode of heat transfer from gas to water/steam.

5) Because the heat transfer coefficient of the water side is much higher than that of the gas side, the evaporator pipe metal temperature is assumed to be equal to the temperature of water/steam mixture, the saturation temperature.
6) Fluid properties are considered constant.

With all the assumptions and equations combined, the heat transfer rate to the water from the gas turbine exhaust stream in the HRSG is modeled as below:

$$\dot{E}_w = \dot{m}_w c_{p_w}\left(T_{w_{out}} - T_{w_{in}}\right) \tag{5.2}$$

$$= h_w A_{Inner}(T_{pipe} - \overline{T_w}) \tag{5.3}$$

Where:

$\dot{E}_w$ …….…..……...…….Heat energy transfer rate on water side (kJ/s)

$\dot{m}_w$ …….…….……Mass flow rate of water (kg/s)

c_{p_w} ……...Specific heat capacity of water (kJ/kg °C)

$T_{w_{in}}$ ……..…….……Water temperature at pipe inlet (°C)

$T_{w_{out}}$ ……..…….……Water temperature at pipe outlet (°C)

h_w ……..Heat transfer coefficient of water (kJ/kg m^2 s)

A_{Inner} .....…....Inner surface area of pipe (m^2)

T_{pipe} ……Temperature of pipe metal (°C)

$\overline{T_w}$ ..…….……..…….. Average temperature of water along pipe (°C)

The heat transfer coefficient of the water side is calculated using the Dittus-Boelter equation, which is an explicit function to calculate Nusselt number for forced convection in a turbulent pipe flow [50]. The equation is only valid for abovementioned conditions of Prandtl number, Reynolds number and length to diameter ratio:

$$\mathrm{Nu_D} = \frac{hk}{D} = 0.023 Re_D^{\frac{4}{5}} Pr^{0.4} \tag{5.4}$$

$$\begin{bmatrix} 0.6 \leq \mathrm{Pr} \leq 160 \\ Re_D \geq 10{,}000 \\ \frac{L}{D} \geq 10 \end{bmatrix}$$

While Prandtl number for water/steam is an off-the-table constant, Reynolds number of the water/steam flow inside pipes is represented differently when a mass flow rate is known instead of fluid velocity.

$$\mathrm{Re_D} = \frac{\rho \mathrm{VD}}{\mu} = \frac{4\dot{m}}{\pi \mathrm{D} \mu} \tag{5.5}$$

Where:

Re_D…….Reynolds number with respect to pipe diameter

ρ …….. Density of fluid (kg/m^3)

V ……..…….Velocity of fluid (m/s)

μ ……Dynamic viscosity of fluid (N s/m^2)

D ...……Diameter of pipe (m)

$\dot{m}$ ……..mass flow rate of fluid (kg/s)

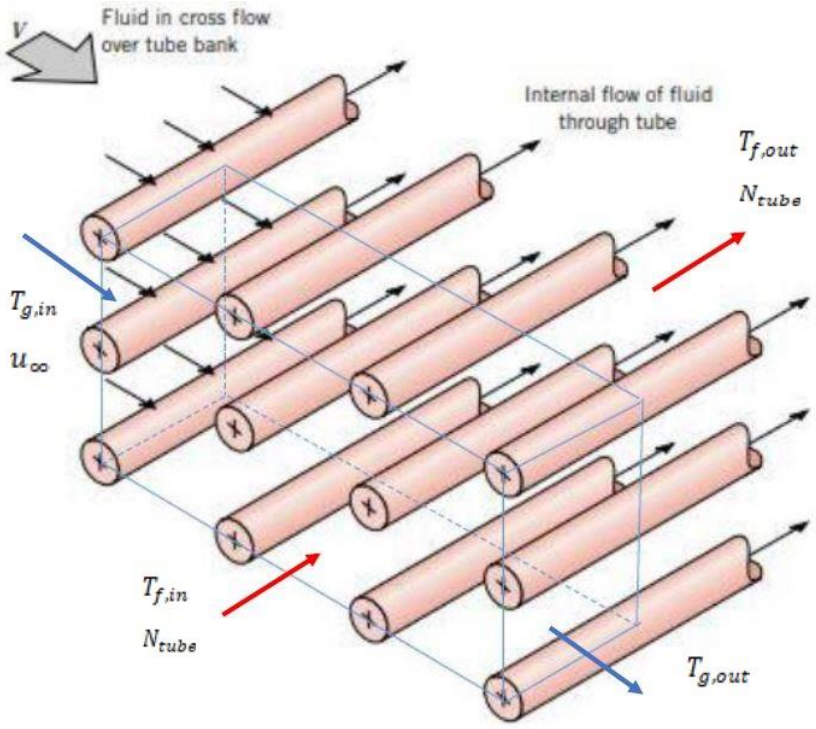

Figure 14: Sectional schematic of a tube bank in cross-flow heat exchanger [50]

While the heat transfer rate on the water side is obtained for fluid flow inside a circular pipe, the heat transfer rate on the gas side is for fluid flow across banks of tubes [50]. The heat transfer rate in gas is modeled as below.

$$\dot{E}_g = \dot{m}_g c_{p_g}\left(T_{g_{in}} - T_{g_{out}}\right) \tag{5.6}$$

$$= h_g A_{outer}(\overline{T_g} - T_{pipe}) \tag{5.7}$$

Where:

$\dot{E}_g$ …….……Heat energy transfer rate from turbine exhaust gas (kJ/s)

$\dot{m}_g$ …….……Mass flow rate of turbine exhaust gas (kg/s)

c_{p_g} ……..……..Specific heat capacity of the exhaust gas (kJ/kg °C)

$T_{g_{in}}$ ……..…….……Gas temperature at pipe inlet (°C)

$T_{g_{out}}$ ……..…….……Gas temperature at pipe outlet (°C)

h_g ……..Heat transfer coefficient of gas (kJ/kg m^2 s)

A_{outer} .....…….....Outer surface area of pipe (m^2)

T_{pipe} ……Temperature of pipe metal (°C)

$\overline{T_g}$ ..…….……..…….. Average temperature of gas along pipe (°C)

The gas side heat transfer coefficient is obtained with Zukauskas correlation [50].

$$\overline{Nu}_D = C\ Re_{D,max}^{m} Pr^{0.36} \left(\frac{Pr}{Pr_s}\right)^{1/4} \tag{5.8}$$

Where:

$\overline{Nu}_D$…….Average Nusselt number with respect to pipe diameter

C, m……..……..…….Constants

$Re_{D,max}$……Maximum Reynolds number

Pr…….…….Prandtl number

Pr_s……..…..Surface Prandtl number

$Re_{D,\max}$ can be obtained with the equation 5.5, but the fluid velocity, V, should be replaced with V_{max}. Depending on a tube arrangement and Reynolds number, the constants, C and m, vary. The varying constant values are shown in Table 2.

Table 2: Constants for Zukauskas correlation for the tube bank in cross flow [50]

Configuration	$Re_{D,max}$	C	m
Aligned	$10–10^2$	0.80	0.40
Staggered	$10–10^2$	0.90	0.40
Aligned	$10^2–10^3$	Approximate as a single (isolated) cylinder	
Staggered	$10^2–10^3$		
Aligned $(S_T/S_L > 0.7)^a$	$10^3–2 \times 10^5$	0.27	0.63
Staggered $(S_T/S_L < 2)$	$10^3–2 \times 10^5$	$0.35(S_T/S_L)^{1/5}$	0.60
Staggered $(S_T/S_L > 2)$	$10^3–2 \times 10^5$	0.40	0.60
Aligned	$2 \times 10^5–2 \times 10^6$	0.021	0.84
Staggered	$2 \times 10^5–2 \times 10^6$	0.022	0.84

[a]For $S_T/S_L < 0.7$, heat transfer is inefficient and aligned tubes should not be used.

In addition, a different configuration of tubes necessitates uses of different expressions for V_{max}.

Two different types of tube arrangements used for HRSG are shown in Figure 15.

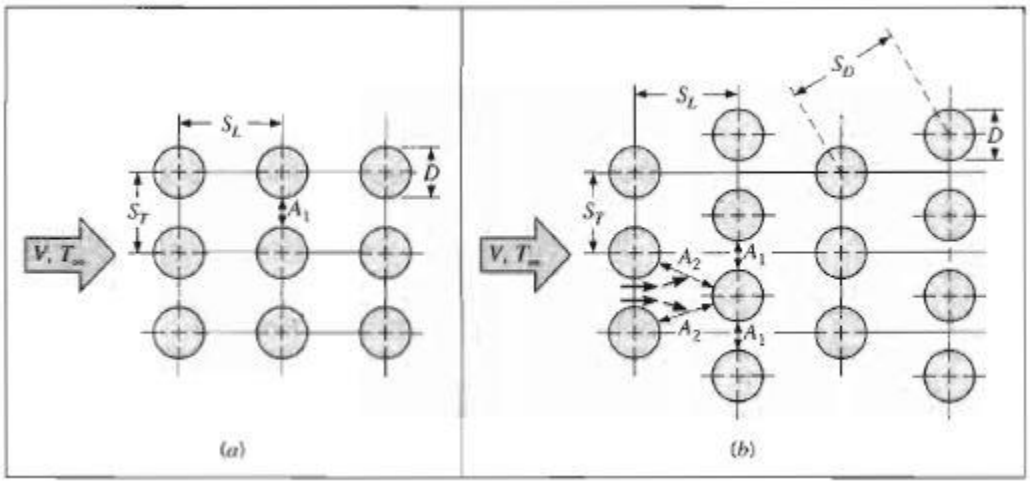

Figure 15: Tube arrangements in a bank [50].

(Left): Aligned. (Right): Staggered.

For the aligned arrangement of tubes, the equation 5.9 is used for V_{max}.

$$V_{max} = \frac{S_T}{S_T - D} V \tag{5.9}$$

For the staggered arrangement of tubes, the equation 5.10 is used.

$$\mathrm{V_{max}} = \frac{S_T}{2(S_D - D)} V \tag{5.10}$$

$$\mathrm{S_D} = \left(S_L^2 + \left(\frac{S_T}{2} \right)^2 \right)^{\frac{1}{2}} \tag{5.11}$$

Where:

S_T……...……Transverse pitch (m)

$\mathrm{S_L}$……...……..Longitudinal pitch (m)

For modeling the UC Irvine HRSG system, the staggered tube arrangement is considered for all parts of the HRSG. For modeling the superheater, the equations 5.6-10 are used along with the gas temperature and mass flow rate at inlet for the gas side to calculate both of the energy transfer rate, $\dot{E}_g$, and the superheater outlet temperature, $\mathrm{T_{g_{out}}}$, at the gas side. At the same time, the equations 5.2-5 are used along with the steam temperature and mass flow rate at inlet for the water side to calculate both of the energy transfer rate, $\dot{E}_{st}$, and the superheater outlet temperature, $\mathrm{T_{st_{out}}}$, at the water side. With the equation 5.1, the metal temperature, which is fed back into both the gas and water side calculations for any changes, can be calculated. The graphical details about the loop associated with the HRSG calculations are demonstrated in Appendix C, Figure 59 and Figure 60.

The above-mentioned assumptions make modeling the evaporator and economizer much easier than modeling the superheater. The assumptions 1) and 5) predetermine steam conditions at the economizer outlet; therefore, there is no need to model the economizer operation. Furthermore, the assumptions 2) and 5) simplify the evaporator operation.

$$\dot{E}_g = \dot{E}_{st} \tag{5.12}$$

$$\dot{E}_{st} = \dot{m}_{st}(h_{sat_g} - h_{sat_l}) \quad (5.13)$$

Where:

$\dot{m}_{st}$……Steam mass flow rate (kg/s)

h_{sat_g}, h_{sat_l}……..Specific enthalpy of saturated steam and saturated water (kJ/kg)

Even after applying the assumptions, the gas side equation used for determining $\dot{E}_g$, stays the same as the equation 5.6. On the other hand, the water side equation can be expressed simply as the enthalpy difference between saturated steam and liquid water as in the equation 5.13. With the economizer outlet conditions on the water side known, the energy required to convert liquid water into steam at a specific temperature and pressure is calculated; the unknown temperature at the evaporator outlet on the gas side can be calculated with the equations 5.12 and 5.6.

At the same time, change in fluid pressure along HRSG is dealt separately from the exchange in heat energy. For scope of this study, because controlling the pressure at the inlet of steam turbine is of the significance, estimating the pressure drop of water and steam within HRSG tubes is important. Although there are many factors that can affect the pressure of fluid flow inside the tubes, friction is the major contributing factor to the pressure drop. The contribution of friction to the pressure drop is determined by the Moody friction factor, a dimensionless parameter defined as the following [50]:

$$f = -\frac{2\left(\frac{dp}{dx}\right)D}{\rho u_m^2} \quad (5.14)$$

Where:

f …….Moody friction factor

D ……..Diameter of pipe (m)

$\frac{dp}{dx}$ …….……Pressure gradient

ρ ……..……..…...Density of fluid (kg/m^3)

u_m …….…….....Average velocity of fluid (m/s)

Using the given fluid conditions and pipe design parameters, dimensionless parameters such as Reynolds number and relative roughness are calculated to characterize the fluid flow inside the pipes. These dimensionless parameters are used to determine the frictional factor, f as shown in the Moody chart, Figure 16. It eventually allows back-calculation of the change in pressure along the length of a pipe.

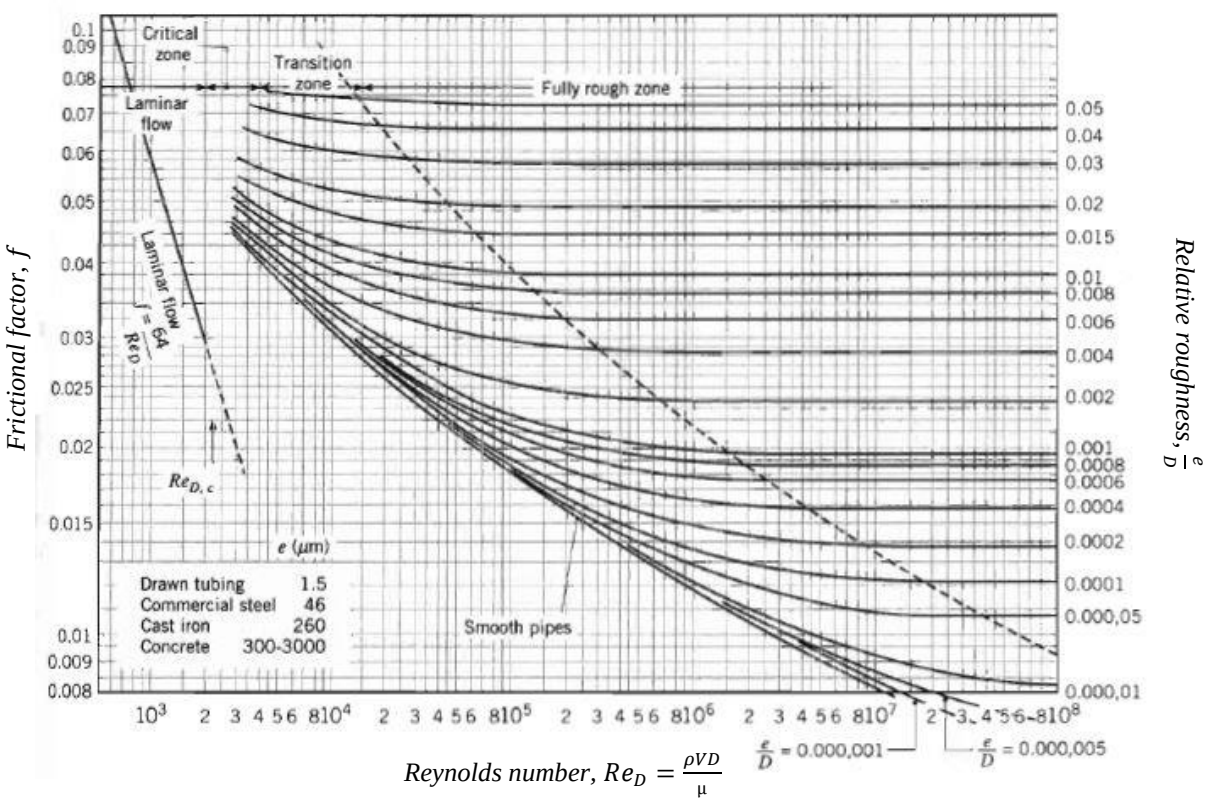

Figure 16: Moody friction factor chart for fully developed flow in a circular tube [50].

5.1.3 Steam Turbine (ST) Model

The main governing equation for turbine operation is Stodola's ellipse equation where it dictates off-design calculations when the turbine nozzles are not choked [51]. Figure 17 demonstrates the graphical representation of Stodola's ellipse.

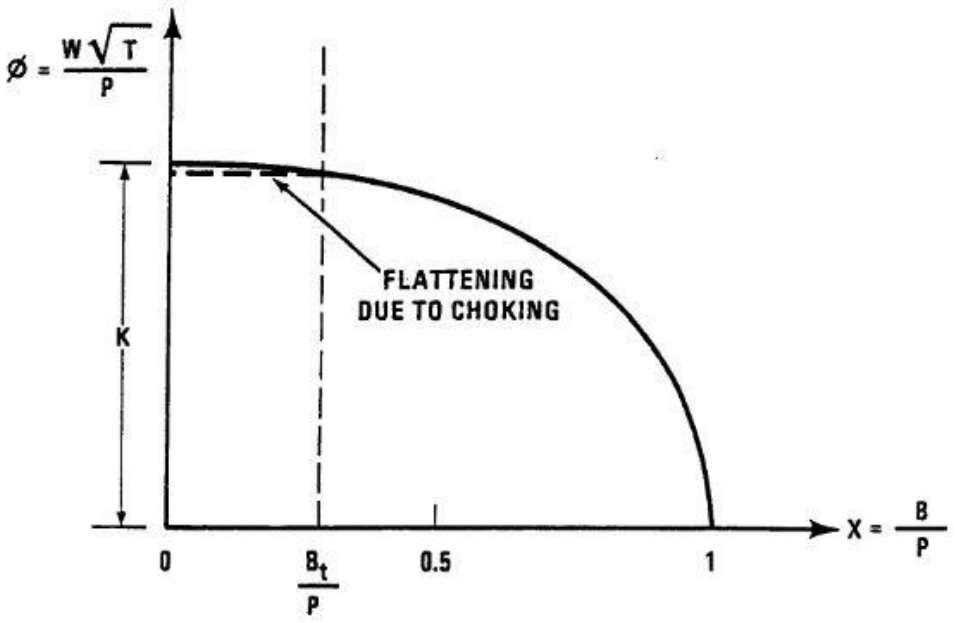

Figure 17: Stodola's ellipse [51]

Representing the off-design turbine operation points, the elliptical path on Figure 17 is dictated by the equation below. There are two versions of the equation; however, for scope of this study, the temperature version of the equation is employed [51].

$$\emptyset = \frac{\dot{m}\sqrt{T}}{P} = K\sqrt{1 - \left(\frac{B}{P}\right)^2} \tag{5.15}$$

Where:

$\emptyset$ ……..Mass flow coefficient

$\dot{m}$ …..……...Mass flow rate (lbs/hr)

P ……..……..Pressure at turbine inlet (psi)

T ……..…Temperature at turbine inlet (°R)

B ....……..…….Back pressure (psi)

K ……...Constant

Provided by manufacturers and shown below in the table 3, the design parameters of the UC Irvine steam turbine are used to calculate the dimensionless mass flow coefficient, $\emptyset$. The calculation of the dimensionless coefficient is calculated depends on structural design of a turbine system such as the number of stages within a turbine and the number of turbines within a system. The number of stages within a turbine comes into effect only when the number of stages is limited to a few. For a turbine with few stages, back pressure, B, in the equation 5.15 has to be replaced by the equation 5.16 [51].

$$B - P_t \tag{5.16}$$

Where:

B …….Back pressure (psi)

P_t ……Pressure in the throat of an isentropic expansion to sonic from P (psi)

P……...Inlet pressure (psi)

On the other hand, the number of turbines does not alter the equation for the mass flow coefficient. Rather, it affects calculation of the number of mass flow coefficients. For modeling purpose, for

example, a dual-pressure turbine requires calculation of the two mass flow coefficients and a three-pressure turbine three. For UC Irvine model, calculation of one mass flow coefficient is needed.

Table 3: UC Irvine steam turbine design parameters, provided by the manufacturer [48]

UC Irvine Steam Turbine, Murray Turbine Serial No. 3 T-5729	
Power (kW)	5438
Speed (rpm)	4500
Flow (lbs/hr)	82114
Normal Temperature (°F)	425
Max. Temperature (°F)	451
Normal Pressure (psig)	240
Max. Pressure (psig)	243
Normal Exhaust Pressure (inHga)	3.5
Max. Exhaust Pressure (inHga)	1.346

Setting the mass flow coefficient, calculated by the design parameters, constant allows back-calculation of corresponding back pressure when all other parameters such as inlet pressure, inlet temperature and mass flow rate are known. With the inlet pressure and temperature known, the steam enthalpy and entropy specific at the inlet can be obtained from the enthalpy table; with the obtained entropy and calculated back pressure, the steam enthalpy at the outlet can be obtained, again from the table. Assuming a quasi-steady equilibrium condition along with the obtained inlet and outlet steam conditions, the following mass and energy equations for the control volume, drawn around a turbine, can be solved [52].

$$\dot{m}_{in} - \dot{m}_{out} = V\frac{d\rho}{dt} \tag{5.17}$$

and

$$\dot{E}_{in} - \dot{E}_{out} - \dot{W}_s - \dot{E}_{gen} = V\frac{d(\rho e)}{dt} \quad (5.18)$$

Where:

$\dot{W}_s$ …… Shaft power (kJ/s)

$\dot{E}_{\text{gen}}$……..……..…… Power to generator (kJ/s)

V ……..Volume of a control volume (m^3)

ρ ……Density of a working fluid (kg/m^3)

e…….. Specific energy of the control volume (kJ/kg)

The quasi-steady assumption, for each time step, sets the mass flow rate at the turbine inlet and outlet equal to each other [52]. For steady-state operation, there is no need to exert any power to change dynamics of the shaft; the shaft power, $\dot{W}_s$, is negligible. Therefore, $\dot{E}_{gen}$in the equation 5.18 can be represented as simple as below.

$$\dot{E}_{gen} = \dot{E}_{in} - \dot{E}_{out} = \dot{m}_{st}\varepsilon_{isen}(h_{in} - h_{out}) \quad (5.19)$$

Where:

ε_{isen} ……Isentropic efficiency

$\dot{m}_{st}$……...Steam mass flow rate (kg/s)

h_{in}, h_{out} ……..Specific enthalpy at turbine inlet and outlet (kJ/kg)

5.2 Utility-scale Model

Table 4 compares the CCPP specifications of the utility and UC Irvine models. The basic principles behind a utility model are the same as those behind the UC Irvine model. However, there have been a few changes in plant configuration and its components' designs.

Table 4: Model Specifications comparison between the utility and UC Irvine models

Utility		**UC Irvine**
2 x 1	Plant configuration (GT x ST)	1 x 1
615 MW	Plant capacity	19.1 MW
190 MW	GT power output	13.5 MW
235 MW	ST power output	5.6 MW
600 kg/s	GT nominal mass flow	50.55 kg/s
200 kg/s*	HRSG steam capacity	16.38 kg/s
3PRH**	ST configuration	Single-Pressure
228.8 kg/s	ST nominal steam flow	10.34 kg/s

*For the utility specifications, HRSG capacity is for one unit of HRSG.

** Three-Pressure with Reheat

For scope of this study, the utility power plant is modeled after General Electric's combined-cycle product, composed of two 7F.04 gas turbines and one STF-D650 steam turbine with total power output up to 615MW.

5.2.1 Gas Turbine Model

The utility gas turbine model used in this study is adapted from the model developed by a former student, Dustin McLarty (now Assistant Professor at Washington State University) [47]. Because Professor McLarty's model utilizes normalized values of pressure and rpm to locate operating points in general compressor and turbine maps that are characteristic of axial turbo-machinery, the nominal power output of the UC Irvine campus CCPP model has simply been scaled up from 14.25 MW to 197.8 MW. At the same time, the nominal mass flow rate of the gas turbine system has been increased significantly from 50.55 kg/s to 593.5 kg/s; the pressure ratio of the system has been increased from 6.2:1 to 16.7:1. In consequence of these changes, the outlet temperature at the gas turbine exhaust has changed from approximately 540 ℃ to 620 ℃ when operated at the turbine's nominal operating conditions.

5.2.2 Heat Recovery Steam Generator Model

Although the utility HRSG model is based on the same assumptions and governing equations used for the UC Irvine model in Section 5.1.2, three main modifications have to be made in order to build a larger and more sophisticated HRSGs that support a larger steam turbine. First of all, a reheating feature is incorporated into the model. The locations of reheating pipes are located in front of superheater tubes. Figure 5 presents configuration of such HRSG in details. Second, changes in tube arrangements and alignments are required to enhance heat exchange for steam of better quality and more quantity. Such changes have been made based on the work of Pearson et al. on "measurement of damaging thermal transidents in F-class horizontal HRSGs" [53]. In comparison to the UC Irvine model, the utility HRSG model has utilized the staggered tube arrangements as well while transverse and longitudinal pitch lengths are adjusted; the length of the

pipes and number of pipes have increased significantly. Last, the UC Irvine campus model has been scaled up in its size and steam-producing capacity for development of HRSG system. The maximum steam production capacity is determined using Steam System Modeler Tool (SSMT), developed by the Department of Energy (DOE). Known design parameters of General Electric's steam turbine STF-D650 such as inlet and outlet steam properties are plugged into the SSMT to find the amount of steam mass flow that matches STF-D650's power output for CCPP application. In consequence, the output steam properties have changed to temperature of 560℃, pressure of 175 bar and mass flow rate of 107 kg/s.

5.2.3 Steam Turbine Model

The utility steam turbine model is based on the same assumption and governing equations used for the UC Irvine steam turbine model in Section 5.1.3. For a larger steam turbine with higher power output and efficiency, the steam turbine is often designed as a set of dual or three-pressure turbines with reheating pipes in-between. Because the UC Irvine steam turbine model is modeled after a single-pressure turbine with a relatively small power capacity, there is no need to include such a complex feature. However, the utility steam turbine model follows the design of GE's STF-D650, a three-pressure turbine with reheaters in-between turbines; STF-D650 steam mass balance has to be modified to keep this complex system under control.

5.2.4 Controllers

Both of the combined-cycle models introduced in this thesis employ two main controllers: one for the GT and the other for the bottoming cycle (HRSG and ST). For the UC Irvine model, its

bottoming cycle is mainly controlled by proportional frequency controller and integral power controller. It is built based on the controller proposed in Ordys [54]. Figure 18 presents the block diagram excerpt from Ordys [54]. In this controller, throttle and bypass valve positions are controlled using difference between design and actual frequency and between design and actual delivered power based on steam pressure at the turbine inlet. The controller employs a feedback control scheme with proportional-integral (PI) control for the frequency difference and integral (I) control for the power difference.

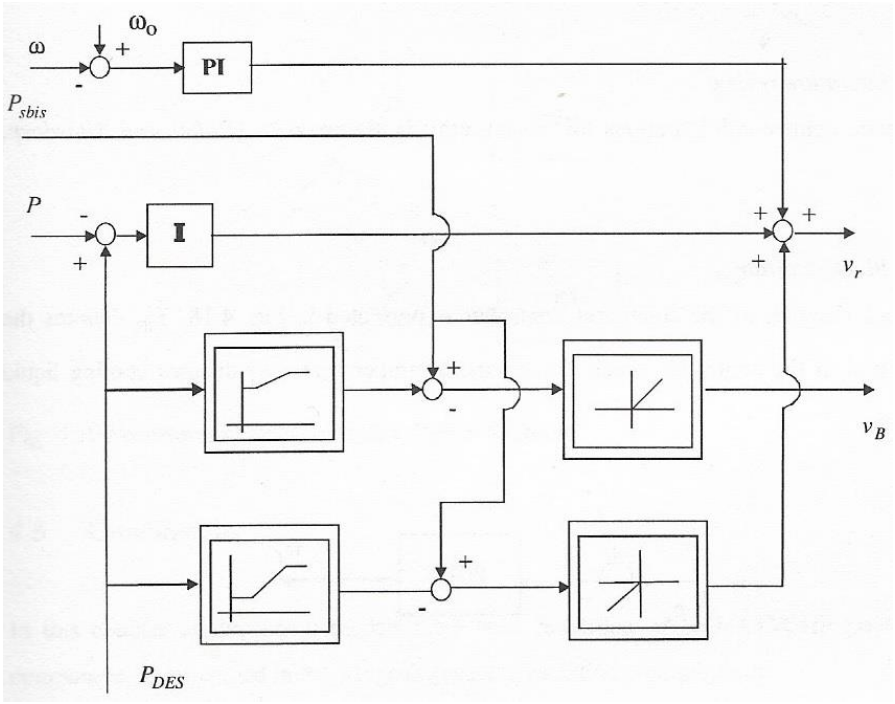

Figure 18: Block diagram for steam turbine control system, excerpted from [54]

Where:

P……..…….....Delivered mechanical power

ω……...Electrical frequency

P_{sbis}……Steam pressure at the inlet

P_{DES}…….….Designed power output

v_r…….……..Throttle valve position

v_B……...……Bypass valve position

The difference between the proposed design and the actual controller is the controller output. The proposed design outputs throttle and bypass valve positions with inputs of electrical frequency error (ω), delivered power error, and steam pressure at the turbine inlet. However, the actual controller outputs a mass flow rate for the steam turbine with inputs of normalized RPM error, normalized power error, and a mass flow rate set point designated to the turbine's nominal operating condition. Although these two controlling schemes may seem different, they are essentially controlling the same variables because the valve positions are the dimensionless measure for the steam mass flow rate.

For the utility model, its bottoming-cycle controller follows the same controlling principles as those used in the UCI model. Figure 65 and Figure 66 in Appendix C demonstrate SIMULINK diagrams of the utility model control system. The controller is composed of a proportional frequency controller, shown in Figure 65, and an integral power controller, shown in Figure 66. The utility model controller employs a cascade control scheme; a normalized RPM error is used as an initial input to the first control loop and normalized error between the power demand and the power, out of the first control loop, is used as an input to the second loop, to ultimately control the steam mass flow rate into the turbine.

Although the utility bottoming-cycle controller utilizes the same types of variables from the UC Irvine counterpart, the utility controller uses a different control scheme from the UC Irvine one. For the UCI bottoming cycle, because the steam turbine is modeled as a single-pressure turbine fed directly from HRSG, its load control is dependent on the steam mass flow rate rather than the steam properties. However, for the utility bottoming cycle, because the steam turbine is modeled

as a three-pressure turbine with reheaters, steam pressure can affect load control in several different parts of the system that it has to be managed more carefully. To do so, the steam pressure is treated as a controlled variable along with the steam mass flow rate; the cascade control scheme is chosen over the simple control scheme not only to avoid any occurrence of algebraic loops that might hinder MATLAB calculation but also to better accommodate the increase in the number of the controlled variables.

5.3 Simulation Scenarios

5.3.1 Future Utility Grid Network Scenario Generation

The tentative scenarios for operation of the combined-cycle power plants in response to higher renewable penetration are generated by HiGRID tool. The developed utility combined-cycle model is to be used to simulate the scenarios for future operation of load-followers in California grid. Because the utility model and Californian grid do not have a matching power capacity, simply inputting the HiGRID-generated load-follower scenarios into the model will not be appropriate for analysis. To resolve the difference, the scenarios are to be normalized with the grid load-follower capacity; the normalization is expected to maintain both validity and dynamicity of the projected load profiles for Californian grid. For scope of this study, three different renewable penetration scenarios are employed. Each of the scenarios is generated to reflect California's future RPS targets: 33% by 2020, 50% by 2030, and 80% by 2050. The specific modeling methodology that HiGRID tool uses to produce future grid projection is shared in details in Eichman et al. [45], [46].

6 RESULTS

6.1 UC Irvine Simulation

6.1.1 Model Verification

Figures 19-22 compare the UC Irvine central plant operation to the simulation results of the UC Irvine models. The red lines represent the operation while the blue lines represent the simulation results. Both GT and ST power outputs match with very high accuracy. In Appendix A, the operation and simulation results are presented separately for every UC Irvine GT and ST operation and simulation from Figure 36 to Figure 43; day-long snapshots for each of the four simulations are shared from Figure 44 to Figure 47.

Figure 19 and Figure 20 are the comparisons for a summer week (August, 2014); Figure 19 shows power output comparison for UC Irvine GT and Figure 20 for ST. Because GT is the primary power generating unit for the campus grid, the GT power output graph demonstrates a weekly pattern very well. The power demand is high during the weekdays (Day 0-3 and 6-7) and work hours while the demand is low during the weekends (Day 4-5) and the non-work hours.

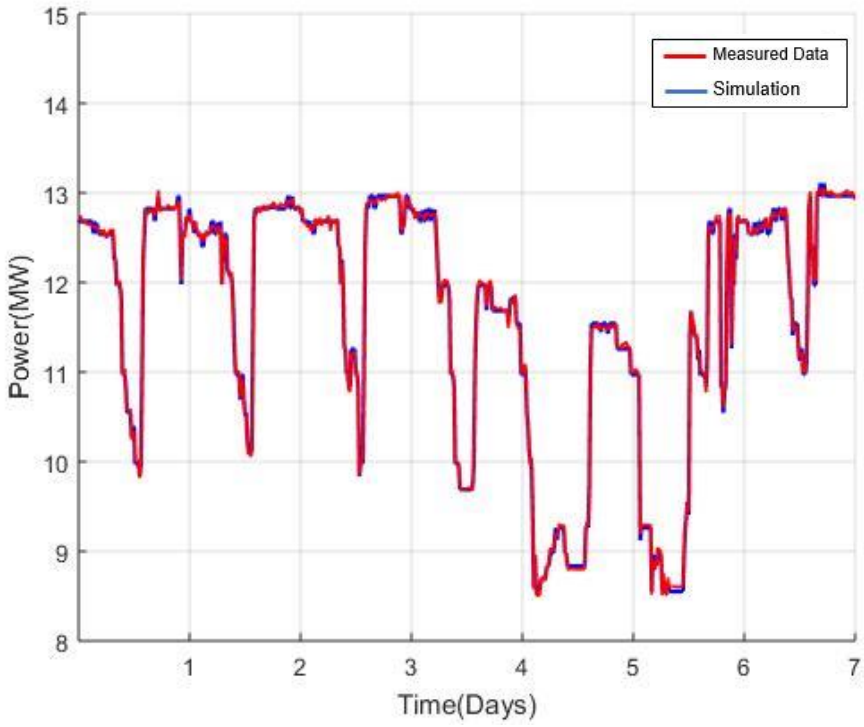

Figure 19: Comparison of UCI GT operation and model simulation in summer.

Due to the nature of the UC Irvine grid and design of the central plant, the steam turbine only uses excess steam for power generation after satisfying hot water and heat demand. Thus, it already tends to operate in very low part-load condition (less than 50%) and experience intermittent shutdowns. Figure 20 demonstrates such characteristics very well. Although the steam turbine is rated at 5438 kW, its actual operation stays at 1-1.5 MW level for most of the times even in the summer when the power demand is higher. For the chosen time frame, the steam turbine has experienced shutdowns twice: once in the beginning of Day 1 and once in-between Day 3 and 4.

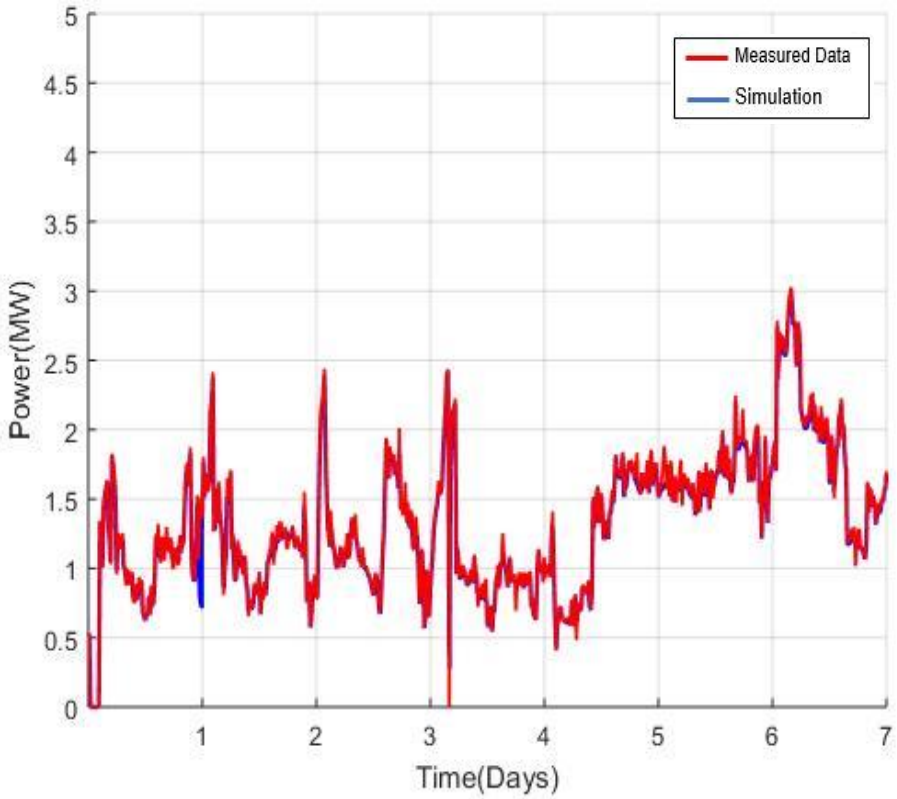

Figure 20: Comparison of UCI ST operation and model simulation in summer.

When zero is inputted as power demand to model a shutdown, the model not only generates a huge peak after the zero that deviates from the GT's operational data but also requires more and more time to stabilize as shutdowns are repeated. In order to avoid these issues and any systematic errors in the modeling regime, the shutdowns are modeled as 0.0001 MW instead of 0 MW.

Figure 21 and Figure 22 are the comparisons for a winter week (January, 2014); Figure 21 shows power output comparison for UC Irvine GT and Figure 22 for ST. Although the daily load profile in winter looks different from that of the summer, the winter shares the same weekly (high during the weekdays and low during the weekends) and daily pattern (high during the work hours and low during the non-work hours) with the summer. Unlike the flat daily load pattern of the summer, the

winter daily load demonstrates sharper profiles. The need for more lighting and electric heating may account for these sharper profiles in the load.

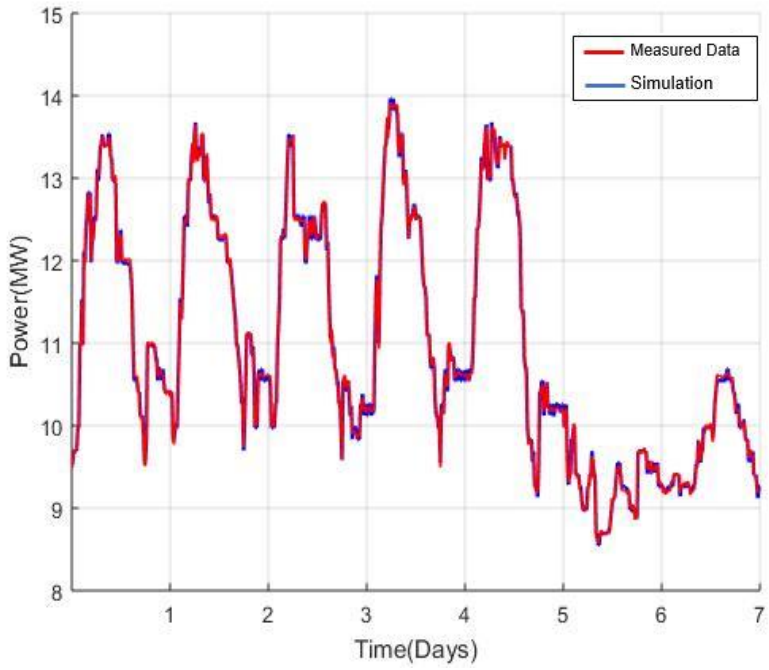

Figure 21: Comparison of UCI GT operation and model simulation in winter.

In the winter, the steam turbine is still operating in part-load condition. However, because most of the steam produced by the HRSG is used to fulfill heat and hot water demand of the campus in the winter, the amount of power generated by the steam turbine in the winter is much less than that in the summer.

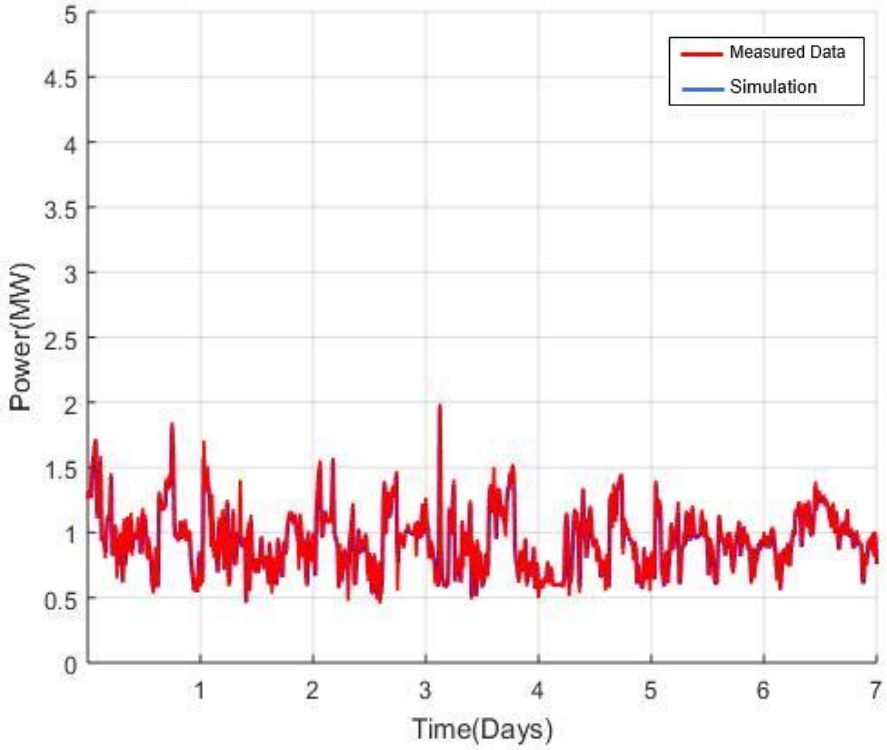

Figure 22: Comparison of UCI ST operation and model simulation in winter.

Composed of three subparts of GT, HRSG and ST, the developed UC Irvine model takes approximately a minute to initialize all parameters to design conditions. Depending on dynamicity of inputs, simulation time may vary; for the week-long simulations like the above, the model takes less than a minute to complete all the required calculations.

6.1.2 Dynamic Operation Scenario for UC Irvine model

As shown in the demand load profiles in Section 3.3.2, GT is the predominant power generator while ST operates as an auxiliary unit within the campus central plant. Thus, for simulation scenario for the campus model, the focus is on dynamic operation of the GT. In the approximately three-hour scenario, shown in Figure 23, the demand load profile changes from GT's full load

capacity down to its lowest possible operation point (~42% of the full) and back to the full. Though a simple scenario, this set of ramping-down and up is the most dynamic set of changes that the UC Irvine GT would experience.

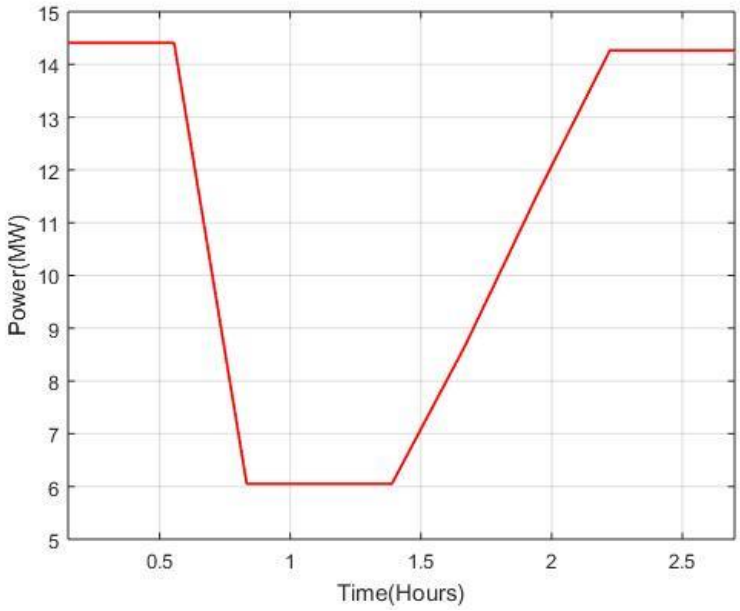

Figure 23: The tentative scenario for UC Irvine GT simulation

Specifically, the 42% (≈ 6MW) is the lowest possible operation point in order to meet criteria pollutant (e.g., nitrogen oxides, carbon monoxide) emissions compliance as dictated by the South Coast Air Quality Management District (SCAQMD). In order to meet the step-like demand load in Figure 23, GT has to ramp down from its full load of 14.25 MW at a rate of 495 kW/min and ramp back up from 6 MW to 14.25 MW at a rate of 166 kw/min.

6.1.3 Simulation with UC Irvine model

The UC Irvine CCPP model had been validated with the seasonal sets of past operational data in Section 6.1.1. The verified model simulated the dynamic operation scenario, presented in Section 6.1.2. Figure 24 demonstrates the whole period of simulation while Figure 25 only shows a snapshot of the period during which the discrepancy between the tentative load profile and simulation result occurs.

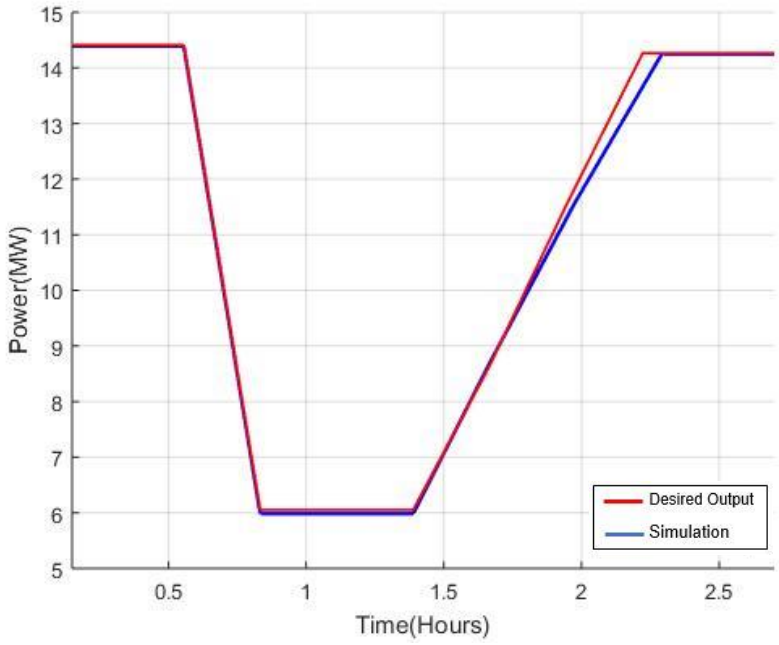

Figure 24: UC Irvine GT simulation result

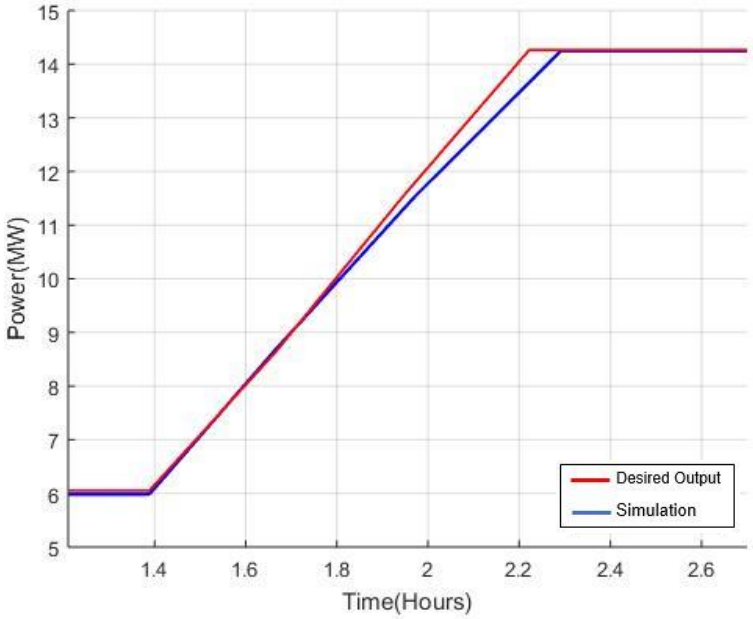

Figure 25: Close-up snapshot of Figure 24

The discrepancy between the scenario and simulation result became more conspicuous beginning at the simulation time of 1.71. As mentioned in Section 6.1.2, GT had to ramp up at a rate of 166 kW/min in order to perfectly meet the load scenario. However, the simulation result demonstrated the ramping-up rate of only 153 kW/min, resulting in the discrepancy shown in Figure 25.

6.2 Utility Model Simulation

6.2.1 Model Verification

The reference power input was put into each component of the utility combined-cycle model to verify performance of the models. The reference input is composed of two sets of positive and negative steps; the larger set of steps consists of 80MW increase and decrease while the smaller consists of 50MW of both. The reference simulation is for a 24-hour timeframe, and each ramping

up-and-down is designed to occur in approximately 15 minutes, 900 seconds. Figure 26 and Figure 27 demonstrate performance verification for the utility GT and ST models using the reference input. The more detailed figures are included in Appendix B**: Utility S**.

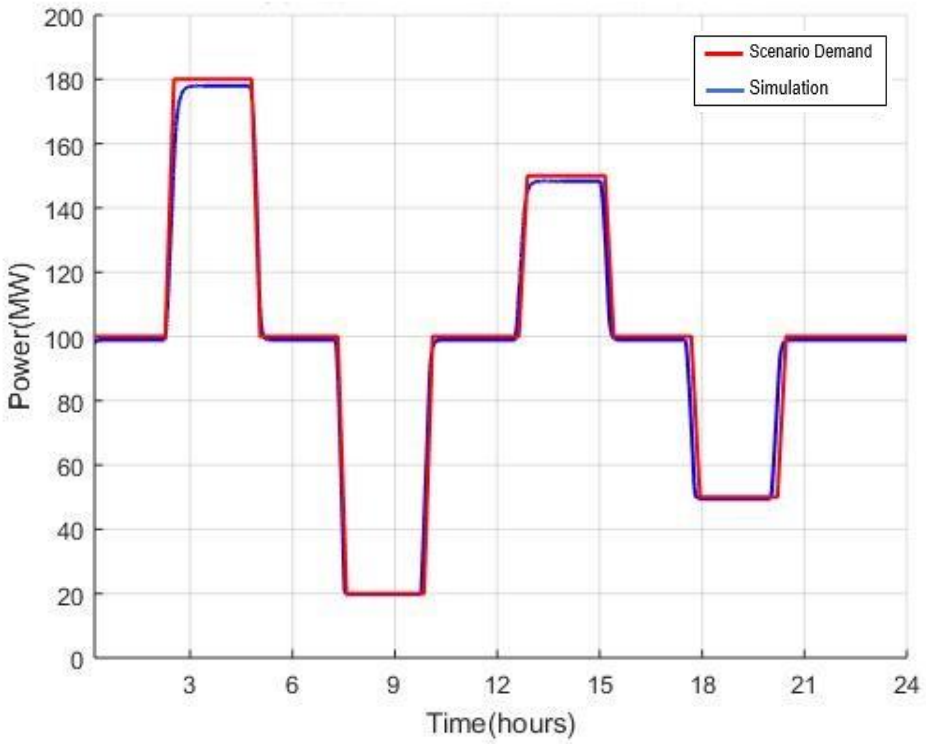

Figure 26: Utility GT model validation

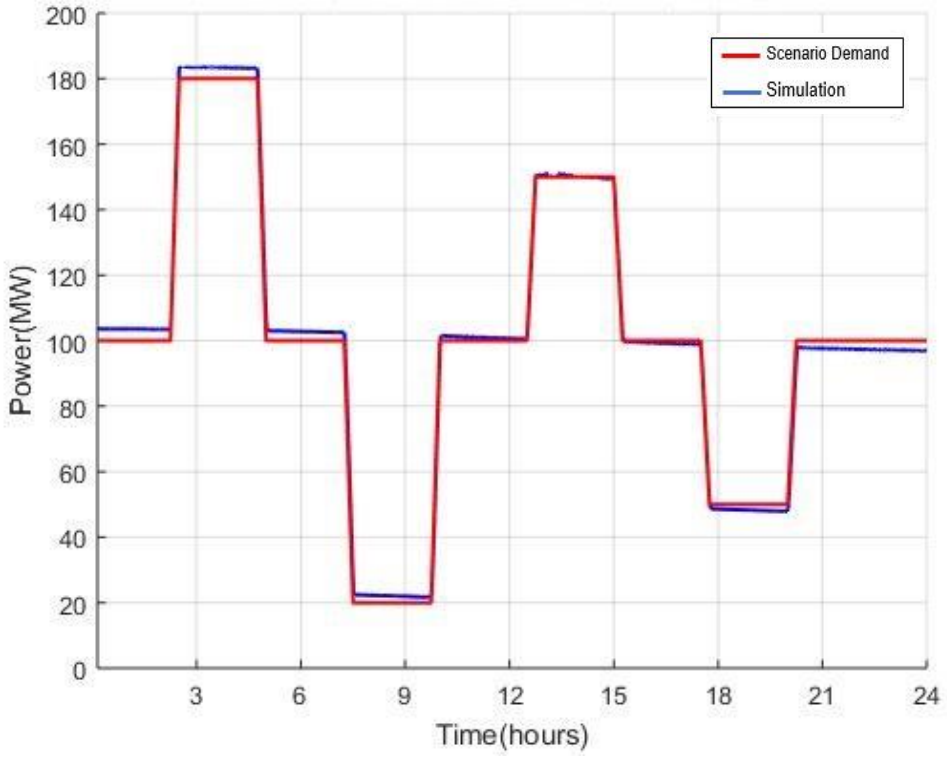

Figure 27: Utility ST model validation

6.2.2 Generated Future Scenarios

Figure 28-30 demonstrate the load breakdown plots for California grid with different renewable penetration, 33%, 50%, and 80% respectively. For all the plots, marked in orange is the power generated by load-followers in the grid. These scenarios were generated by HiGRID tool. From 33% to 50% scenario, actual grid penetration of renewables has simply been increased to meet the requirements. However, 80% target cannot be achieved without implementing energy storage; for scope of this study, the 80% scenario is essentially 80% potential renewable penetration with actual renewable penetration of 72.5%. In addition, the renewable penetration values in the HiGRID generated scenarios (from Figure 28 to Figure 30) are calculated including power generated by hydroelectric facilities as renewable.

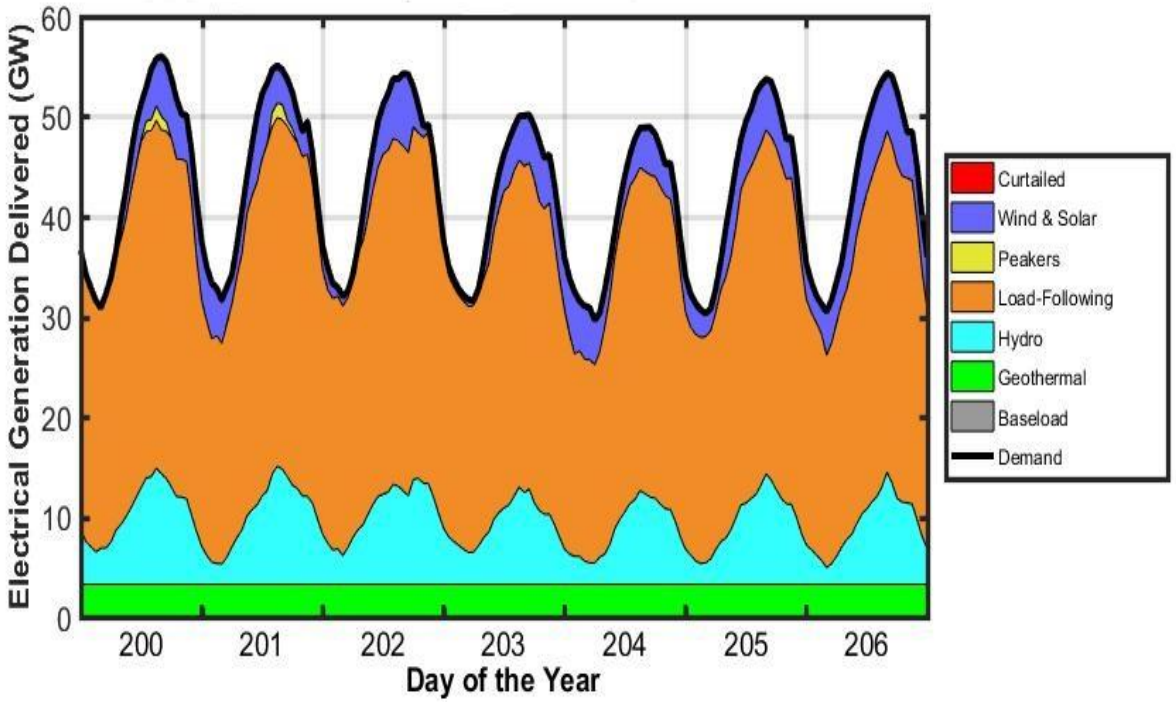

Figure 28: Energy portfolio with 33% renewable penetration into California grid

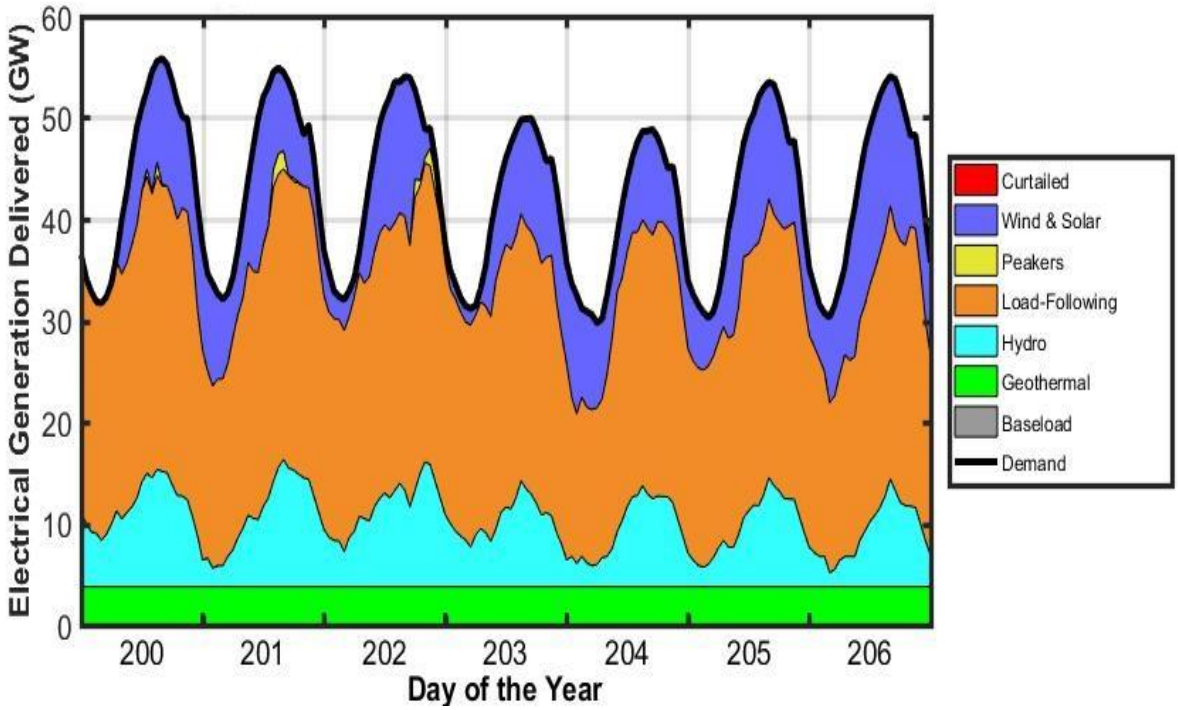

Figure 29: Energy portfolio with 50% renewable penetration into California grid

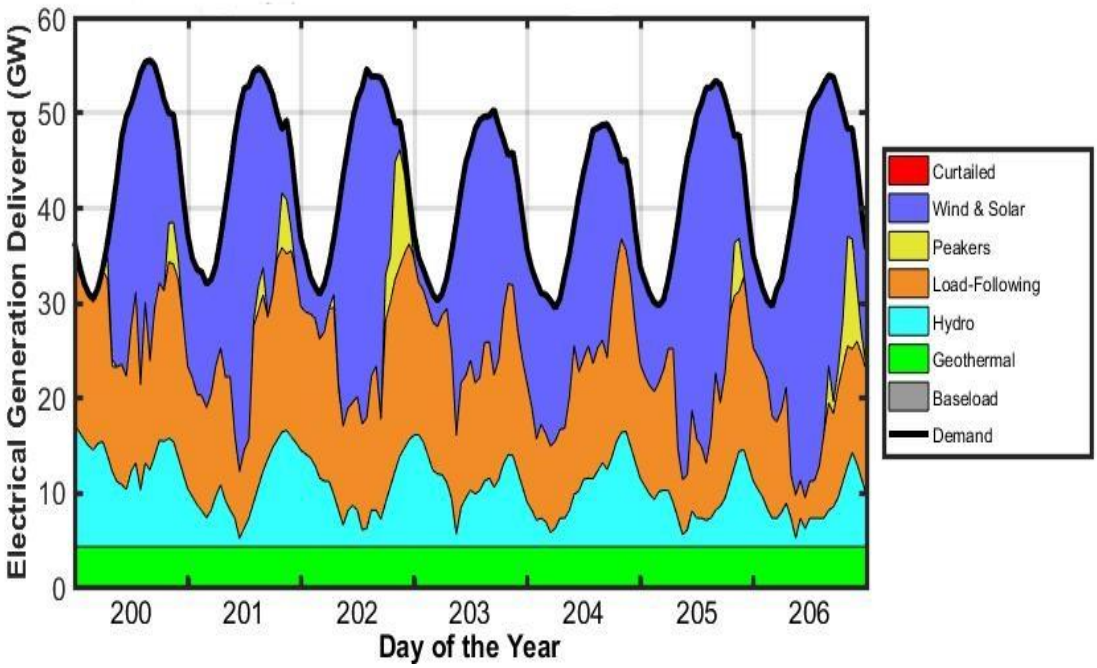

Figure 30: Energy portfolio with 80% renewable penetration into California grid

The hydroelectric facilities are distinguished into two categories: large and small hydro. This distinction is based on the capacity of a facility. If the capacity of a facility is larger than 30 MW, the facility is considered a large hydro. If the capacity of a facility is smaller than 30 MW, the facility is considered a small hydro. In the state of California, only small hydros qualify as renewable under the Renewables Portfolio Standard [55].

6.2.3 Simulation of the Scenarios

Shown in Figure 31 are the three HiGRID-generated load-follower profiles for a 365-day period. As the renewable penetration increases from 33% to 50% to 80%, the average capacity factor over the year has decreased from 53% to 39% to 17%. At the same time, the maximum capacity of the CCPP needed in California grid to meet the load-follower demand profile has decreased from 40

GW to 35 GW to 25 GW. On the other hand, for the same increase in the renewable penetration, the maximum up and down ramp rates have increased. For the 33 % scenario, the maximum ramp-up rate is 13% and maximum ramp-down rate is 11%; for the 50% scenario, 24% and 14%; for the 80% scenario, 29% and 28%.

In order to analyze the dynamics for a fleet of a CCPP in details, a seven-day period (from day 200 to day 206) was extracted from each scenario, normalized and inputted into the utility combined-cycle model for simulation. The load-follower contribution to the grid electricity mix had to be normalized not only to capture the grid dynamics but also to study the grid dynamics in terms of operation of the complementary technology. The CCPP model simulation results of normalized 33%, 50%, and 80% scenarios are respectively demonstrated in Figure 30-32; all of the simulation results of the GT and ST models for the three scenarios are separately shown in Figure 51-56 in Appendix B.

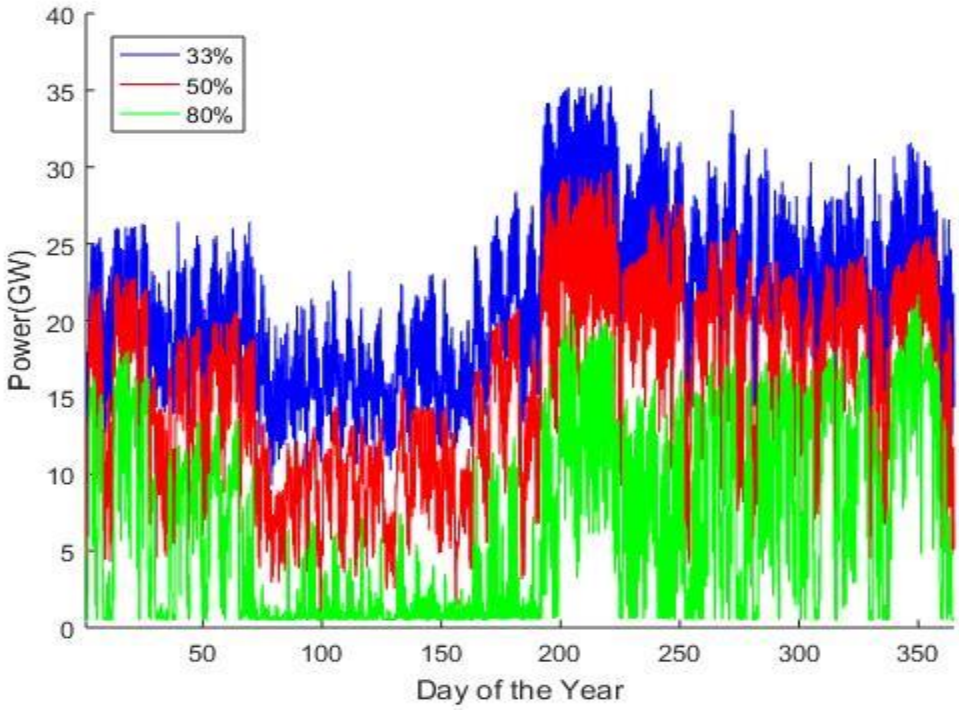

Figure 31: Comparison of load-follower contribution for the three scenarios

As grid penetration of renewables increases, load profiles for load-followers become more dynamic. In the 33% penetration scenario as shown in Figure 32, the load profile for load-followers, combined-cycle power plants in this case, is simply diurnal: high during days and low during nights. Although there is a slight variation in the actual day-to-day operation, the regular diurnal pattern does not go through any dramatic change.

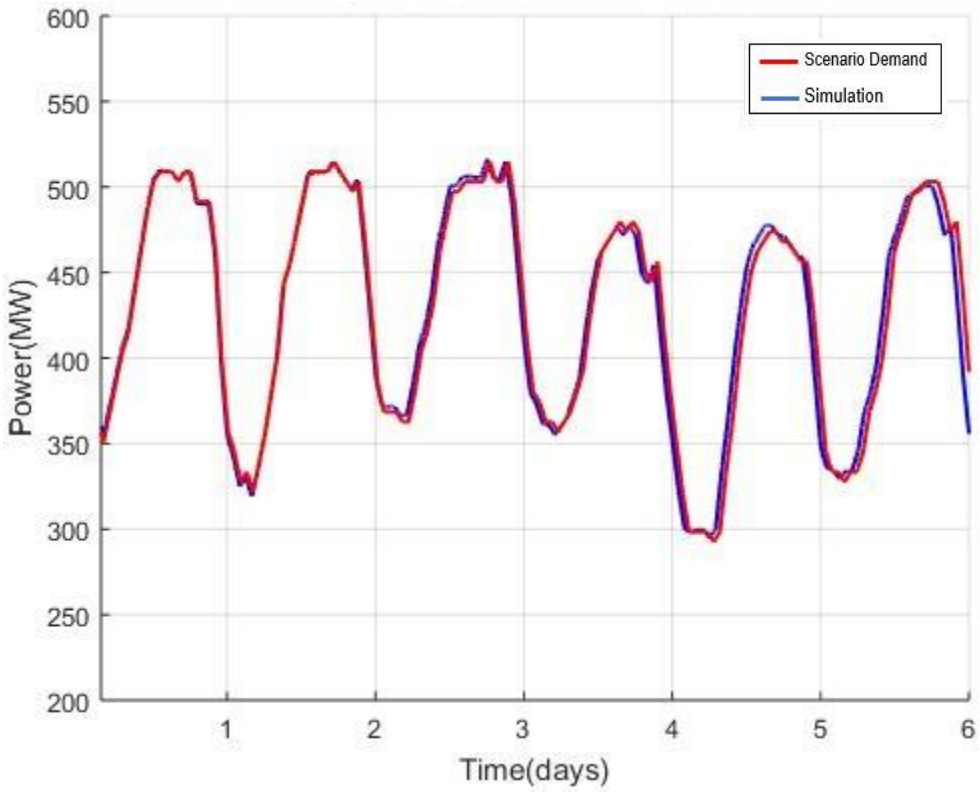

Figure 32: CCPP model simulation for 33% renewable penetration scenario

In the 50% penetration scenario, the diurnal pattern from the 33% scenario still exists; however, as shown in Figure 33, day-to-day operation varies much more. Specifically, the daily load curve has become less smooth in the 50% scenario due to an increase in the number of sharp peaks and larger discrepancy in the daily demand. Such changes in the operational load profile can be accounted for the conspicuous increase of renewables, mainly solar and wind, penetration to the grid.

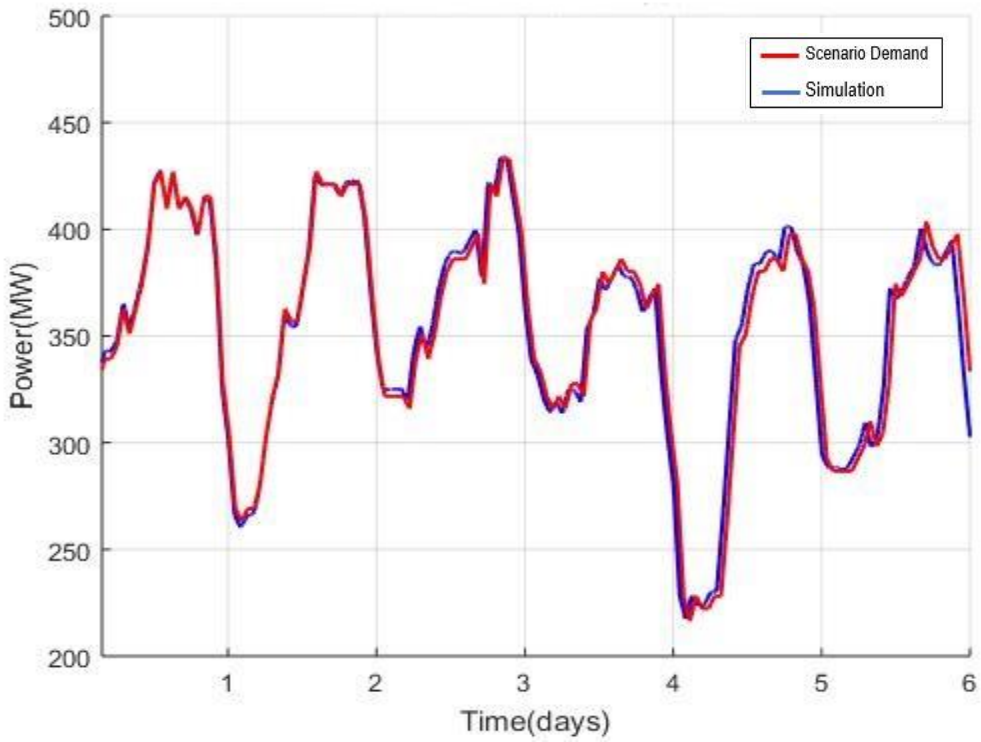

Figure 33: CCPP model simulation for 50% renewable penetration scenario

In the 80% penetration scenario, as shown in Figure 34, the load profile does not demonstrate any specific pattern. That is because, along with the dramatic increase in solar and wind penetration, the load-followers mainly operate to complement these resources with highly variable availability.

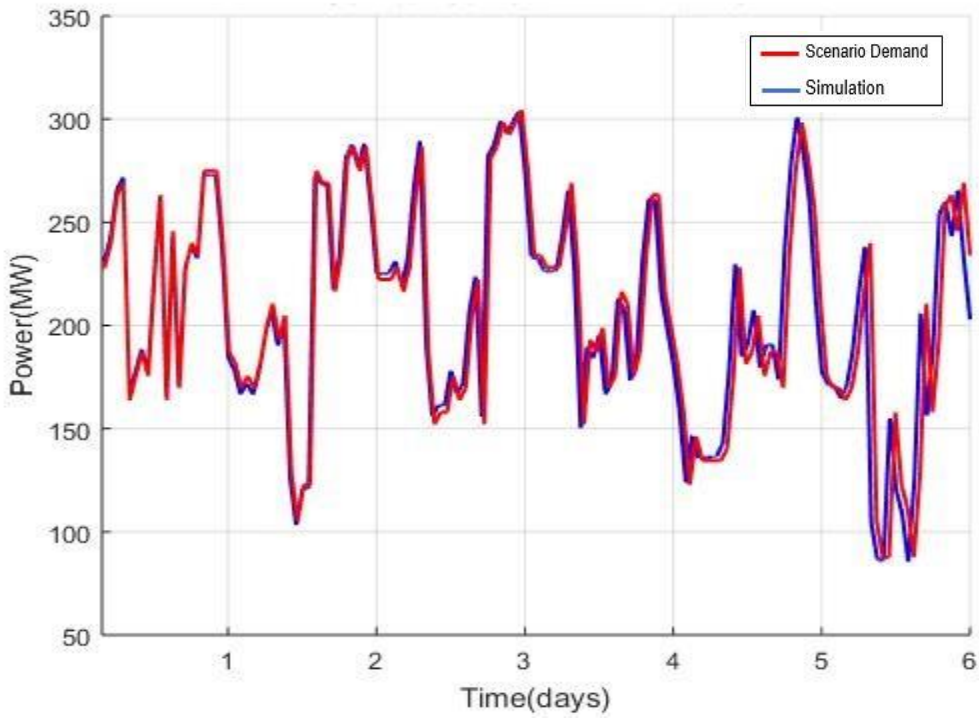

Figure 34: CCPP model simulation for 80% renewable penetration scenario

For the given simulation time period (between day 200 and day 206), Figure 35 demonstrates the changes in the combined-cycle power plant's average thermal efficiency, estimated by the model. It has been previously shown that as the grid penetration of renewables increases, the combined-cycle power plant has to be operated in a more dynamic manner and in a lower part-load condition.

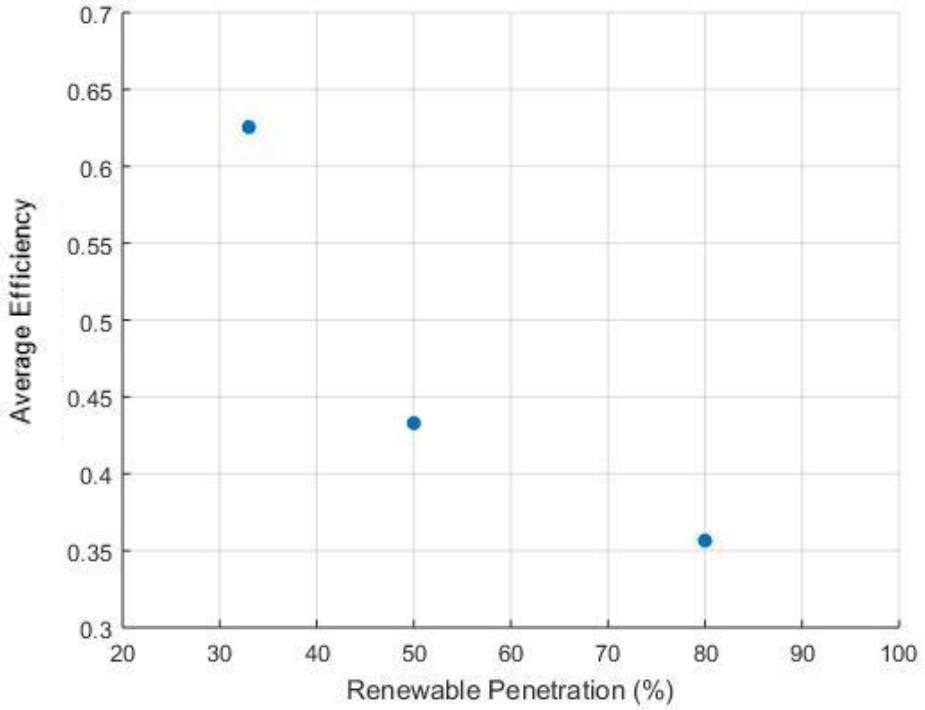

Figure 35: Graph of average efficiency vs. renewable penetration for the simulation period

Due to lower part-load operation, the model's average efficiency decreases from 63% to 44% and to 36% as the renewable penetration increases from 33% to 50% and to 80%. Despite the compromise in efficiency, the comparison between the simulation results and operation data in Figure 32, Figure *33*, and Figure *34* demonstrates that reliability of power generation and supply process to the associated grid is well-maintained.

7 SUMMARY AND CONCLUSIONS

In this thesis, operational dynamics of combined-cycle power plant technology were studied through a physical modeling approach in the MATLAB/SIMULINK environment. The models were developed to simulate: 1) a 19MW UC Irvine central power plant; 2) a 600MW utility-scale power plant. The UC Irvine model was verified with past data from the campus central plant while the utility model was verified with a dynamic set of data associated with a series of fast ramping ups and downs.

Three scenarios with different values of renewable penetration were generated using the HiGRID tool. The renewable penetration percentages were set according to the original California RPS targets of 33%, 50% and 80%. For the scope of this study, load-follower power plant contributions to the general load profile for a week-long period were extracted from each scenario and inputted as demand load profiles into the models for simulation.

From this research, several conclusions have been made. Each major conclusion is followed by a brief descriptive paragraph:

1. *Natural gas combined-cycle power plant technology is technically capable of serving as a dynamic load-following power plant for associated grids with increasing levels of renewable penetration.*

   Natural gas combined-cycle power plant technology is known to have advantages in dynamic operation over other conventional power generation technologies such as nuclear and coal-fired power plants. In this thesis, the natural gas combined-cycle power plant technology was selected and simulated for producing electricity to meet all of the load-follower portions of

demand for three scenarios with increasing renewable penetration from 33% to 50% and to 80%. Although the load profile that the model had to simulate became more irregular and highly dynamic, the figures comparing the simulation results and demand load profiles demonstrated not only the matching dynamics but also the reliable power output status that such power plants can technically achieve. A major caveat is associated with the emissions control equipment used for catalytic reduction of nitrogen oxides and oxidation of carbon monoxide, which is known for the UCI central power plant to limit emissions-compliant performance to about 50% part-load. The dynamics of the selective catalytic reduction emissions control equipment were outside the scope of this effort.

2. *A significant decrease in fuel-to-electricity conversion efficiency of these power plants results from dynamic operation in response to high renewable penetration.*

   The utility natural gas combined-cycle power plant model simulated three scenarios with different renewable grid penetration percentages for a week-long period. The simulation results demonstrated that maximum efficiency within the given time period decreased with increasing renewable penetration. For the given week-long period, the 33% simulation demonstrated average efficiency of approximately 63%; the 50% simulation approximately 44%; the 80% simulation approximately 36%.

3. *Higher grid penetration of renewables and longer periods of simulation require implementation of different controlling schemes to improve modeling capability.*

The figures comparing the simulation results and demand load profiles for the three different scenarios demonstrated several interesting patterns. As the renewable penetration increased, the discrepancy between each scenario's load profile and simulation result appeared to be more pronounced. The overarching pattern for all scenarios, however, was that as the time progressed, the discrepancy became more noticeable. Although there had been difference in degree that the discrepancy between the load profile and simulation result appears in each scenario's simulation plot, the discrepancy followed a specific pattern: an underestimated peak preceded by an overestimated peak and vice versa. The discrepancy was not large enough to impact the grid reliability within the scope of this thesis; however, for future studies with longer periods of simulation and higher grid penetration of renewables, implementation of more sophisticated controlling schemes would be recommended.

8 RECOMMENDATIONS

The results presented above motivate the need for further work in dynamic simulation of the combined-cycle power plant technology. The modeling efforts presented in this work focused on simulating the CCPP power outputs, thus developing matching profiles for the given demand load profiles. However, due to adoption of emissions control measures, the operation of fossil fuel plants is to be optimized rather based on emissions than based on power outputs. The follow-on work should consider how the emissions control equipment could be operated over a larger dynamic operating range as renewable penetration is increased. This will require the development of a dynamic selective catalytic reduction (SCR) model that incorporates a chemical reaction converting NO_x into nitrogen, water and carbon dioxide using ammonia.

In addition, the current work focused on the dynamic operation of the CCPP as the load-follower in California grid. Because renewable resources are spatially and temporally variable, this work could be extended to various regions around the nation and the world with different climatic characteristics and renewable policies.

Another possibility for further work in terms of physical modeling is to develop a model for a system that can substitute the NGCC's role as a load-follower within the utility grid. With the increase in renewable penetration requirement, these fossil fuel-based facilities will gradually lose their standings. In preparation for the future, further research in the substituting power plant technology is required. One possible option is a utility scale power plant utilizing a fuel cell-gas turbine (FC/GT) hybrid system that is known to achieve ultra-high efficiency of approximately 75%. The follow-on work should consider developing a model for this system in utility scale and evaluating its dynamic operability as a load-follower to substitute NGCC in the utility grid.

9 REFERENCES

[1] Guo, Zhan, Ning Ai, and Karen R. Polenske. 2008. "Evaluating environmental and economic benefits of yellow dust storm-related policies in north China." *International Journal of Sustainable Development & World Ecology* 457-70.

[2] Miri, Abbas, Hasan Ahmadi, Mohammad R. Ekhtesasi, Naser Panjehkeh, and Ahmad Ghanbari. 2009. "Environmental and socio-economic impacts of dust storms in Sistan Region, Iran." *International Journal of Environmental Studies* 343-55.

[3] Liu, Yongbo, and Yaning Chen. 2006. "Impact of population growth and land-use change on water resources and ecosystems of arid Tarim River Basin in Western China." *International Journal of Sustainable Development & World Ecology 13.4* 295-305.

[4] Deutsche Gesellschaft fur Internationale Zusammenarbeit (GIZ) GmbH. 2012. "Legal Frameworks for Renewable Energy."

[5] Zhous, Ella. 2015. "U.S. Renewable Energy Policy and Industry." National Renewable Energy Laboratory, October.

[6] U.S. Department of Energy, TITLE XVII. Accessed Aug. 14, 2018. https://www.energy.gov/lpo/title-xvii

[7] California Energy Commission. 2018. *California Energy Commission.* Accessed July 2018. http://www.energy.ca.gov/portfolio/.

[8] California legislative Information, Senate Bill No.100. Accessed Feb. 17, 2019. https://leginfo.legislature.ca.gov/faces/billNavClient.xhtml?bill_id=201720180SB100.

[9] McLarty, Dustin, Jack Brouwer, and Scott Samuelsen. 2014. "Fuel cell-gas turbine hybrid system design part I: Steady state performance." *Journal of Power Sources* 412-20.

[10] McLarty, Dustin, Jack Brouwer, and Scott Samuelsen. 2014. "Fuel cell-gas turbine hybrid system design part II: Dynamics and control." *Journal of Power Sources* 412-20.

[11] Maton, Jean-Paul, Li Zhao, and Jacob Brouwer. 2013. "Dynamic modeling of compressed gas energy storage to complement renewalbe wind power intermittency." *International Journal of Hydrogen Energy* 7867-80.

[12] Wiser, Ryan, Dev Millstein, Trieu Mai, Jordan Macknick, Alberta Carpenter, Stuart Cohen, Wesley Cole, Bethany Frew, and Garvin Heath. 2016. "The environmental and public health benefits of achieving high penetrations of solar energy in the United States." *Energy* 472-86.

[13] Gonzalez, Arnau, Jordi-Roger Riba, Antoni Rius, and Rita Puig. 2015. "Optimal sizing of a hybrid grid-connected photovoltaic and wind power system." *Applied Energy* 752-62.

[14] Valverde-Isorna, L., D. Alli, D. Hogg, and M. Abdel-Wahab. 2016. "Modelling the performance of wind-hydrogen energy systems: Case study the Hydrogen Office in Scotland/UK." *Renewable and Sustainable Energy* 1313-32.

[15] Molina, M. G., and E.J. Espejo. 2014. "Modeling and simulation of grid-connected photovoltaic energy conversion systems." *International Journal of Hydrogen Energy* 8702-07.

[16] Prăvălie, R., Cristian Patriche, Georgeta Bandoc. 2019. "Spatial assessment of solar energy potential at global scale. A geographical approach." *Journal of Cleaner Production*, Volume 209. 692-721

[17] Niblick, B., Amy E. Landis. 2016. "Assessing renewable energy potential on United States marginal and contaminated sites." *Renewable and Sustainable Energy Reviews*, Volume 60. 489-497.

[18] Feng, C., Mucun Sun, Mingjian Cui, Erol Kevin Chartan, Bri-Mathias Hodge, Jie Zhang. 2019. "Characterizing forecastability of wind sites in the United States." Renewable Energy, Volume 133. 1352-1365.

[19] Huang, Yu W., Noah Kittner, Daniel M. Kammen. 2019. "ASEAN grid flexibility: Preparedness for grid integration of renewable energy." *Energy Policy*, Volume 128. 711-726.

[20] Sharma, T., P. Balachandra. 2019. "Model based approach for planning dynamic integration of renewable energy in a transitioning electricity system." *International Journal of Electrical Power & Energy Systems*, Volume 105. 642-659.

[21] Alobaid, F., Nicolas Mertens, Ralf Starkloff, Thomas Lanz, Christian Heinze, Bernd Epple. 2017. "Progress in dynamic simulation of thermal power plants." *Progress in Energy and Combustion Science*, Volume 59. 79-162.

[22] Liu, Z., Iftekhar A. Karimi. 2018. "Simulating combined cycle gas turbine power plants in Aspen HYSYS." *Energy Conversion and Management*, Volume 171. 1213-1225.

[23] Liu, Z., Iftekhar A. Karimi. 2018. "New operating strategy for a combined cycle gas turbine power plant." *Energy Conversion and Management*, Volume 171. 1675-1684.

[24] Babrowski, S., Patrick Jochem, Wolf Fichtner. 2016. "How to model the cycling ability of thermal units in power systems." *Energy*, Volume 103. 397-409.

[25] U.S. Department of Energy, the Water-Energy Nexus. n.d. "US-China UC Proposal: Task 4.3 Climate Impacts on Power Plant and Electric Grid Operations in Drought Susceptible Regions of the U.S. and China."

[26] Dev, N., Samsher, Surendra Kachhwaha, Rajesh Attri. 2014. "GTA modeling of combined cycle power plant efficiency analysis." *Ain Shams Engineering Journal*.

[27] Gobbato, P., M. Masi, A. Toffolo, and A. Lazzaretto. 2011. "Numerical simulation of a hydrogen fuelled gas turbine combustor." *International Journal of Hydrogen Energy* 7993-8002.

[28] Ditaranto, M., H. Li, and T. Løvås. 2015. "Concept of hydrogen fired gas turbine cycle with exhaust gas recirculation: Assessment of combustion and emissions performance." *International Journal of Greenhouse Gas Control* 377-383.

[29] Cappelletti, A., and F. Martelli. 2017. "Investigation of a pure hydrogen fueled gas turbine burner." *International Journal of Hydrogen Energy* 10513-10523.

[30] Abed, S., Khir Tahar, Ammar Ben Brahim. 2016. “Thermodynamic and Energy Study of a Regenerator in Gas Turbine Cycle and Optimization of Performances.” *International Journal of Energy Optimization and Engineering*. 5. 25-44. 10.4018/IJEOE.2016040102.

[31] Kim, T. S., Lee, D. K., & Ro, S. T. 2000. “Dynamic behaviour analysis of a heat recovery steam generator during start-up.” *International Journal of Energy Research*, *24*(2), 137–149.

[32] Borgnakke, C., and Richard E. Sonntag. *Fundamentals of Thermodynamics*. , 2017. Print.

[33] Sanpasertp, T. (2011). Energy Procedia n in an Ab w a Series of Intercooler Circuits, *4*, 1676–1682.

[34] General Electric Company. Aug, 2016. *Powering a new record at EDF: 9HA.01 sets efficiency world record.*

[35] Ducker M. The fall of the F-class turbine; 21 August 2015. [Online]. Available: <http://www.power-eng.com/articles/print/volume-119/issue-8/features/the-fall-of-the-f-class-turbine.html>.

[36] Balling, Lothar. 2010. "Flexible future for combined cycle." *Modern Power Systems* 61-65.

[37] He, Gang, and Daniel M. Kammen. 2016. "Where, when and how much solar is available? A provincial-scale solar resource assessment for China." *Renewable Energy* 74-82.

[38] He, Gang, and Daniel M. Kammen. 2014. "Where, when and how much wind is available? A provincial-scale wind resource assessment for China." *Energy Policy* 116-22.

[39] Wang, Meina, Paul Ullrich, and Dev Millstein. 2018. "The future of wind energy in California: Future projections with the Variable-Resolution CESM." *Renewable Energy* 242-257.

[40] Bukhary, Saria, Sajjad Ahmad, and Jacimaria Batista. 2017. "Analyzing land and water requirements for solar deployment in the Southwestern United States." *Renewable and Sustainable Energy Reviews* 3288-3305.

[41] Mikkola, Jani, and Peter D. lund. 2016. "Modeling flexbility and optimal use of existing power plants with large-scale variable renewable power schemes." *Energy* 364-75.

[42] Shafiullah, G. M. 2016. "Hybrid renewable energy integration (HREI) system for subtropical climate in Central Queensland, Austrailia." *Renewable Energy* 1034-53.

[43] Koussa, Djohra saheb, Mustapha Koussa. 2016. "GHGs (greenhouse gases) emission and economic analysis of a GCRES (grid-connected renewable energy system) in the arid region, Algeria." *Energy* 216-230.

[44] Novoa, Laura D. (2016). An Integrated PV/Battery Energy Storage for EV Charging in a Microgrid Topology. Master of Science. University of California, Irvine.

[45] Eichman, J., F. Mueller, B. Tarroja, L.S. Schell, and S. Samuelsen. 2013. "Exploration of the integration of renewable resources into California's electric system using the Holistic Grid Resource Integration and Deployment(HiGRID) tool." *Energy* 353-363.

[46] Eichman, Joshua D. (2013). Energy Management Challenges and Opportunities with Increased Intermittent Renewable Generation on the California Electrical Grid. Ph.D. University of California, Irvine.

[47] McLarty, Dustin F. (2013). Thermodynamic Modeling and Dispatch of Distributed Energy Technologies including Fuel Cell-Gas Turbine Hybrids. Ph.D. University of California, Irvine.

[48] UC Irvine Cogeneration Plant Specifications. Print.

[49] Spakovszky, Z. S..*Thermodynamics and Propulsion*, edited by Douglas Quattrochi, Sept. 2007. Available: <web.mit.edu/16.unified/www/FALL/thermodynamics/notes/node61.html>.

[50] Incropera, Frank P., and David P. DeWitt. 2002. *Fundamentals of heat and mass transfer*. New York: J. Wiley.

[51] Cooke, D. H. (1985). On Prediction of Off-Design Multistage Turbine Pressures by Stodola's Ellipse. *Journal of Engineering for Gas Turbines and Power*.

[52] Kim, T. ., Park, H. ., & Ro, S. (2001). Characteristics of transient operation of a dual-pressure bottoming system for the combined cycle power plant. *Energy*, *26*, 905–918.

[53] Pearson, M., J.Michael Pearson, Robert Anderson. (2005). Measurement of Damaging Thermal Transients in F-Class Horizontal HRSGs. *ETD International Seminar on Cyclic Operation of Heat Recovery Steam Generators*. London, UK.

[54] Ordys, Andrzej W, A.W. Pike, Michael A. Johnson, Reza M. Katebi, and Michael J. Grimble. 1994. *Modelling and Simulation of Power Generation Plants.* London: Springer-Verlag.

[55] California Energy Commission. *Hydroelectric Power in California.* Accessed Feb. 2019. Available: <https://www.energy.ca.gov/hydroelectric/>

10 APPENDICES

Appendix A: UCI Simulation Results

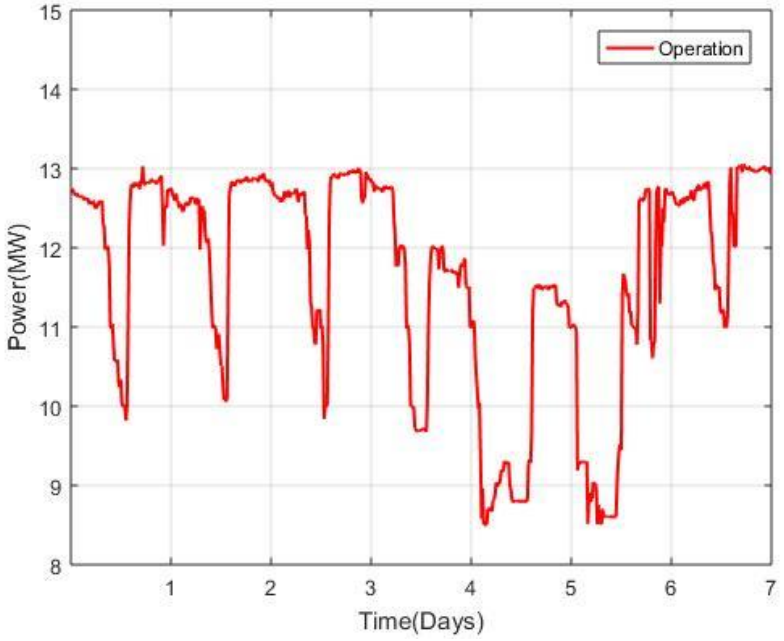

Figure 36: A week-long operation of UCI GT in summer

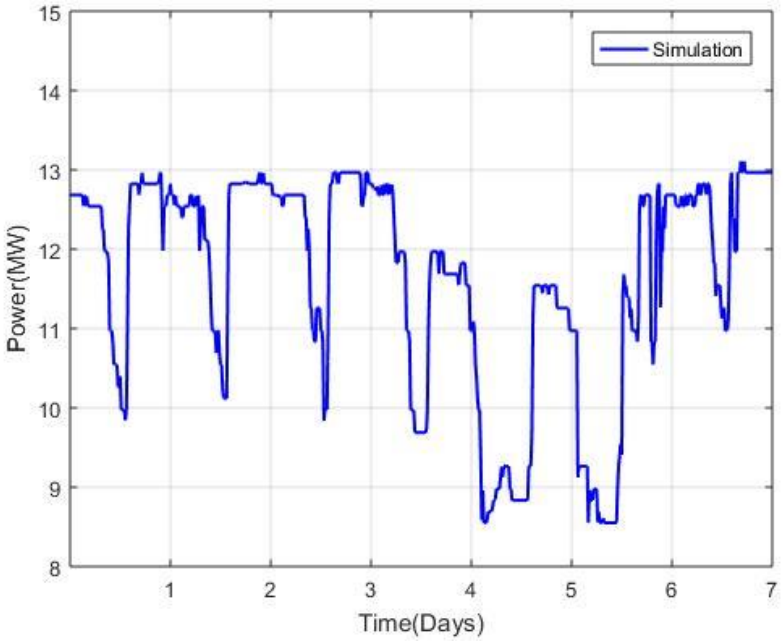

Figure 37: A week-long simulation of UCI GT in summer

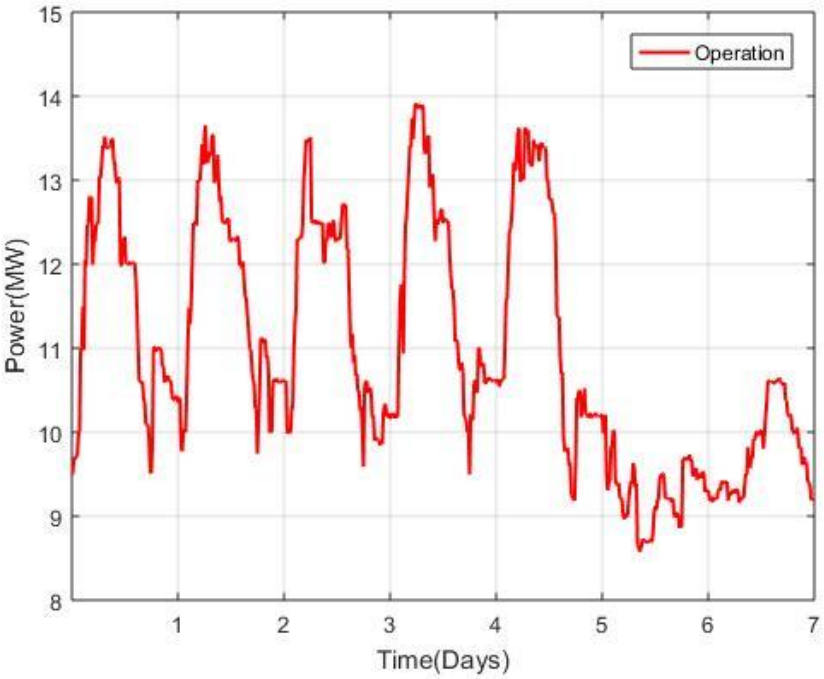

Figure 38: A week-long operation of UCI GT in winter

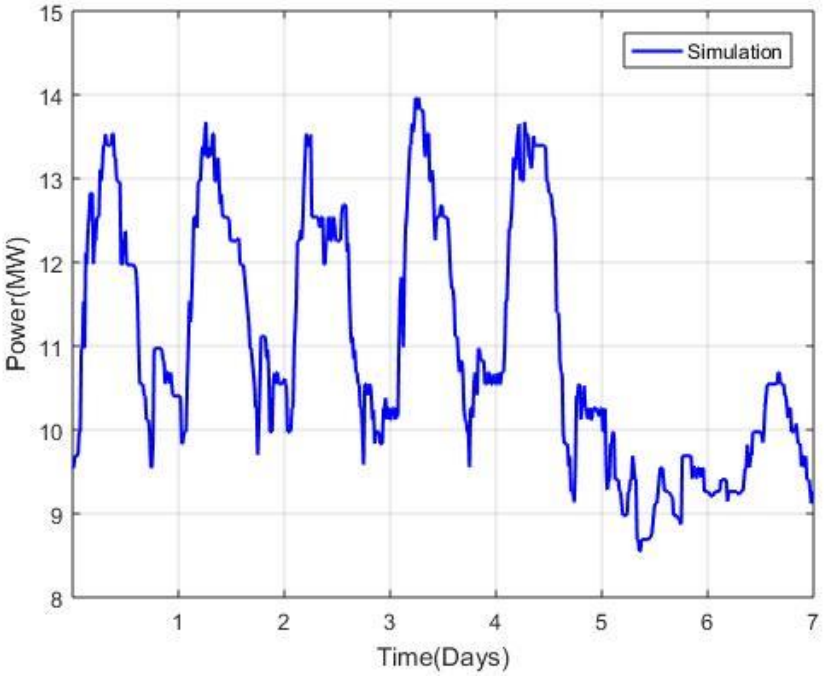

Figure 39: A week-long simulation of UCI GT in winter

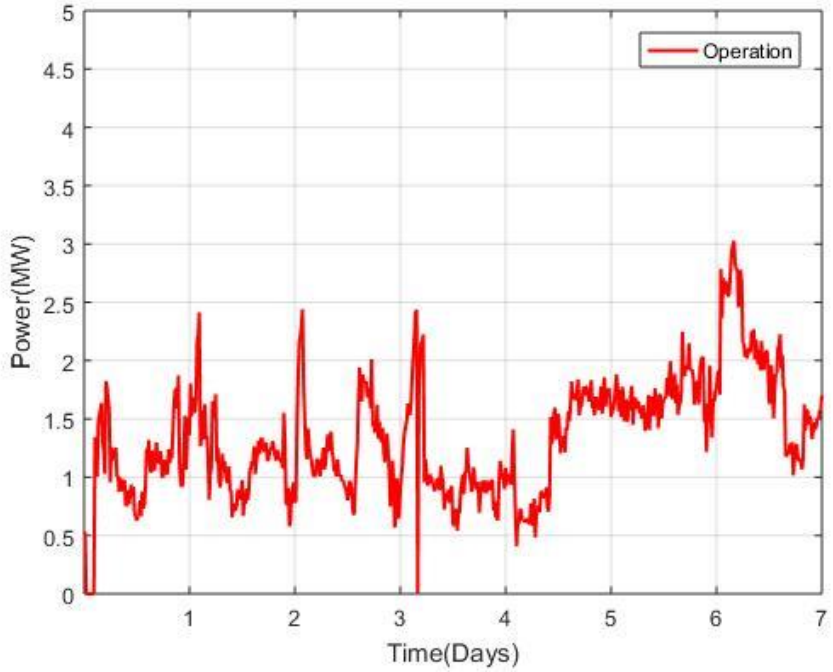

Figure 40: A week-long operation of UCI ST in summer

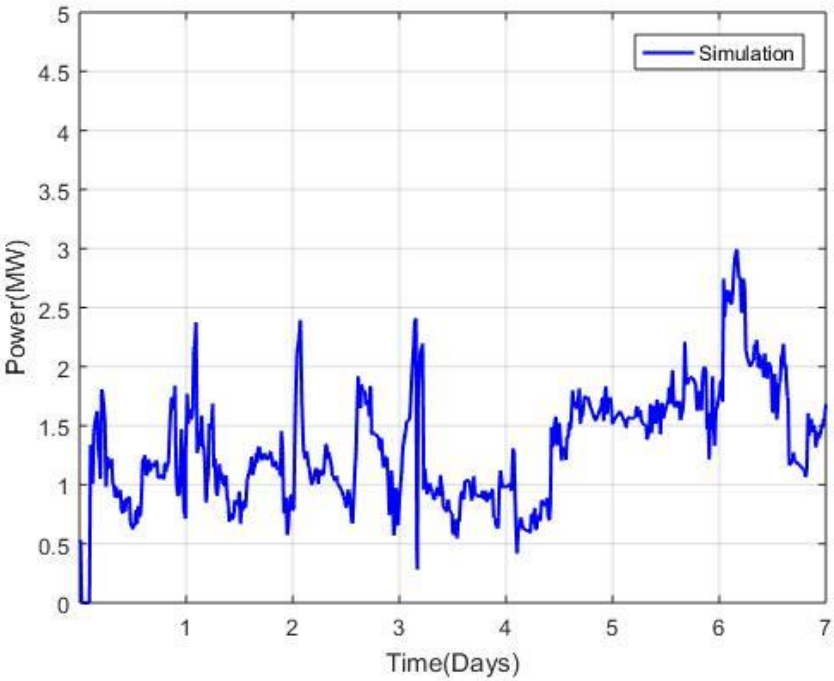

Figure 41: A week-long simulation of UCI ST in summer

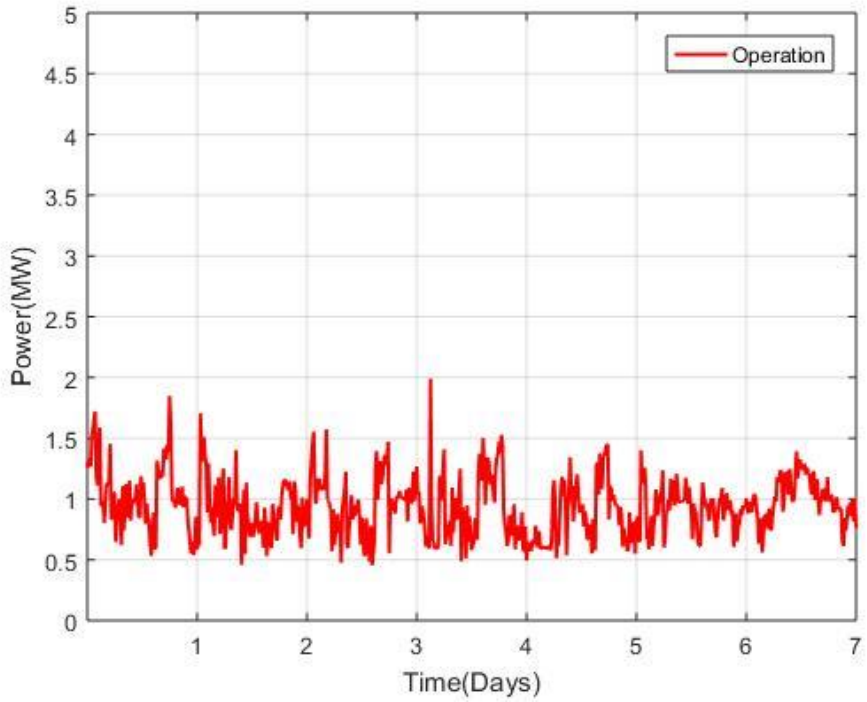

Figure 42: A week-long operation of UCI ST in winter

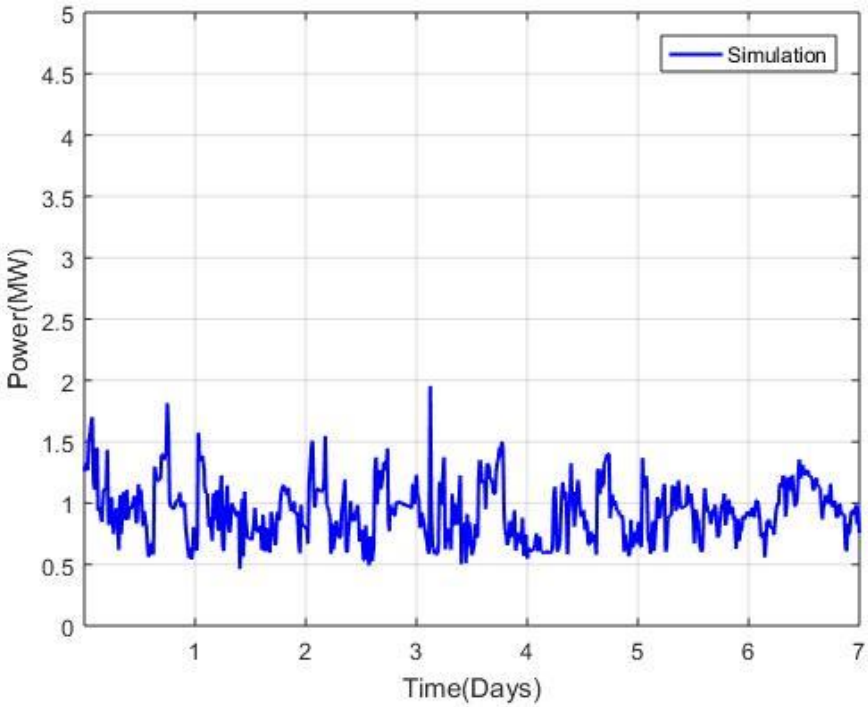

Figure 43: A week-long simulation of UCI ST in winter

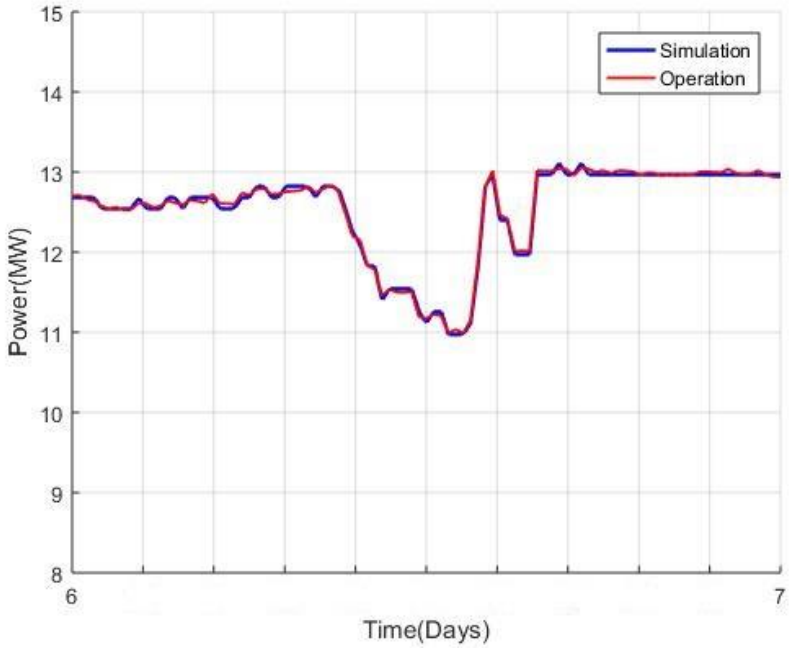

Figure 44: Day-long snapshot of UCI GT operation and simulation comparison in summer

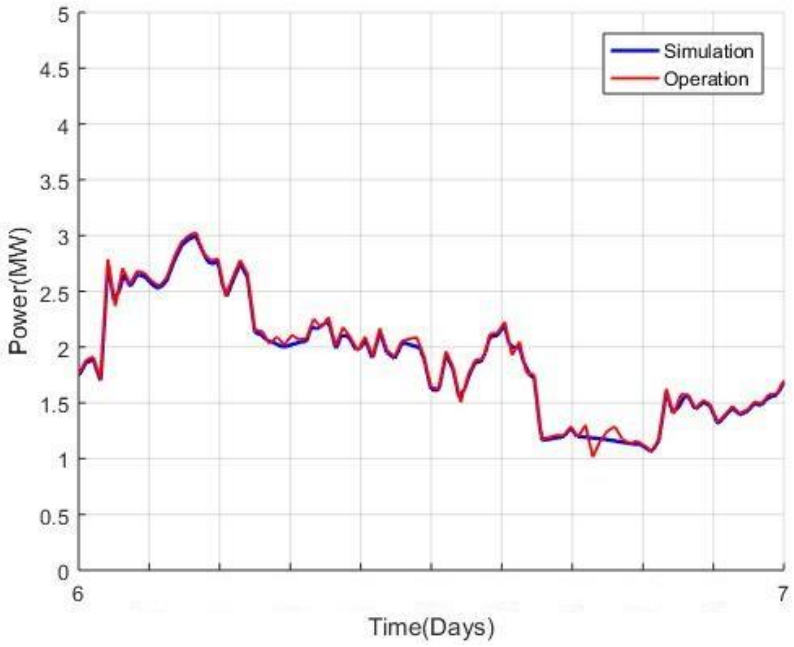

Figure 45: Day-long snapshot of UCI ST operation and simulation comparison in summer

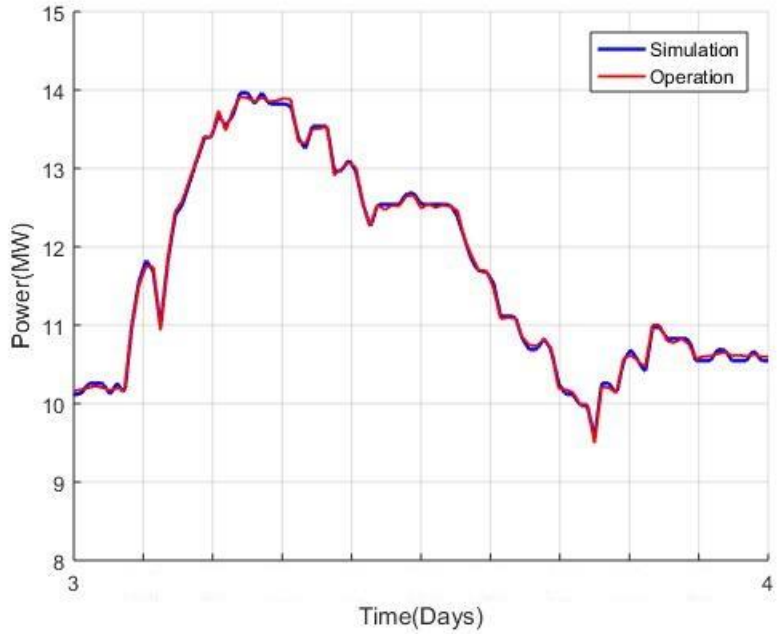

Figure 46: Day-long snapshot of UCI GT operation and simulation comparison in winter

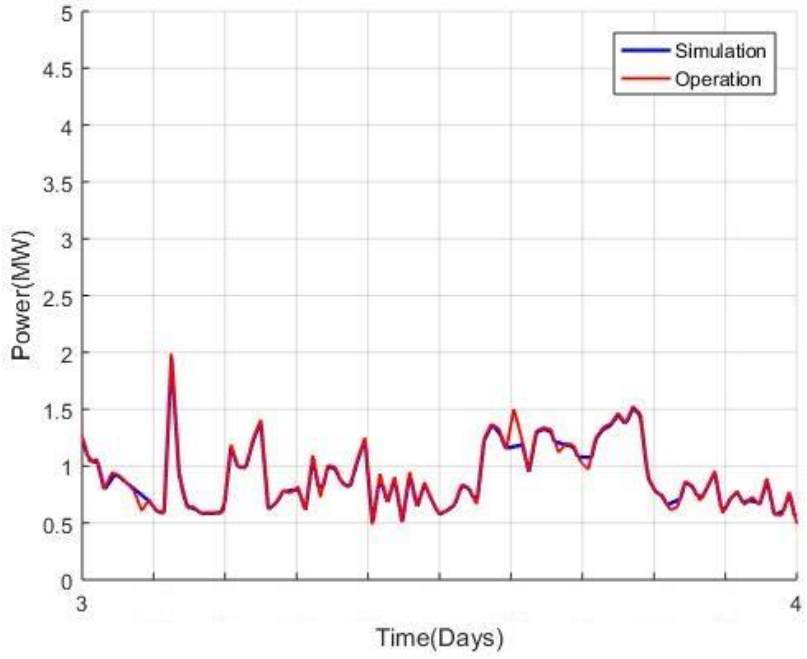

Figure 47: Day-long snapshot of UCI GT operation and simulation comparison in winter

Appendix B: Utility Simulation Results

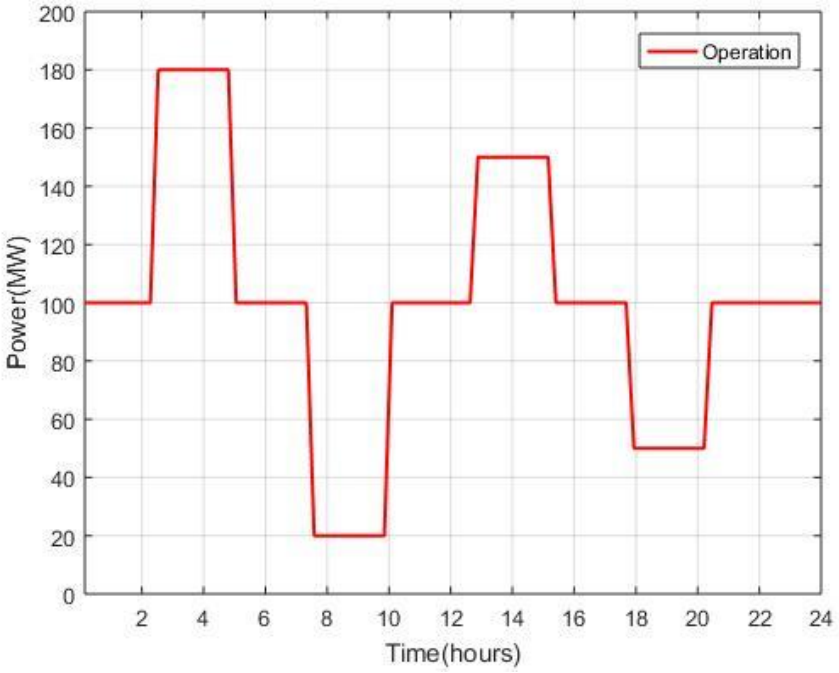

Figure 48: Reference power input for utility model

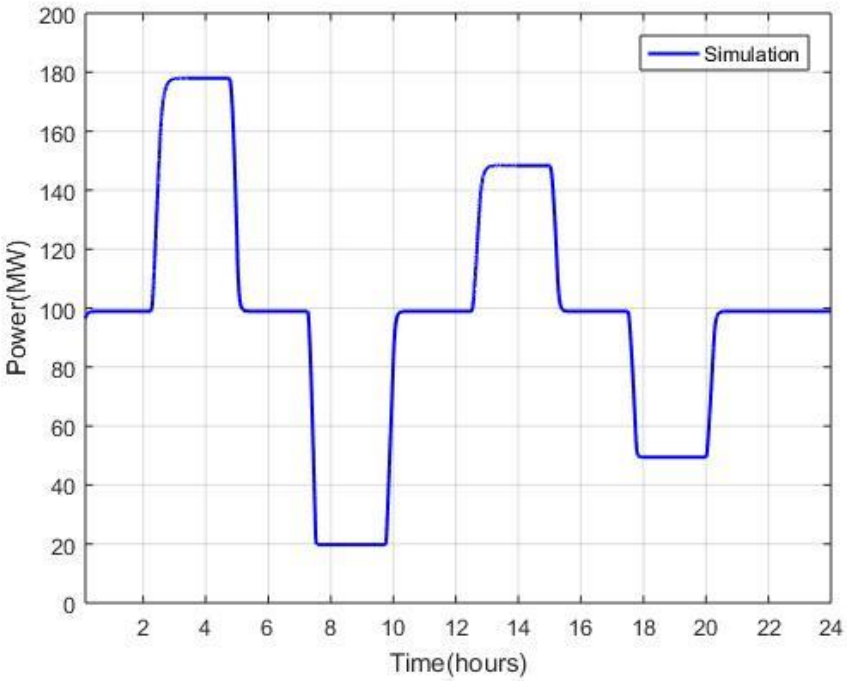

Figure 49: Utility GT model simulation with the reference input

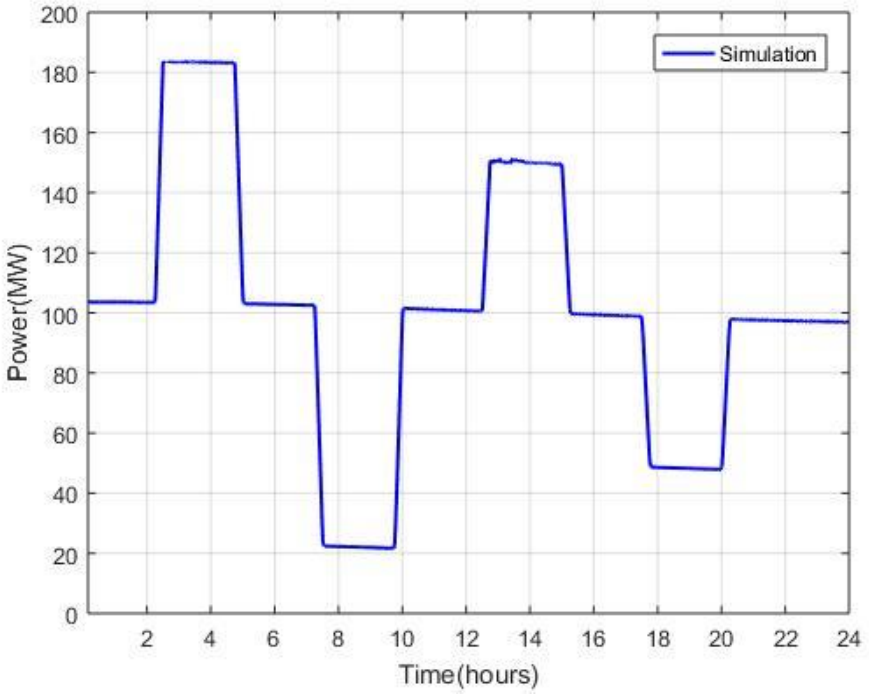

Figure 50: Utility ST model simulation with the reference input

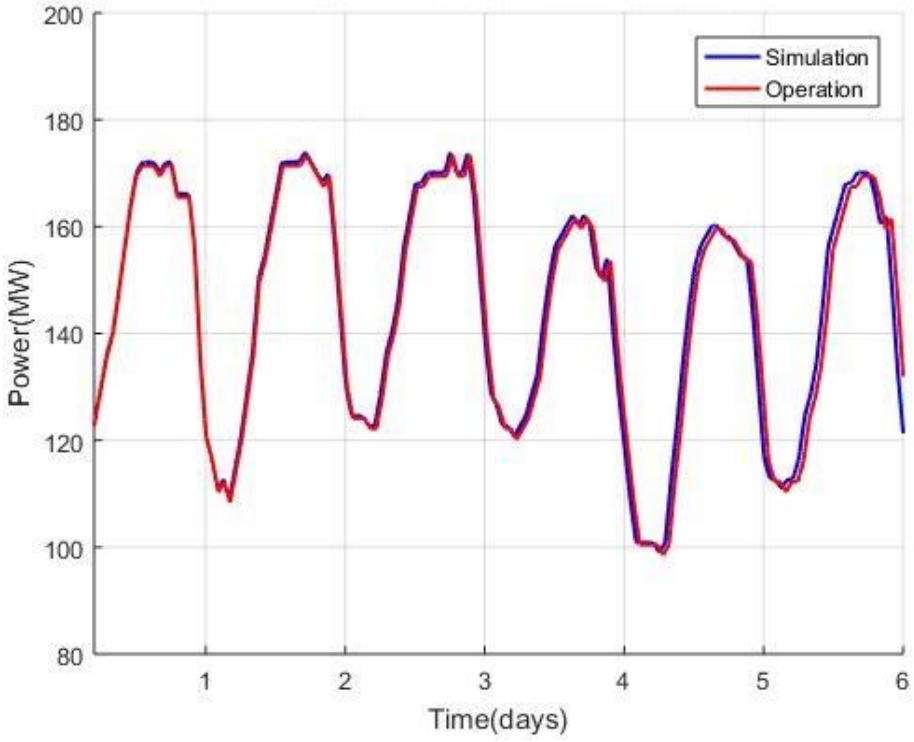

Figure 51: GT model simulation for 33% renewable penetration scenario

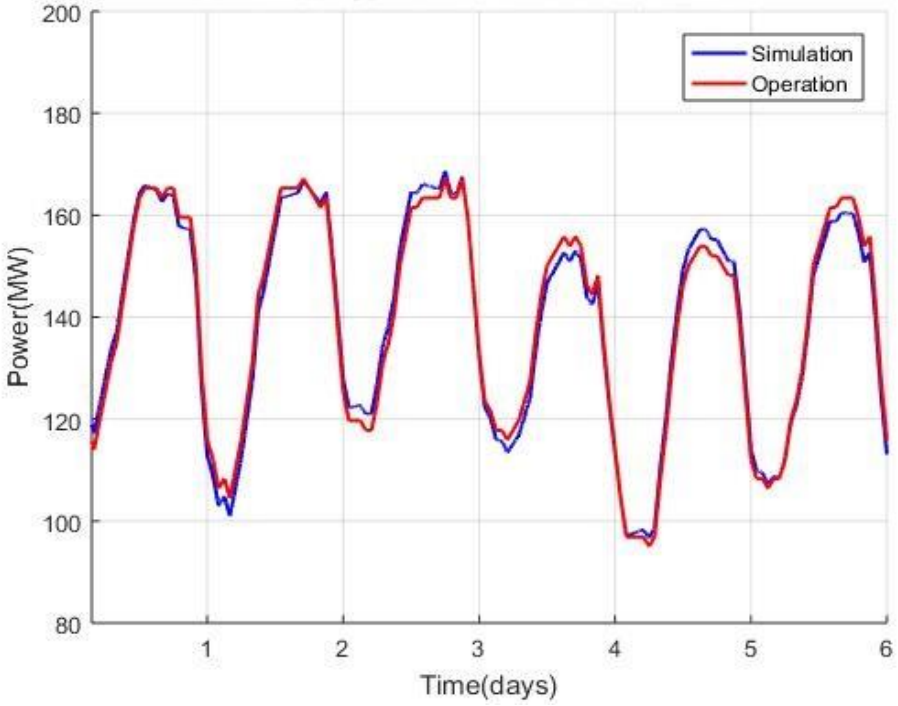

Figure 52: ST model simulation for 33% renewable penetration scenario

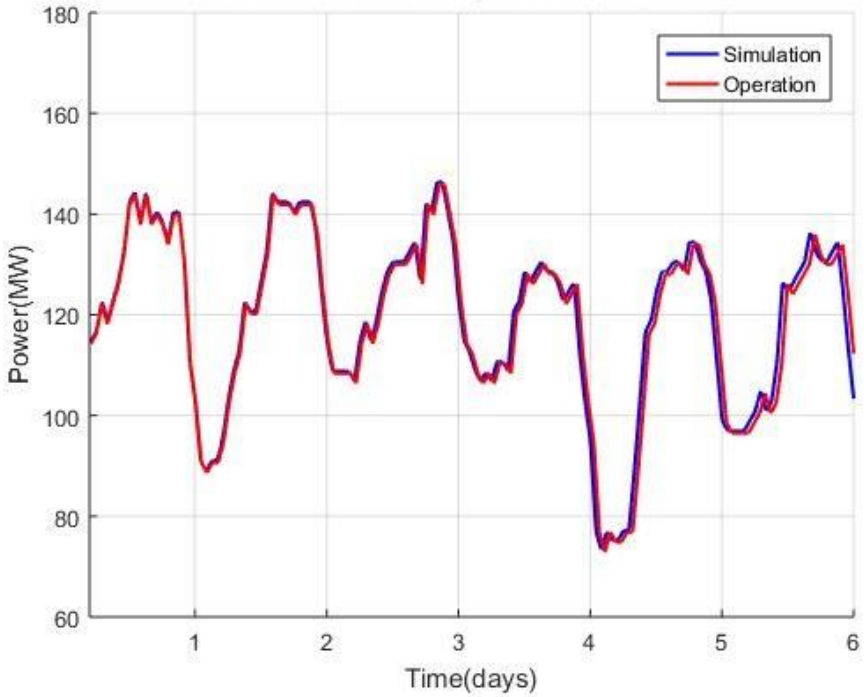

Figure 53: GT model simulation for 50% renewable penetration scenario

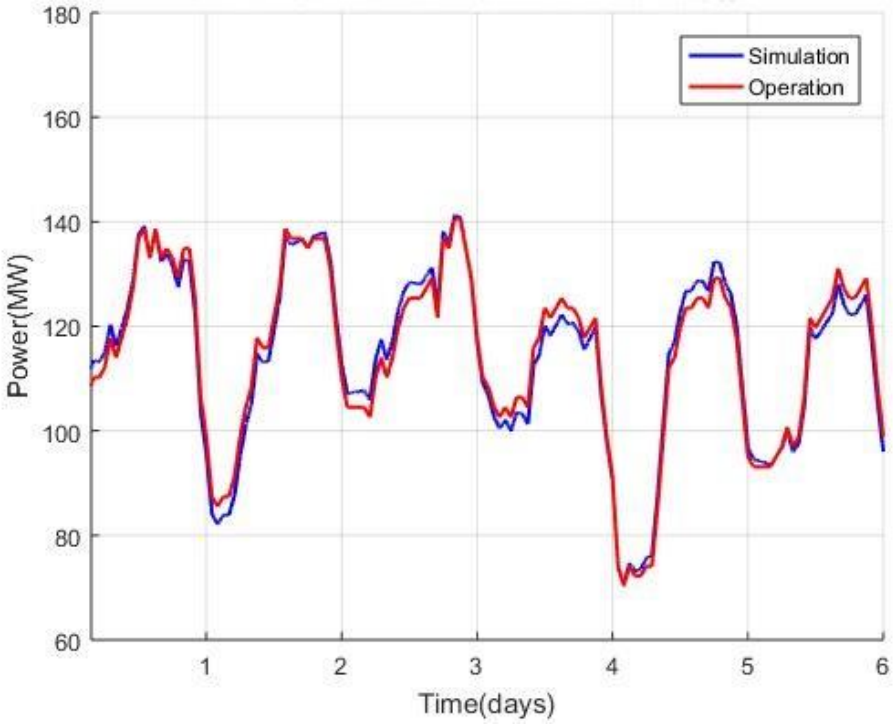

Figure 54: ST model simulation for 50% renewable penetration scenario

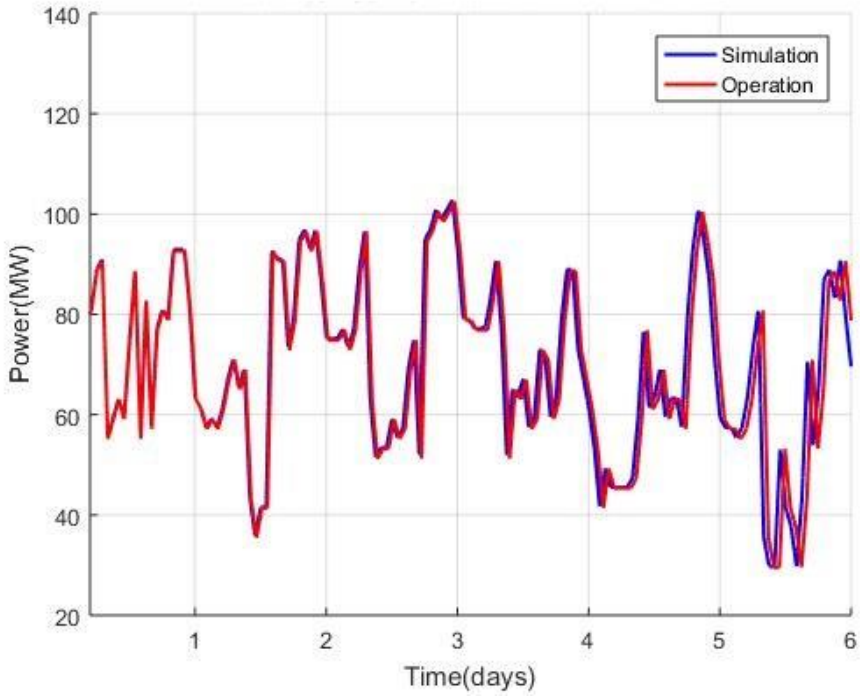

Figure 55: GT model simulation for 80% renewable penetration scenario

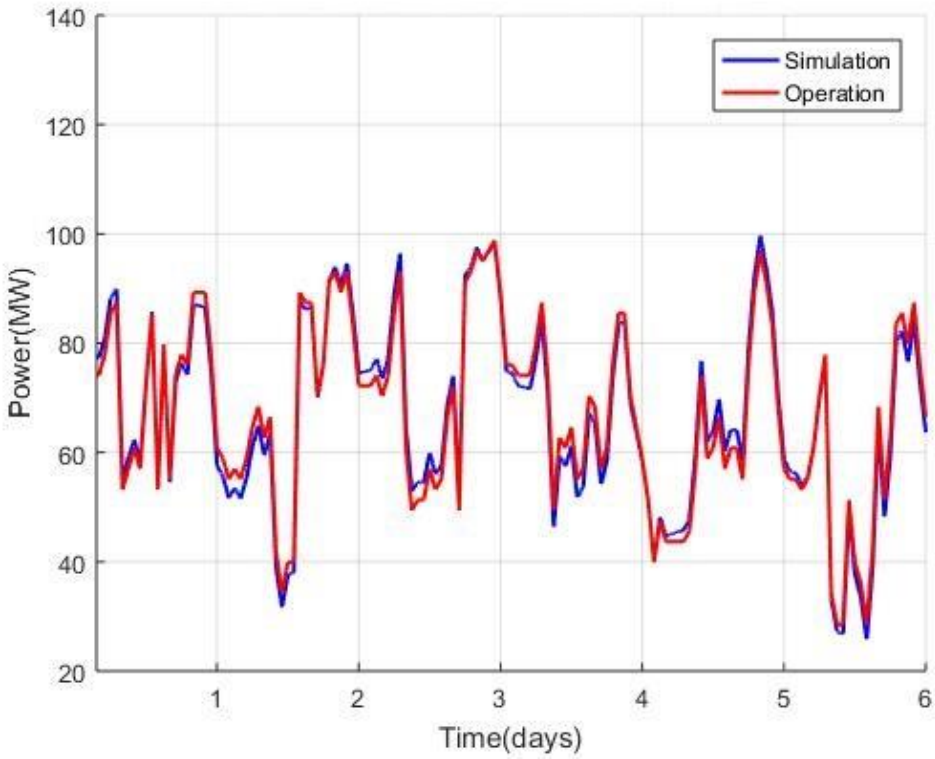

Figure 56: ST model simulation for 80% renewable penetration scenario

Appendix C: Models

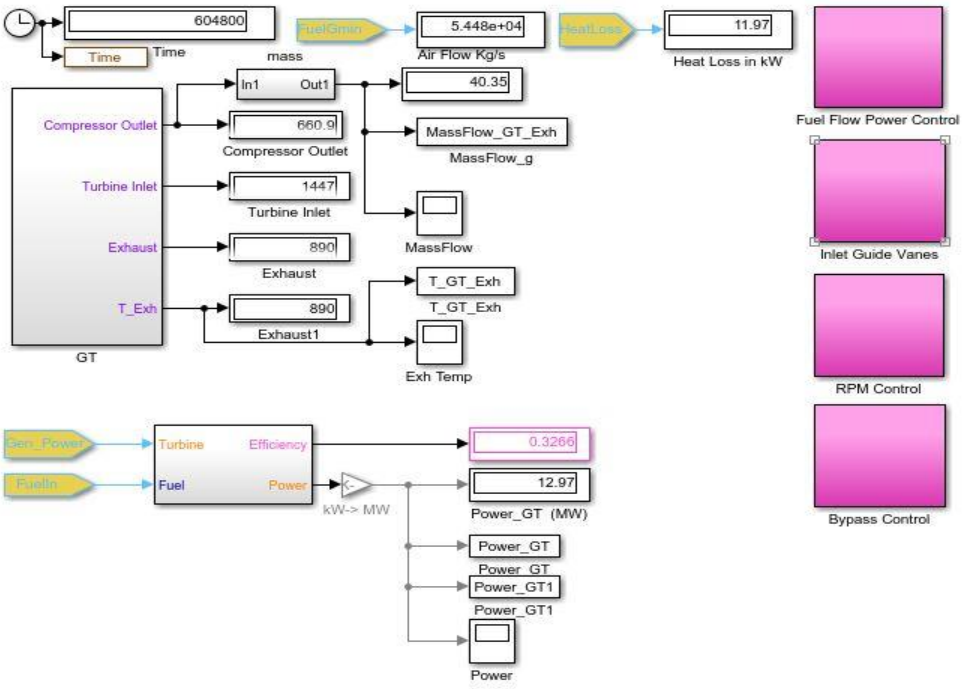

Figure 57: UC Irvine GT model configuration, Interface

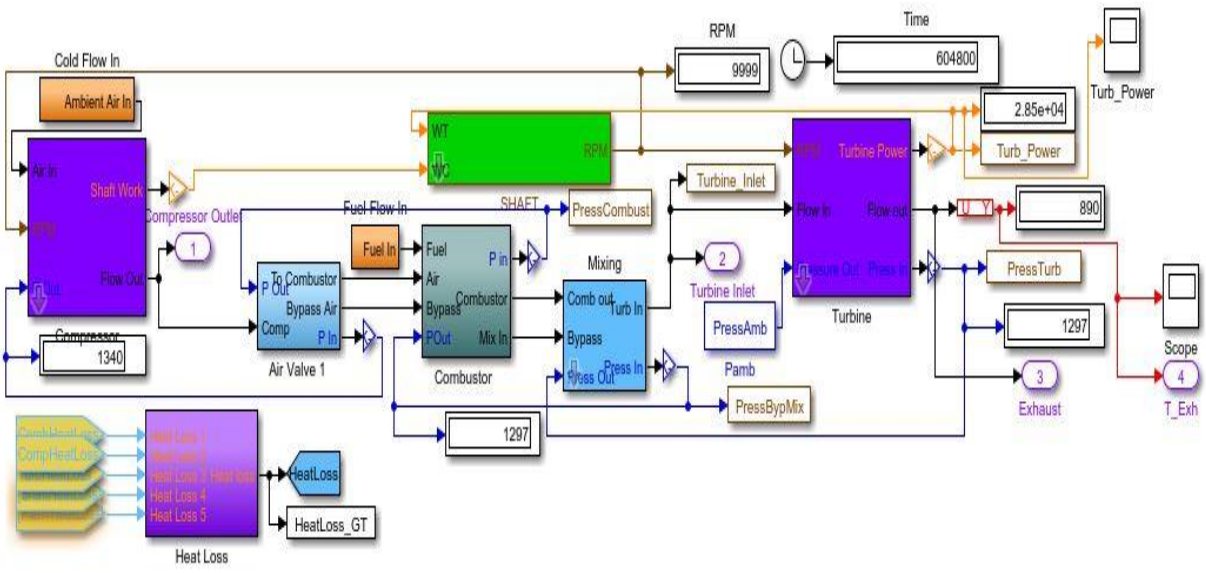

Figure 58: UC Irvine GT model configuration, Flow diagram

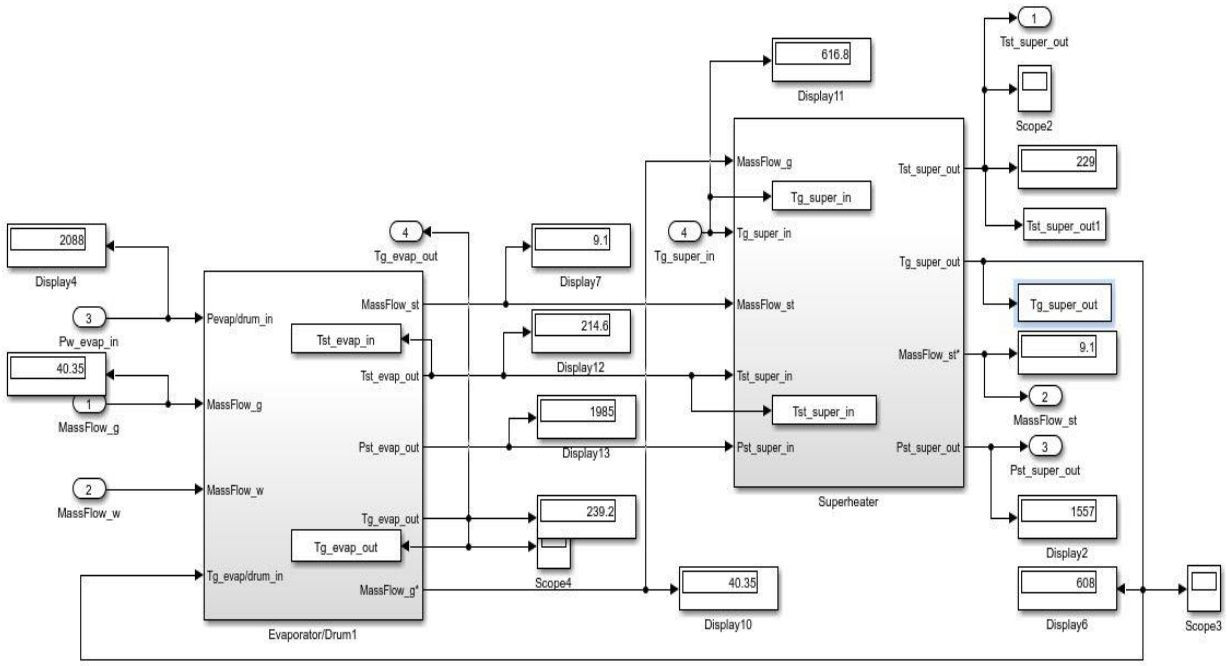

Figure 59: UC Irvine HRSG model configuration

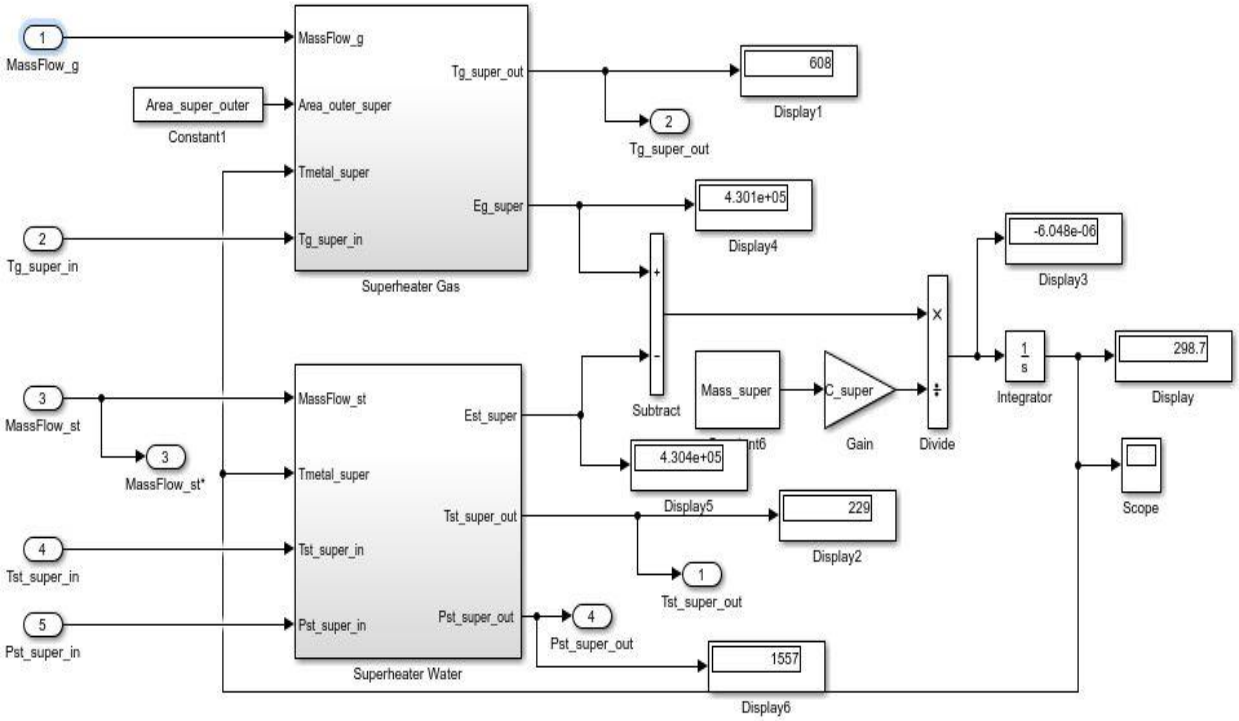

Figure 60: UC Irvine HRSG model configuration, Superheater

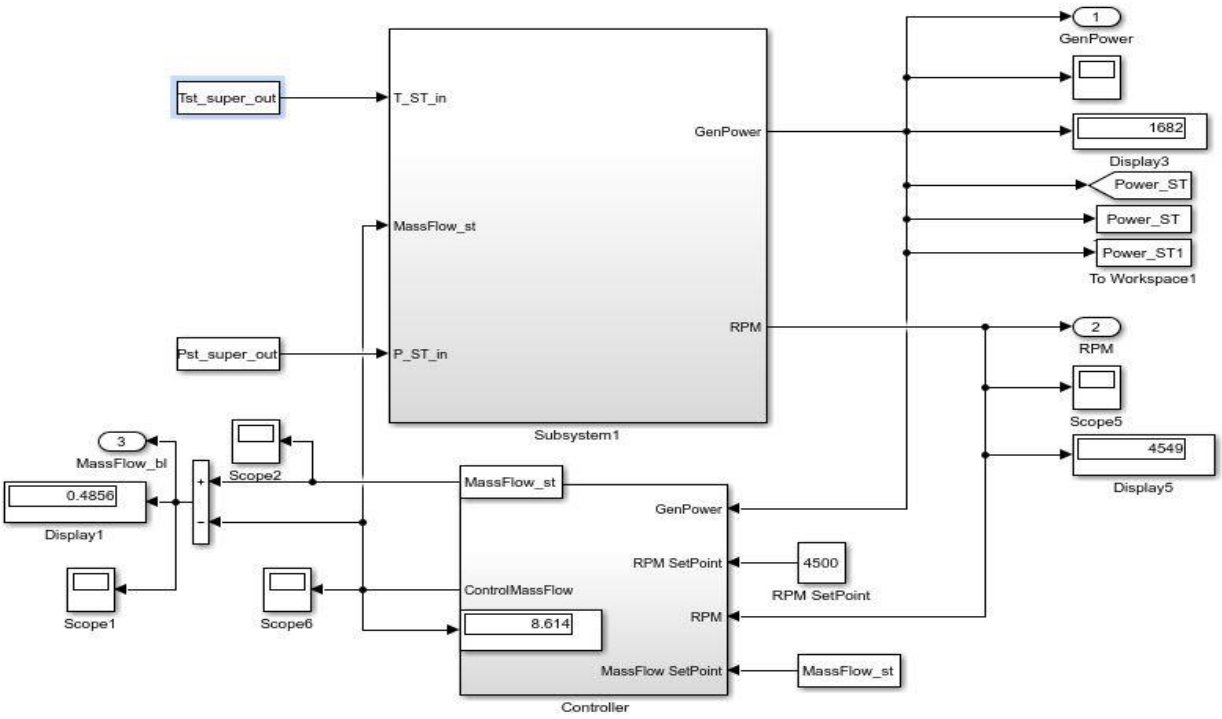

Figure 61: UC Irvine ST model configuration, Interface

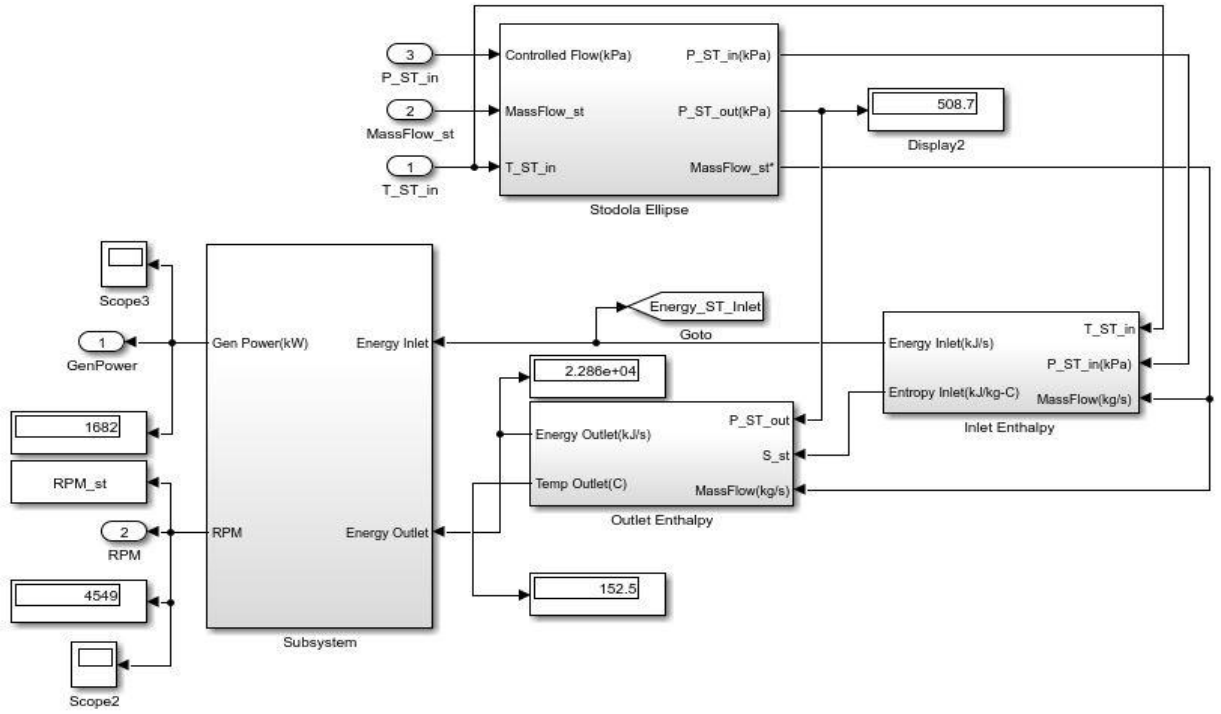

Figure 62: UC Irvine ST model, Flow diagram

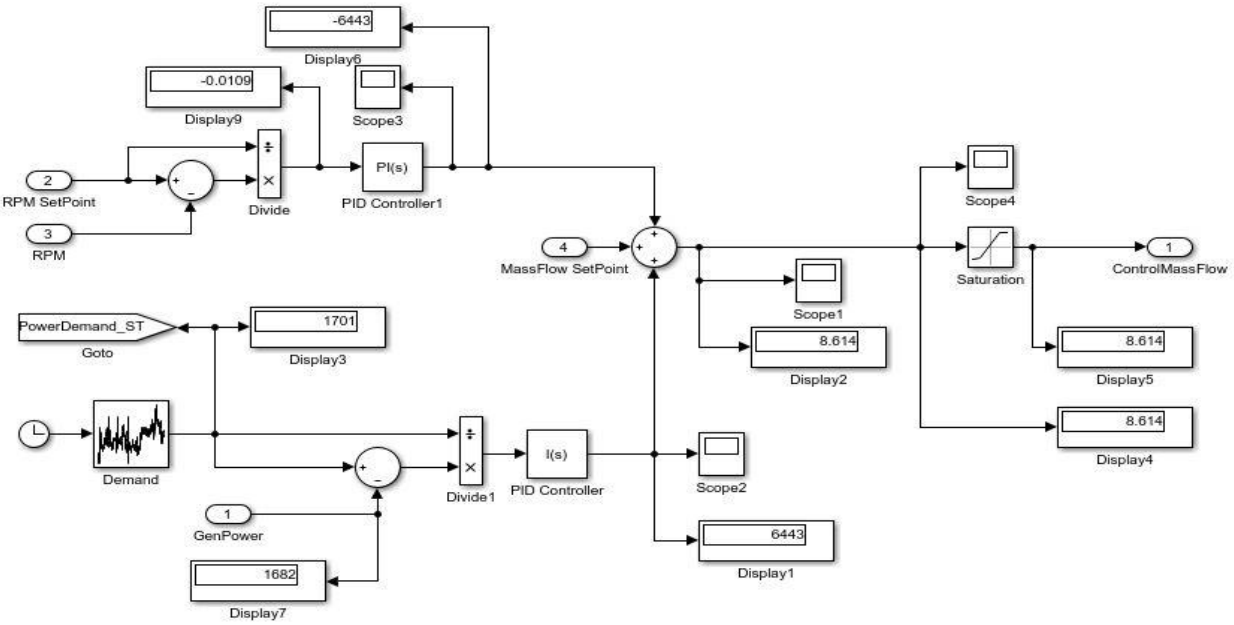

Figure 63: HRSG/ST controller configuration

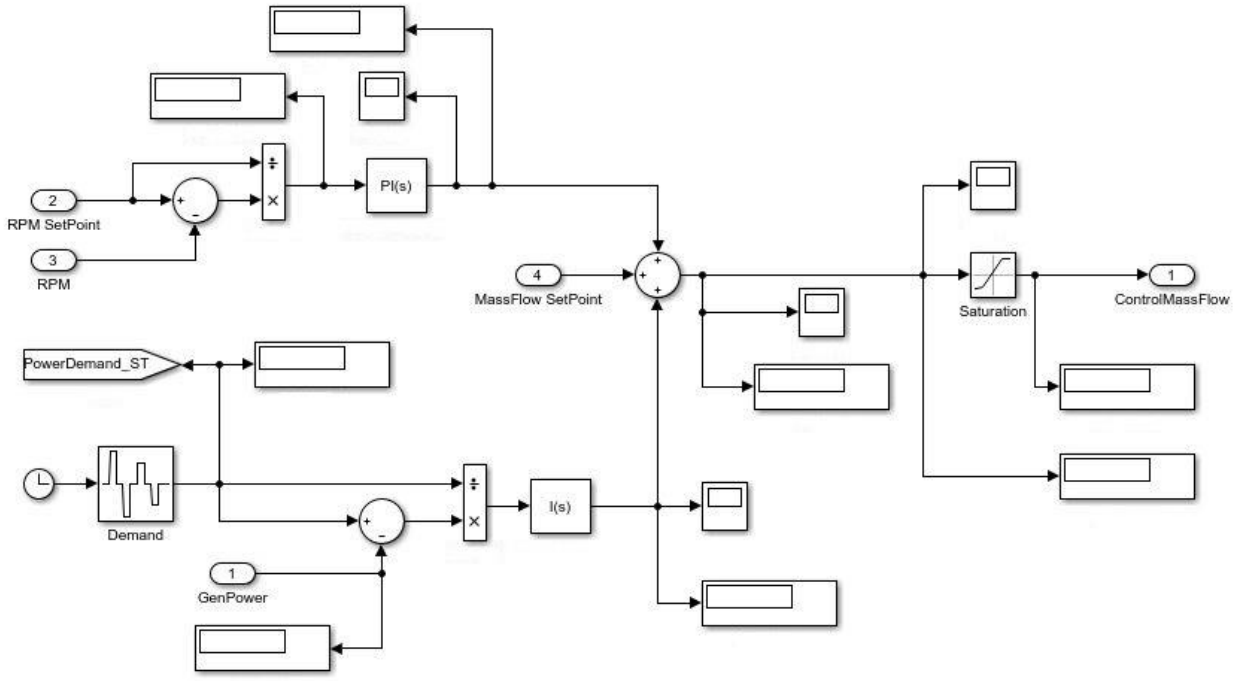

Figure 64: SIMULINK diagram of UC Irvine model bottoming cycle controller system

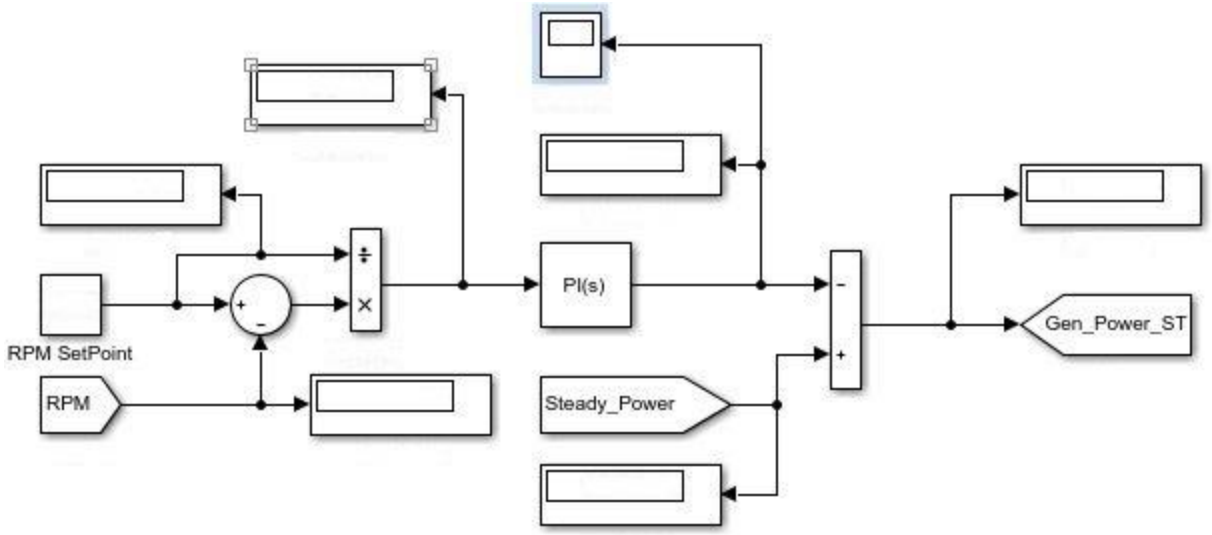

Figure 65: SIMULINK diagram of utility model bottoming cycle control system, part 1

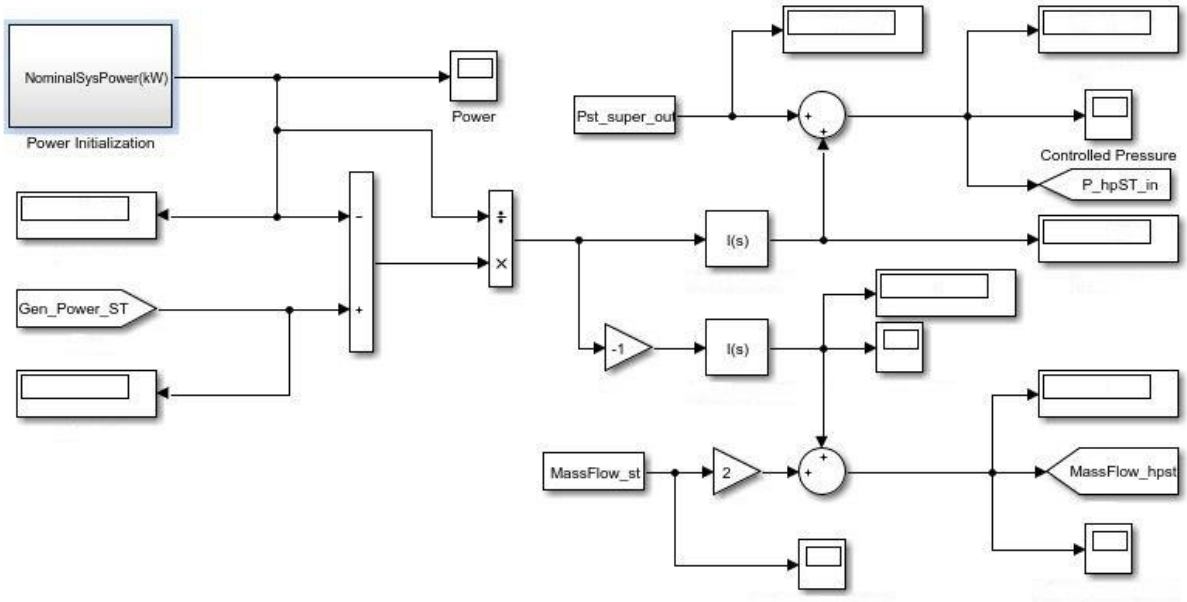

Figure 66: SIMULINK diagram of utility model bottoming cycle control system, part 2

Appendix D: Miscellaneous Figures

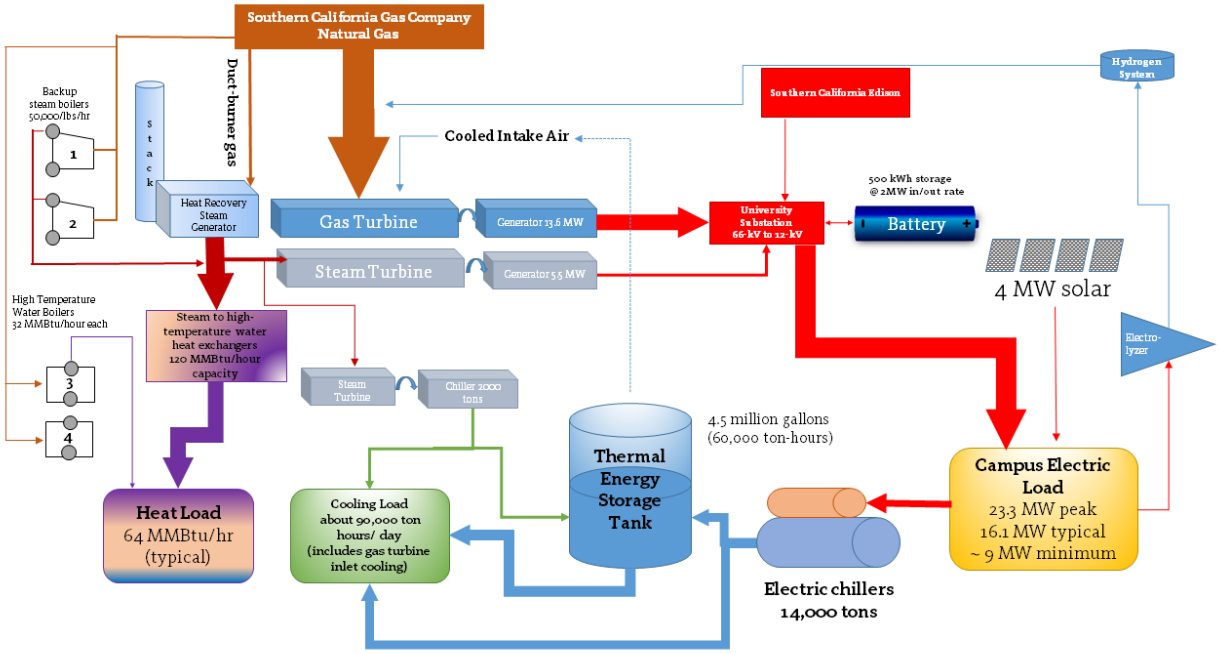

Figure 67: A schematic of UC Irvine campus energy infrastructure